Low Velocity Impact Energy Absorption of Fibrous Metal-Matrix Composites using Smart Materials

AUTHOR

Ajith Karamshiel Gopal

University of Natal

Supervisor : Prof. Sarp Adali

Submitted in fulfillment of the academic requirements for the degree of Doctor of Philosophy in Engineering (PhD (Engineering)) in the Department of Mechanical Engineering, University of Natal, August 2003.

PREFACE

I, Ajith Karamshiel Gopal declare that the whole thesis, unless specifically indicated to the contrary in the text, is my own work and has not been submitted in part, or in whole to any other university.

The research work has been carried out at CSIR Mining Technology and Kentron, A Division of Denel, under the supervision of Professor S. Adali of the University of Natal.

ACKNOWLEDGEMENTS

I would like to acknowledge the contributions made by the following people:

- Professor S. Adali from the University of Natal, for his insight, guidance and assistance throughout this study.
- My wife, Mandy Gopal, for all her support and encouragement.
- My mum, Mrs. S. Gopal, for instilling in me the importance of education.

ABSTRACT

In general, the basic concept of an intelligent material is defined as the multifunctional material that has a sensor, a processor and an actuator function in the material that allows it to maintain optimum conditions in response to environmental changes. Despite the fact that these materials have demonstrated varying degrees of success in shape and position control, active and passive control of vibration and acoustic transmission of materials subjected to dynamic loads, impact damage and creep resistance in structures and have been applied in industries from aerospace to biomechanics to civil engineering structures, very little literature is available on the subject.

Thus, the objective of this dissertation is to add to the fundamental understanding of the behaviour of these special materials by investigating the possibility of a magnetostrictive SMA hybrid metal-matrix composite beam with piezoelectric actuator, to enhance the materials load attenuation and energy absorption characteristics under low velocity impact loading.

The methodology employed in this investigation is driven by two primary factors. The first is the unique approach that the author puts forward to attempt to simplify the characterisation of damage in not just metal matrix composites, but in materials in general. The second factor is the lack of available literature on smart material energy absorption as well as a lack of precise theory for short fibre composites. The methodology includes an extensive literature review, the development of an analytical model, based on the new damage modulus approach, verification of the model using experimental results presented by Agag et. al., adjustment of the model to include smart material effects and finally numerical simulation using the MATLAB® software to predict the effect of smart materials on the energy absorption capacity of the material under impact.

The results show that the damage modulus (E_D) is a material characteristic and can be derived from the stress strain diagram. Further, it takes into account degradation of the material through the plastic region, up to the point just before ultimate failure. Thus, E_D lends itself to the simplification of many damage models in terms of a reducing sustainable load and energy absorption capacity. Only the energy consumed through material rupture remains to be characterised. The results also show that smart fibres diminish the capacity of the beam to sustain a load, but increase the displacement to failure. Thus, for a compatible substrate material, this increased displacement translates to a significant enhancement of energy absorption characteristics. The effect of prestrain on energy absorption is also considered and there appears to be a definite turning point where the maximum energy absorption is experienced.

The dissertation thus achieves its objective in investigating the ability of smart materials to enhance the energy absorption characteristics of regular fibre reinforced metal-matrix composite materials subject to low velocity impact loading. Of equal importance to the achievement of this objective is the introduction in the dissertation of the unique damage modulus that goes to the foundation of material characterisation for mechanical engineering design and has profound implications in damage theory and future design methodologies. Significant learning has taken place in the execution of this PhD endeavour and this dissertation will no doubt contribute to other investigations in the field of smart materials.

CONTENTS

LIST OF FIGURES

LIST OF TABLES

CHAPTER 1

1 INTRODUCTION

"Forget dumb old bricks and mortar: engineers are designing future devices from exotic materials that incorporate chemical switches or mechanical sensors to improve their performance." (W. Wayt Gibbs : Scientific American staff writer, 2000)

The objectives of this introductory chapter are to provide a brief description of the general characteristics and typical current applications of relevant smart materials as well as a summary review of related works, to give the reader an appreciation for the type and extent of literature available in this field of study. This chapter is also used to describe the objectives of the current investigation and put forward the methodology that is used to achieve them.

1.1 General Description and Applications of Smart Materials

Generally, the basic concept of an intelligent material is defined as the multifunctional material that has a sensor, a processor and an actuator function in the material that allows it to maintain optimum conditions in response to environmental changes. The class of intelligent or smart materials include shape memory alloys (SMA), piezoelectric materials, electrorheological fluids and electrostrictive and magnetostrictive materials. Cumulatively, these materials have demonstrated varying degrees of success in shape and position control, active and passive control of vibration and acoustic transmission of materials subjected to dynamic loads, impact damage and creep resistance in structures and have been applied in industries from aerospace to biomechanics to civil engineering structures.

The novel performances of shape memory materials include high damping capacity, large recoverable strain and recovery stress and property changes due to thermal or stress induced microstructural transformations. The shape memory effect of SMA is based on the crystal lattice deformation mechanism shown schematically in Figure 1-1 (Furuya : 1996).

Thus, austenite can be transformed into martensite by the application of temperature or stress or both and vice versa, thereby allowing control of the material's physical properties. SMA are also, commercially, easily fabricated into the useful forms of fibres, wires, ribbons, particles and thin films to be used with polymer (and more recently metal) matrices to form smart composites that

have enjoyed an amazingly broad range of applications in mechanical, electronic and automotive engineering, aerospace industries, sensors, domestic appliances and medical applications.

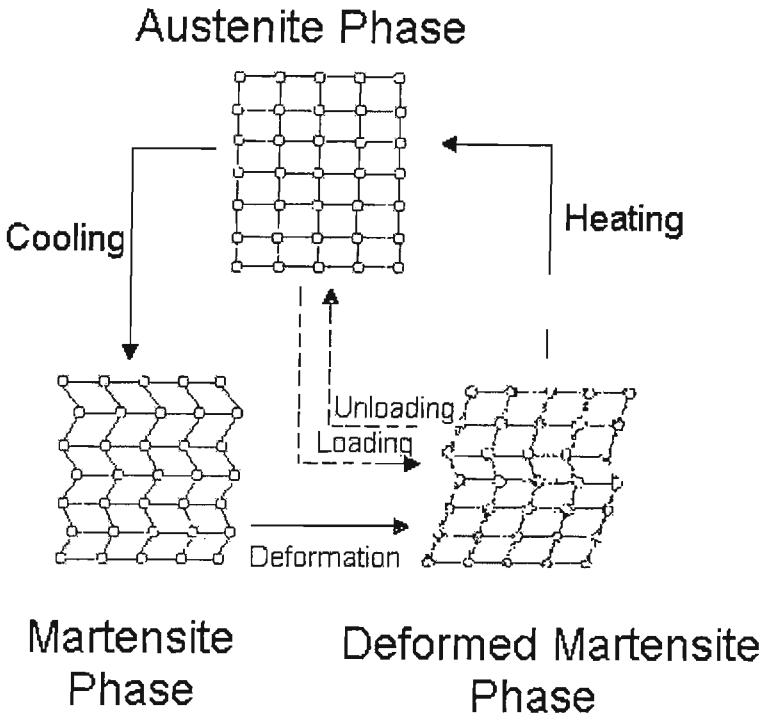

Figure 1-1: Crystal lattice deformation mechanism in SMA (modified after Furuya : 1996)

SMA have been applied to activate a hinge mechanism used for the deployment of reflector surfaces for satellite antennas, to aircraft wings as torque tubes for the control of face sheets, to aircraft in the form of nitinol springs that vary the spring stiffness and consequently improve aeroelastic roll performance and to control fuselage bending, reduce stresses in structures and control helicopter rotors (Birman : 1997). In addition to aerospace applications, SMA are, for example, proposed to control deflections of traversing beams that can be found in bridges and large space structures. Numerous projects have been concerned with possible applications of SMA in the medical field as well.

Also due to their special characteristics, piezoelectric materials can be used in distributed behaviour sensing and control of flexible structures. The two basic phenomenon that permit piezoelectric materials to be used as sensors and actuators in a control system are the direct piezoelectric effect and the converse piezoelectric effect. The direct piezoelectric effect implies

that the application of mechanical force or pressure to a piezoelectric material produces electrical charge, and conversely, the application of electrical charge to a piezoelectric material induces mechanical strain or displacement (Rao & Sunar : 1999). A classical example of these two effects is shown in Figure 1-2.

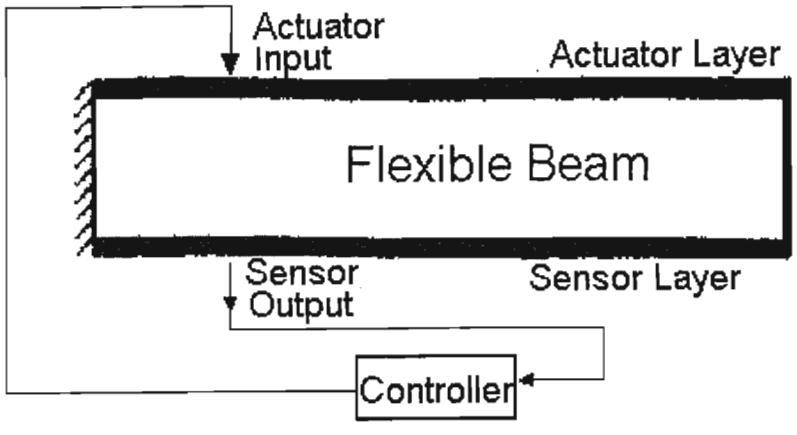

Figure 1-2: Distributed piezoelectric control system
(after Rao et. al. : 1999)

Two piezoelectric layers acting as sensor and actuator are surface bonded to a flexible beam host structure. The piezoelectric sensor senses the disturbance of the beam and generates charge proportional to the beam strain. The charge is tuned and accordingly manipulated by the controller and fed back to the piezoelectric actuator. The actuator causes a pinching action that helps attenuate the vibration motion of the beam.

Piezoelectric materials have found various applications in structural control schemes, such as position, displacement and velocity feedback, force feedback, wave absorption and fuzzy control. Other applications include vibration control and trajectory tracking of flexible robots, the manipulation of blade twists of helicopter rotors, the control of rotor motion in helicopter rotor blades and the flutter vibration suppression of cantilever tubes transporting high speed moving fluid, to name just a few.

Magnetostrictive materials and electrostrictive materials are analogous in that they respond quadratically to an applied field. Giant magnetostrictive materials, however, provide large displacements and output energy density, and superior manufacturing capabilities as compared to ferroelectrics. An example of a magnetostrictive material is Terfenol-D, and it is fabricated using conventional magnetron sputtering techniques. Magnetostrictive materials are fairly new to the

smart materials domain and its application has been limited by poor fracture toughness, eddy current losses at higher frequencies and bias and prestress requirements. These materials are currently being investigated in hybrid SMA composites to induce martensitic transformation of the SMA by the application of a magnetic field.

1.2 Summary of Related Studies

The review of impact damage resistance and low velocity impact presented by Miyazaki, Sandstrom and Wei (1998) is used as a basis for this summary as it incorporates most of the relevant and important conclusions pertinent to this investigation.

The high strain energy absorption capacity of SMA, evident from Figure 1-3, has been used by, Li, Liang and Rogers (1991) to extend material lifespan by accelerating closure of fatigue cracks and lowering crack propagation speed.

As an extension to the application proposed by Li et. al. (1991), Du and Nie (Miyazaki et. al. : 1998) showed that stress concentrations at notch tips can be reduced by placing prestrained Ti-Ni wires on the surface of tensile test specimens and causing them to contract with shape memory through the application of electric heating. Recent attempts have been made by Paine and Rogers and colleagues (Chaudhry, Kiesling, Paine and Rogers : 1996; Ellis, Jia, Lalande and Rogers : 1997; Paine and Rogers : 1994a; Paine and Rogers : 1994b) to improve the impact damage resistance of brittle thermoset matrix composites by hybridising with SMAs. The response of various SMA hybrid composites with different interaction configurations to low velocity impact was examined.

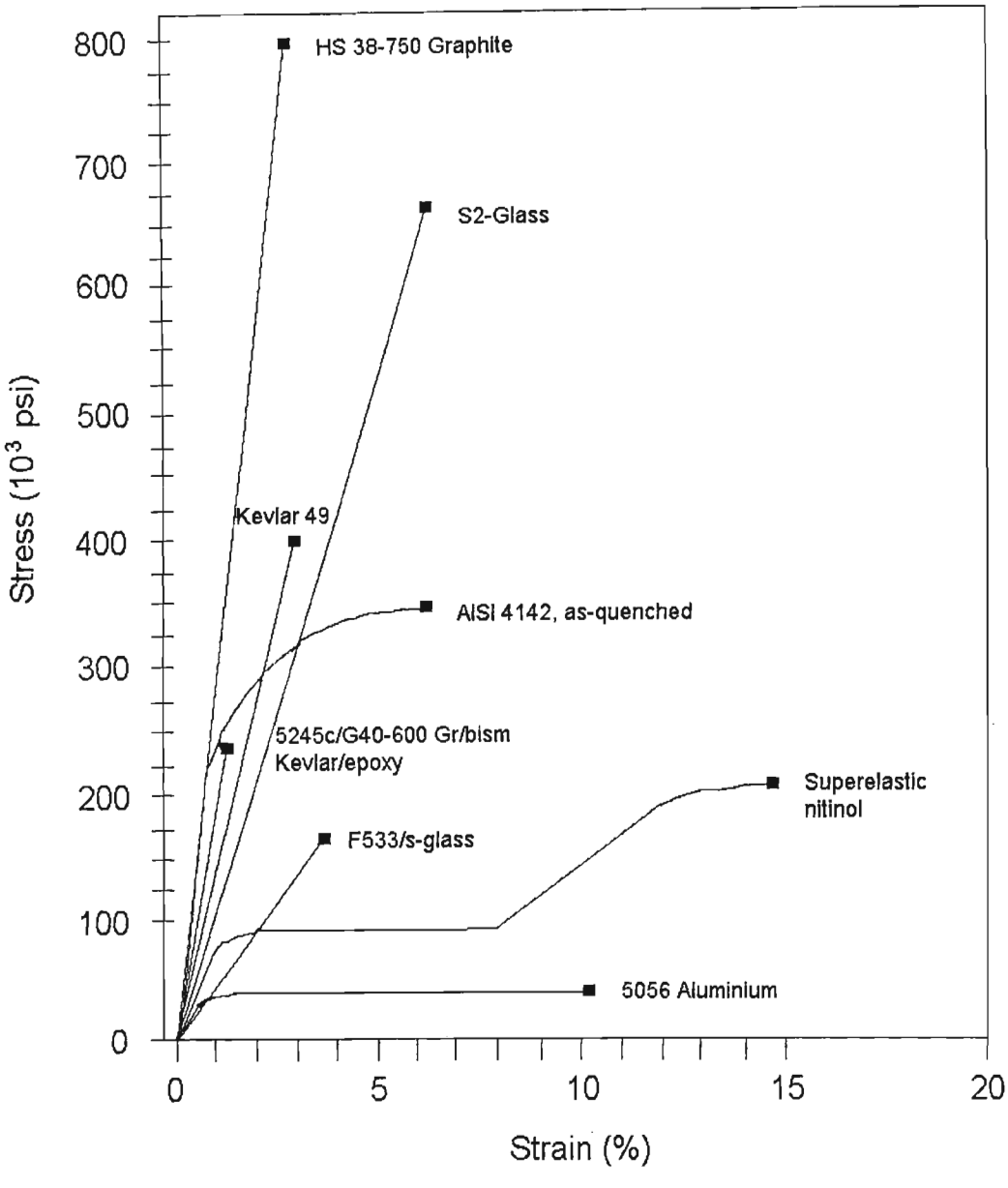

Figure 1-3: Stress-strain curves for various engineering materials (modified after Miyazaki et. al. : 1998)

To facilitate observation of the failure modes and to simplify fabrication, Ti-Ni fibre/epoxy composite materials were laminated to host composites as surface layers instead of being embedded. Graphite/bismaleimide (gr/bis) and glass/epoxy were used as the two host composites. An aluminium epoxy composite and Kevlar epoxy composite were also used as comparison hybrid layers. The dissipated impact energy and deflection during impact were determined from force-time data through low velocity impact tests conducted using an instrumented drop weight impact

tester. The results are summarised in Figure 1-4. The normalised energy values represent the amount of energy per unit volume required to perforate the various materials.

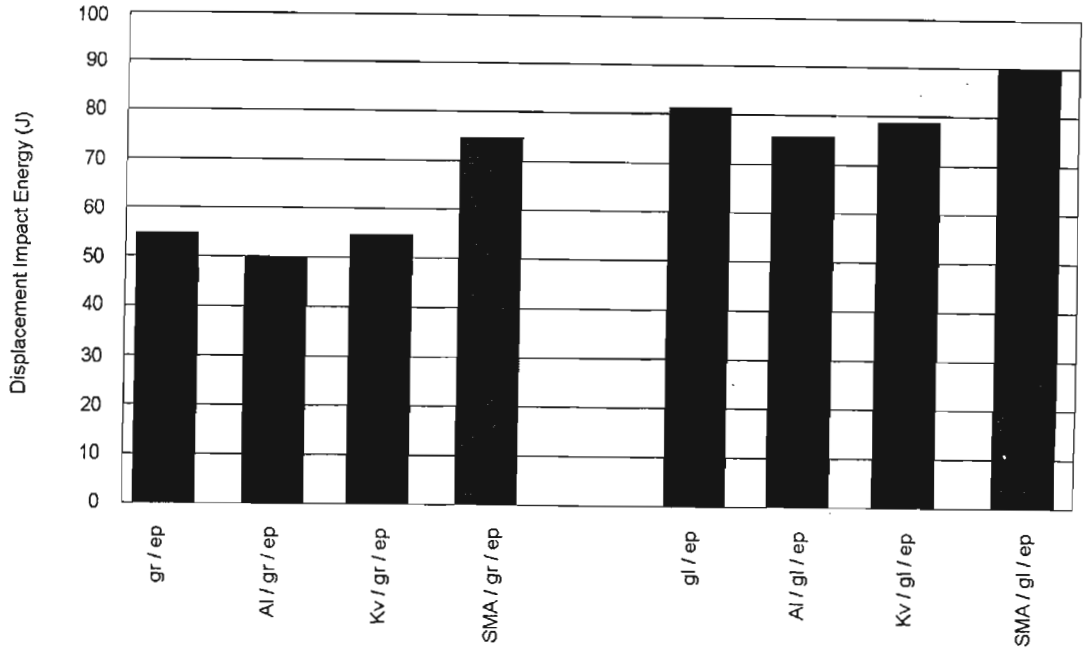

Figure 1-4: Comparison of the impact energy absorption for various composites under low velocity impact (modified after Miyazaki et. al. : 1998)

Evident from Figure 1-4 is that the Ti-Ni/graphite composite produces an increase of 35 % for the volume normalised perforation energy over the monolithic gr/ep host composite, whereas the aluminium and Kevlar hybrids produce little or no increase at all in perforation energy. The differences in perforation energy for the glass/epoxy system is not as pronounced. Visual inspection revealed that the composite with SMA fibres resisted the cutting action through distribution of the impact load over a greater surface area, because the SMA remained intact during the perforation event. The monolithic gr/ep and gl/ep and the aluminium and Kevlar hybrids all failed locally from a punched or cut hole from the local transverse shear stresses at the edge of the impact site (Miyazaki et. al. : 1998).

Low velocity impact experiments on gr/bis composite laminates with embedded SMA fibres also revealed that the impact resistance is greatly improved through the SMA fibres. The embedded fibres caused an increase in peak impact force and reduced the impact-induced delamination area by as much as 25 %. Independent tests conducted by Chaudhry et. al. (1996) with thin gr/bis composites embedded unidirectionally and bi-directionally with Ti-Ni fibres showed that while the

stiffness and ultimate strength of the composite remained unchanged, an increase in absorbed impact energy of 41 % was observed in the bi-directional SMA hybrids and 23 % in the unidirectional SMA hybrids. The bi-directional hybrids, however, suffered from a 22 % larger delamination area as compared to plain gr/ep composites. Contact deformation, global bending deformation and transverse shear deformation were identified as the energy absorption mechanisms for the SMA/graphite/epoxy composites under low velocity impact. At very low velocities, contact energy absorption is the most effective mechanism, while the shear deformation absorbs most of the impact energy at higher impact velocities. The total energy absorption of the SMA hybrid composites increases when the stress-induced martensitic transformation occurs.

Birman, Chandrashekhara and Sain (1996a; 1996b) studied the effect of low velocity impact on global deformations of composite plates and show that global deflections of composite plates can be reduced by a factor of two or more by using SMA fibres embedded within the composite material. It is also shown that SMA fibres are more effective when they are orientated along the shorter edges of rectangular plates.

Finally, by coupling Ti-Ni SMA to PZT via a TiO_2 buffer layer, the final composite material can sense and actuate to dampen structural vibration without the use of external control as depicted in Figure 1-5 (Miyazaki et. al. : 1998).

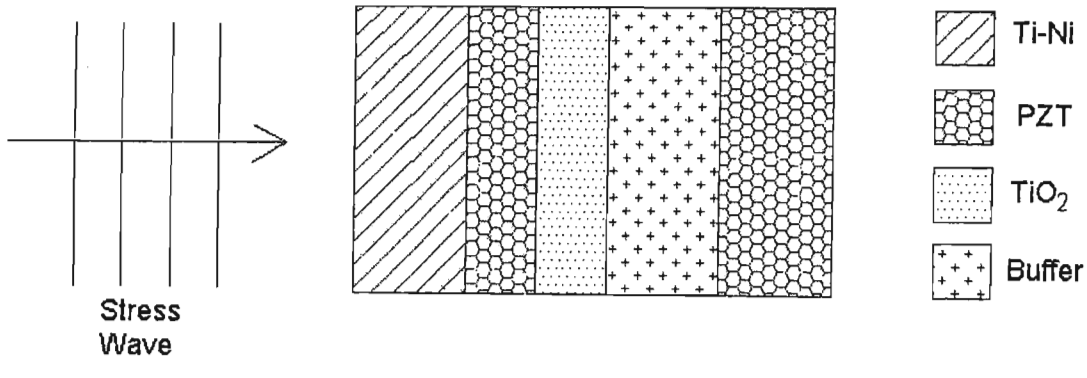

Figure 1-5: Self sensing and actuation of a SMA PZT smart material (after Miyazaki et. al. : 1998)

The stress wave propagates through the Ti-Ni SMA producing a stress induced martensitic transformation where some of the mechanical energy is converted into heat. The wave further produces a voltage across the first ferroelectric layer that can be used to produce an out-of-phase

stress wave by the second ferroelectric layer, and in turn attenuate the stress wave. A mechanical metallic impedance buffer (such as aluminium, titanium or Ti-Ni) is used to provide time for the counter-stress attenuation to occur.

This brings to a close a very brief summary of relevant work in the area of impact load attenuation and smart composites. A more detailed review follows in Chapter 2.

1.3 Objectives and Overview

Smart materials have enormous potential in a wide variety of industries, not only in aerospace, biomechanics and civil engineering, as highlighted earlier. However, due to a lack of understanding, these materials are still considered hi-tech and too sophisticated to be used in ordinary day-to-day design applications. Thus, in a broader context, the aim of this thesis is to increase the understanding of the behaviour of smart materials, and in so doing help to erase the perception that these materials are beyond the reach of the vast majority of designers and engineers.

To this end, the focus of this investigation is on the ability of smart materials, specifically SMA, magnetostrictive materials and piezoelectric materials, to enhance the performance of an ordinary metal-matrix composite beam in terms of load carrying capability and energy absorption capacity (The understanding behind this concept is that a SMA must be a better energy absorber than traditional materials because of their larger strain to failure characteristic). This is the primary objective of the investigation and includes a study on the effect of magnetostrictive inclusions on the energy absorption capacity of the SMA.

The second important aspect of the objectives of this investigation is the increase in understanding and competence for the author in peripheral activities such as numerical modelling and simulation techniques, data interpretation and evaluation, as well as a broader understanding of material behaviour in general.

Thus, the outputs of the study can be summarised as follows:

- The investigation of a magnetostrictive SMA hybrid composite with piezoelectric actuator, smart material that is capable of enhancing load attenuation and energy absorption characteristics.

- Fundamental understanding of the microstructural behaviour of SMA, magnetostrictive materials, piezoelectric materials and smart composites in general.
- Fundamental understanding and competence development in numerical modelling and simulation techniques, data interpretation and evaluation.

The investigation towards the design of an impact resistant smart composite includes a detailed literature review and analytical and numerical modelling.

The literature review encompasses general impact loading, the micromechanic behaviour of shape memory alloys, magnetostrictive materials and piezoelectric thin films. The output of this phase is the familiarisation of all relevant work conducted in the said fields, as well as a thorough understanding of the behaviour of the various material types. A competence is thus established to facilitate the theoretical modelling of the individual materials under various environmental stimuli.

With the competence in individual material modelling developed, the next phase combines this knowledge into a single analytical model characterising the smart composite under investigation. This is achieved in a step-wise procedure, beginning with a standard SMA composite model, then introducing the magnetostrictive inclusions activated by an external magnetic field and then finally attaching a piezoelectric actuator to the model in the attempt to generate the required magnetic field, under impact, to stimulate the magnetostrictive inclusions to cause martensitic transformation in the SMA. Attention is given to the energy absorption characteristics of the designed smart composite.

The theoretical modelling is executed together with numerical modelling using an appropriate software package. Thus, the scope of this investigation also includes the thorough understanding of numerical analysis in general as well as the specific software. The numerical modelling tool is used at each step in the analytical modelling procedure as a qualitative verification of results and to develop competence and proficiency in various modelling techniques used in the set-up and execution of the final model.

1.4 Methodology

The methodology employed in this investigation is driven by two primary factors. The first is the unique approach that the author puts forward to attempt to simplify the characterisation of damage in not just metal matrix composites but in materials in general. The second factor is the lack of

available literature on smart material energy absorption as well as a lack of precise theory for short fibre composites.

The characterisation of the energy absorption of a structural system is relatively simple in the elastic region of the materials involved. This is as a result of well-defined, predictable material behaviour and mature analytical models. However, once one enters the realm of plasticity, the characterisation gets very complex due to complex theories surrounding various damage models. Having a practical engineering background, the author finds these complex analytical descriptions extremely frustrating and limiting to practical engineering predictions. Thus, in an attempt to facilitate simple engineering models, the concept of an 'instantaneous' modulus is introduced. This instantaneous modulus, which from now on will be referred to as the damage modulus ED, is to the plastic region what Young's Modulus, is to the elastic region of a materials physical characterisation. The distinct difference is that unlike Young's modulus, the damage modulus is not a slope (differential) but a physical factor describing the stress behaviour of a material through its strain range i.e.

$$\sigma = E\varepsilon \qquad \text{for } 0 \leq \varepsilon \leq \textit{plasticity strain}$$

and

$$\sigma = E_D\varepsilon \qquad \text{for all strain}$$

The importance of the damage modulus is two fold. Firstly, it is a single factor that describes a material through its entire strain range. Thus, it easily accommodates materials with a defined plasticity point, such as steel, as well as materials without a defined plasticity point such as aluminium, for example. The second contribution that the damage modulus makes is that it takes into account 'damage' in material modelling and thus simplifies analyses by a considerable amount. To substantiate this new concept, the damages modulus will be used in this investigation.

As a starting point, E_D is derived from the stress-strain curve for the various materials involved, i.e. aluminium (AC8A alloy), aluminium oxide (Al_2O_3) and Nitinol. It should be noted that in the elastic region $E_D = E$. The simplification is that now Elastic theory can be used in the in the plastic strain range as well. Further, damage is taken into account by incorporating and effectively reducing Young's Modulus in the plastic zone.

The second factor driving the methodology of this investigation is the lack of available literature on energy absorption of smart metal matrix composites. This is particularly important, as every proposed model needs some kind of basis to reflect its applicability and serve as a measure of

accuracy. The route using experimental investigation as a tool to provide this basis is, unfortunately, not viable as South Africa views the use of smart materials, especially SMA such as nitinol, as military orientated and special clearances are required to import these materials. Thus, the only remaining option is to use published experimental results of other authors as a means of verifying this particular analytical model and, after a detailed literature investigation (as summarised in the previous chapter), the article by Aggag, Han, Nam and Takahashi is found to be most pertinent to the objectives of the current investigation.

In this investigation the author develops an analytical model, based on the damage modulus concept, to predict the behaviour of a short fibre metal matrix composite during a Charpy impact test. The model is verified using the experimental results given by Aggag et al. A smart composite Charpy test is then simulated by replacing the instantaneous modulus characteristics of some of the fibres with the damage modulus of a SMA. The results obtained are then compared to those obtained by Aggag et al to quantify the effect of the SMA on impact energy absorption. To accommodate the lack of precise theory describing the characteristics of short fibre systems, the analytical model is based on continuous unidirectional fibre reinforced composite theory adapted by a strength factor and geometric factor to make it more representative of a short fibre system. The former reduces the strength of the system, while the latter reduces the stiffness of the system. Once these two factors are set during the verification phase of the investigation, they remain unchanged through the remainder of the analyses, as they are only affected by geometry. The onset of failure of a system is initiated when either the system strain reaches the failure strain of the fibres or when the system stress reaches the strength of the composite. Once failure is initiated, the stress in the system is kept constant until the load that the system can support goes to zero. Also simulating failure is the decreasing depth of the system. This is modelled simplistically as a linear function from the original depth to the final depth of the system. The final depth is obtained by determining the minimum cross-sectional area required to support the failure load.

Finally, to simulate the effect of the magnetostrictive inclusions, the SMA model is subject to varying degrees of pre-strain to represent the reaction of the magnetostrictive elements to varying degrees of magnetic field. Numerical simulation is accomplished using the Matlab software package.

To refresh the reader's memory, a brief excerpt of the Charpy impact test is given.

The Charpy impact test was developed prior to the development of fracture mechanics and was used as a means of measurement of the fracture toughness parameters that are required to perform a structural integrity assessment during the design process. The test continues to be used today as

an economical quality control method to assess the notch sensitivity and impact toughness of engineering materials. While it is usually used to test the toughness of metals, similar tests can be used for polymers, ceramics and composites.

The Charpy impact test measures the energy absorbed by the high strain rate fracture of a standard notched specimen. The specimen is broken by the impact of a heavy pendulum hammer, falling through a fixed distance to strike the specimen at a fixed velocity (constant kinetic energy). Tough materials absorb a lot of energy when fractured, and brittle materials absorb very little energy. Figure 1-6 gives a graphical representation of the Charpy impact test.

The impact energy measured by the Charpy test is the work done to fracture the specimen. On impact, the specimen deforms elastically until yielding takes place (plastic deformation), and a plastic zone develops at the notch. As the test specimen continues to be deformed by the impact, the plastic zone work hardens. This increases the stress and strain in the plastic zone until the specimen fractures. The Charpy impact energy therefore includes the elastic strain energy, the plastic work done during yielding and the work done to create the fracture surface. The elastic energy is usually not a significant fraction of the total energy, which is dominated by the plastic work. The total impact energy depends on the size of the test specimen, and a standard specimen size is used to allow comparison between different materials.

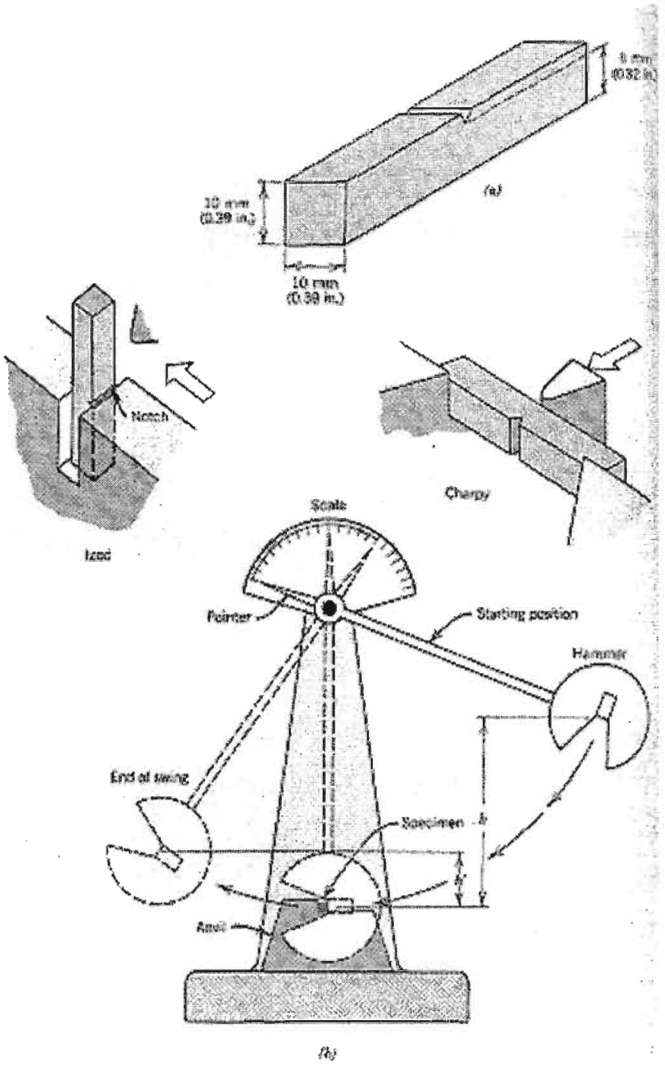

Figure 1-6: Graphical representation of the Charpy impact test

CHAPTER 2

2 LITERATURE REVIEW

The objective of a literature review is to familiarise oneself with relevant up to date information so that the investigation does not repeat previous work and is expedited by the knowledge and understanding consequently gained. The author has identified four review areas for the current study and includes impact loading, shape memory alloys, magnetostrictive materials and piezoelectric materials. It is practically impossible to peruse all the available literature in a realistic time period and as a result the number of articles sourced and reviewed has been limited to the most relevant in each area. A summary of the information and understanding gained is presented below. A selected bibliography, together with the initial review that was conducted, is presented in Appendix A.

2.1 Impact Loading

Composite materials are finding increasing use in engineering applications, because of their high specific strength, where the ability to withstand impact loading is an important design criterion. The application of composites to such dynamically loaded structures requires knowledge and understanding of the response of the composites to high strain rates. Numerous studies on the mechanical behaviour of composite materials under impact loading have been conducted. However, while the author has sourced an abundance of such articles dealing with polymeric matrix composites, there seems to be a lack of investigations into the impact behaviour of metal matrix composites. One such article that deals solely with polymeric matrix composites is by Harding and Ruiz (1998) where an elastic stress analysis using average elastic constants for the composite in the principle directions of reinforcement is used as a basis for initial estimates of the maximum stress reached for the specific loading conditions. While this approach forms a good starting point, it needs to be used with caution as the values of the various elastic constants may vary with the rate of loading; a point also alluded to by Harding et. al. (1998). Also, it is important to estimate the critical stress levels below which the composite deforms elastically and above which catastrophic failure occurs. To accomplish this task the use of data from small specimen tests is proposed. Small-scale structural tests should follow, in which loads and deflections on plates or beams, for example, as well as the damage can be monitored. This data is then used to develop and / or validate methods of modelling of the composite in general. (It is important to design tests and generate results that are not too restrictive in their application. This point is further examined later in the review.)

Thus, Harding et. al. (1998) give the overriding requirement, when designing a test specimen for determining material properties, that the values of the properties measured should be independent of the specimen dimensions and geometry. While standard specimen designs are available for homogenous isotropic ductile metallic materials, these are not applicable for material properties at impact rates of strain, in general. The most versatile technique available for such application is based on the split Hopkinson pressure bar (SHPB). The constraints on this approach are that the length of the test section must be sufficiently short for force equilibrium to be established across the specimen early in the test and that the interface between the specimen and the loading bars must not introduce extraneous stress waves that interfere with the standard wave analysis. The limitation of this approach, as applicable to composite materials, is that the specimen dimensions need to be large in relation to the scale of reinforcement if the measured properties are to be characteristic of the material. This directly conflicts with the SHPB requirement of a small gauge length. A further limitation is that the process of damage initiation and propagation in composite materials is more sensitive to the specimen geometry than the corresponding deformation process in ductile metallic materials. Typical small specimen tests include through the thickness shear tests, compression tests, tension tests (in-plane tension test and through the thickness tension test) and interlaminar shear tests (single and double lap shear test).

Harding et. al. (1998) further describes two types of small-scale structural tests, viz. the plate test and the beam test (Figure 2-1). In both cases, an instrumented bar is accelerated by a projectile to the required velocity before it comes into contact with the specimen.

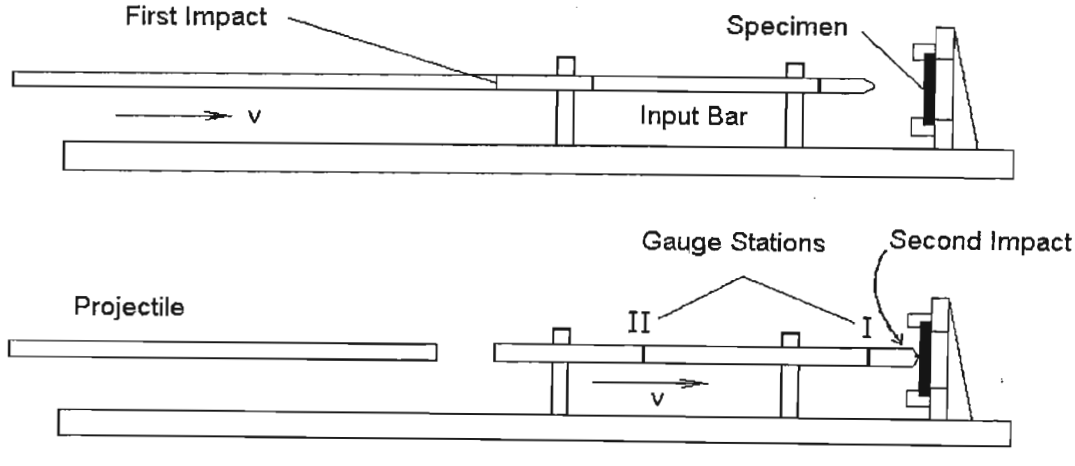

Figure 2-1: Schematic of small-scale structural test

(modified after Harding et. al. : 1998)

The initial gap between the bar and the specimen is made sufficiently large so that the bar is unstressed when it subsequently impacts the centre of the specimen but not so large that the bar velocity has decayed to any significant extent. The advantage of the beam test over the plate test is that high-speed photography may be employed to study the progressive accumulation of damage. Beam tests with high-speed photography showed the stages in the process of failure as follows.

1. Initiation of fibre fracture at the rear surface.
2. Crack extension into the beam across several 0° and 90° laminate layers.
3. Blunting of the crack by delamination, allowing the delaminated plies to unload.
4. As bending deflection continues to increase, the crack propagates a little further and the process repeats itself.

An important observation is that delamination plays a more significant part in the process for longer beam specimens while cracking predominates in short beam specimens and only becomes significant in longer specimens in the later stages when the remaining uncracked thickness is quite small.

The experimental portion of the investigation by Harding and Ruiz (Harding et. al. : 1998) considered the problem of a transverse impact of a simply supported laminated beam. The model is broken up into two phases, viz. a) initiation of failure and b) extension of damage. Failure is assumed to be initiated when the tensile strain in the outermost fibres reaches a critical value. In this first stage the velocity of the input bar is approximately constant. This initial loading is treated as quasi-static and conventional beam theory is used to determine the time to fracture initiation. In the second phase two processes combine to extend the initial damage. The crack is extended by fibre fracture of fibres aligned along the beam or matrix cracking along fibres aligned across the beam. This process is governed by the same equations as the first phase, but with the appropriate reduced values of the effective beam depth and stiffness taken into account. The second process of the second phase is delamination. Delamination causes portions of the beam to be unstressed and thus, a new beam geometry is defined to take this into account. The central deflection of the new geometry beam is obtained using elementary beam theory and in turn used to determine the strain energy. The release of strain energy due to delamination is also determined. The extent of delamination is dependent on the energy release rate. Figure 2-2 shows an excerpt of the experimental results obtained by Harding et. al. (1998).

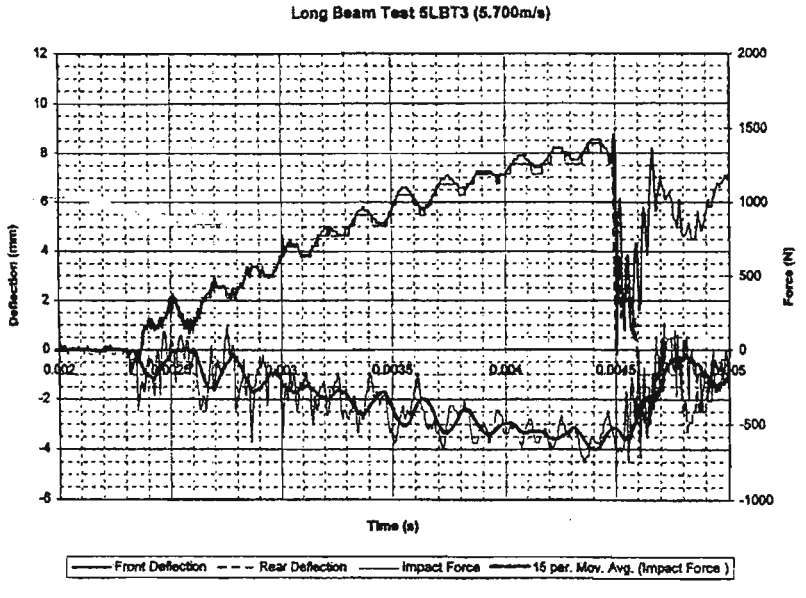

Figure 2-2: Test record for a beam specimen that failed under transverse impact (after Harding et. al. : 1998)

While deflections and forces are in good agreement with experimental results, this method under estimates the extent of damage and it is the opinion of the author that this is as a result of redefining specimen properties based on new effective beam depth and stiffness only, i.e. the model does not appear to take into account the reduced crack or delamination propagation energy as compared to initiation energy. Further, for a crack to propagate through the beam all fibres aligned across the beam should experience delamination to varying degrees up to the crack tip. The Harding and Ruiz model (Harding et. al. : 1998) only predicted delamination of two layers out of a twenty-one layer beam and eight layers out of a forty-one layer beam. The basing of delamination on energy release rate also contributes to ineffective predictions because of the wide range of variance in most composite materials.

Numerical modelling of the transversely impacted simply supported beam is accomplished using the DYNA-3D finite element code that uses the Chang and Chang criterion of failure of composites.

Hamouda and Hashmi (1998) expand on the issue of testing of composite materials at high rates of strain by citing their important considerations to the design of experiments for dynamic testing of

composite materials, viz. a) devising launch mechanisms to produce the desired stress state, b) fixing specimens in the test assembly, c) selection of specimen geometry, d) test duration and equilibrium time, e) the complexity of composite failure mechanisms, f) measuring transient parameters accurately and g) data collection, management and interpretation. Hamouda and Hashmi (Hamouda et. al. : 1998) proceed to present a useful table (Table 2-1 below) categorising various experimental techniques for high strain rate testing and thereafter discuss eight such techniques including Charpy-Izod, drop weight, expanding ring, SHPB, compression SHPB, tension SHPB, shear and plate impact tests.

Review of the above mentioned discussion yields important considerations that the author feels need to be borne in mind when designing an experimental investigation. Results of the Charpy-Izod tests are dependant on the specimen dimensions and hence cannot be used to obtain fundamental data on the impact response of a composite material.

The drop weight tests are used to determine the compressive stress-strain behaviour of materials at medium strain rates of the order of 10^{-2} s^{-1} and greater. Investigation of e-glass fibre reinforced epoxy indicates a dynamic failure stress 25 % greater in magnitude than the corresponding static value. Also, drop weight testing of chopped strand mat reinforced polyester shows that increasing the angle of impact (angle of inclination) results in a decrease in the corresponding damage area and a reduction in the depth of surface indentation, for any given incident kinetic energy.

The expanding ring test is difficult to perform and requires very precise displacement measurement and is hence limited in its use. One of the advantages, however, is the ability to test extremely high strain rates (of the order of 500 s^{-1}). Tests conducted on graphite-epoxy rings show that for a matrix controlled failure (90° fibre orientation) the material properties exhibit higher elastic modulus and strength than the static values. In both cases (0° and 90° fibre orientation) the static ultimate strain was three times higher than the dynamic value.

Table 2-1 : Experimental techniques for high strain rate testing

(after Hamouda et. al. : 1998)

Mode	Applicable Strain Rate (s^{-1})	Testing Techniques
Compression	< 0.1	Conventional testing machine
	0.1 – 100	Servo-hydraulic machine
	0.1 – 500	Cam plastometer and drop test
	200 – 10^4	Hopkinson pressure bar
	10^4 – 10^5	Direct impact using air gun apparatus
Tension	< 0.1	Conventional testing machine
	0.1 – 100	Servo-hydraulic machine
	100 – 10^4	Hopkinson pressure bar in tension
	10^4	Expanding ring
	> 10^5	Flyer plate
Shear	< 0.1	Conventional testing machine
	0.1 – 100	Servo-hydraulic machine
	10 – 10^3	Torsional impact
	100 – 10^4	Hopkinson pressure bar in torsion
	10^3 – 10^4	Double notch shear and punch
	10^4 – 10^7	Pressure-shear plate impact

As previously discussed, the major complication of the SHPB test is the antagonistic requirements of the test procedure and material constraints. Also, load transfer between the loading bars and the specimen has to be carefully designed to avoid stress wave reflections due to an impedance mismatch. Compression SHPB tests conducted on short cylindrical specimens of woven glass-epoxy laminates show an increase in the ultimate compressive strength under impact loading that appeared unaffected by specimen geometry (Hamouda et. al. : 1998). Hamouda and Hashmi also modified the standard SHPB test to be applicable to tensile tests, though the results are not very accurate. To increase accuracy it is recommended that a set of strain gauges be attached directly to the specimen. Recently a new electrical resistance technique for detecting failure in balanced angle-ply carbon fibre reinforced plastics has been developed that uses the variation of electrical resistance of tubes during expansion when subjected to internal explosive loading pulses.

Unfortunately, all the shear property determination techniques described are based on the SHPB and none can be used with confidence due to the difficulty in inducing pure uniform shear in the specimen.

In general, plate impact experiments provide the most versatile technique for material property evaluation and provide the highest strain rates available today. A full description of the experiment is referred to by Hamouda and Hashmi (Hamouda et. al. : 1998).

Dang and Liu (1998) conducted instrumented impact tests of laminated composites under low velocity impact concluding that matrix cracking and delamination are the major damage modes in composite laminates subjected to low velocity impact. An indentation law based on quasi-static tests is used to model the composites response. This approach is known to usually give good predictions of composite responses under low velocity impact because it has a strong dependence on parameters obtained from experiment. Consequently, the model developed by this approach is only suitable for its specific experimental configuration, i.e. the model ceases to be applicable if the material or geometry of the composite or impactor is altered. Figure 2-3 shows the experimental force-displacement results obtained for laminates subjected to various impact velocities.

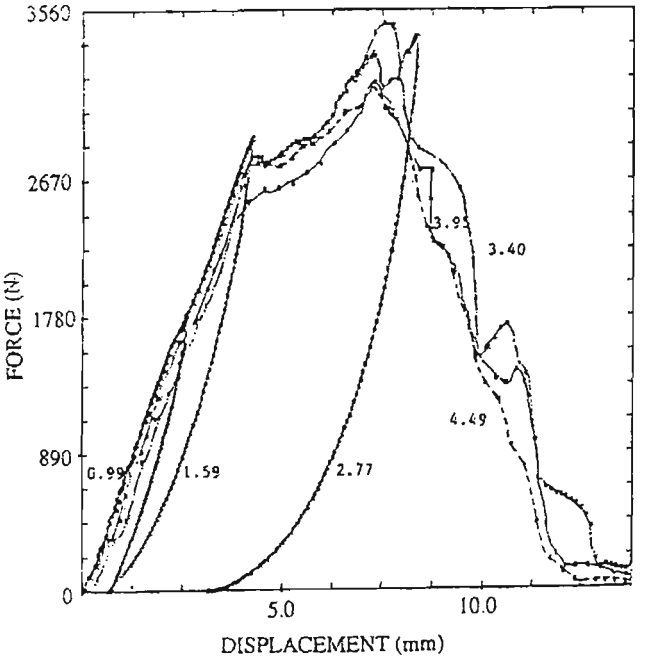

Figure 2-3: Force-displacement relations for laminates subjected to various impact velocities (after Dang and Liu : 1998)

The results of the testing and simulation show that as the laminate thickness increases the stiffness and strength increases causing a subsequent increase in peak contact force and decrease of contact duration, maximum deflection and energy absorption. Fibre angle does not play a significant role in impact response. The contact duration and peak contact force decreases once penetration takes place while the maximum deflection remains relatively constant as the impact velocity increases. Increase in impact velocity does not affect energy absorption, though there is a significant jump in energy absorption due to penetration.

According to Dharani and Flocker (1998), while standard finite element wave propagation codes are useful for easy determination of stresses caused by impact loading, it is difficult to model the important interlayer delamination process. Thus, their paper presents a method that allows traditional wave propagation codes to model this interlayer debonding of laminated architectural glass subjected to low velocity impact. While the application presented in the paper is specific to architectural glass, the author believes it contains inherent generic conclusions that will assist in this investigation. One such conclusion is that limited debonding results in a more compliant structure that can absorb more energy. Further, when glass is impacted by a spherical projectile, the cone crack is of primary concern and the stress of concern is the maximum principle stress on the inner surfaces directly beneath the impact site. A typical cone crack with cone angle ϕ formed in a brittle material after an impact from a spherical projectile is shown in Figure 2-4a while Figure 2-4b illustrates a cone crack formed in the outside layer of a laminated architectural glass unit. This is significant because if a ceramic piezoelectric material is used on the surface of the smart material in the current investigation, the formation of a cone crack can interrupt the piezoelectric effect and nullify the intended results.

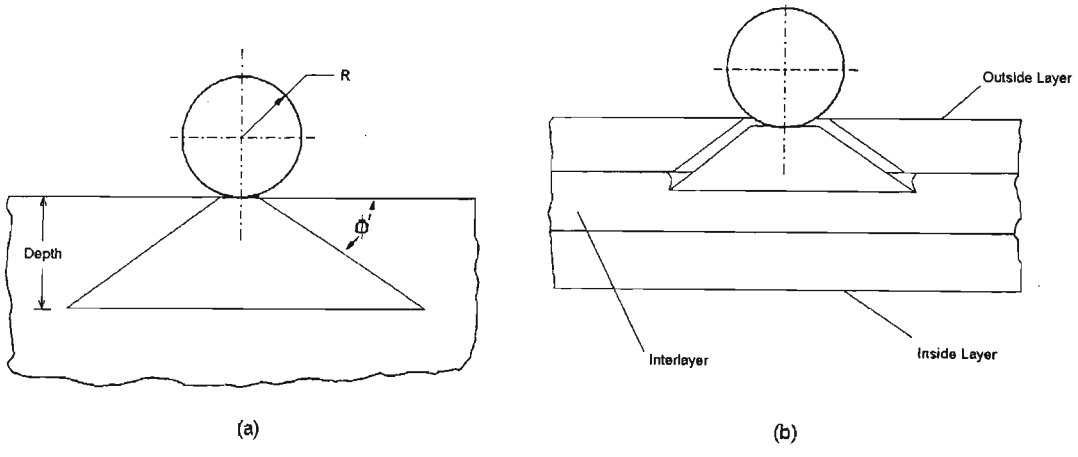

Figure 2-4: Cone crack in an infinite half-space and a laminated glass unit

(after Dharani et. al. : 1998)

A propagating cone crack is modelled in a finite element mesh by setting deviatoric stresses and hydrostatic tension to zero at the appropriate time and location. Thus, a cracked element will not support shear or tension but will support compression. The interface debonding model is based on the primary assumption that debonding is a propagating phenomenon that starts and then progresses away from the point where a crack meets an interface layer. Analysis of interface debonding (mechanics of peel adhesion) show that at high peel angles tensile forces dominate at the point of debonding, while at low peel angles shear forces dominate (Dharani et. al. : 1998). Similar to cracking, debonding is modelled by relaxing the element stresses by setting deviators and hydrostatic tension to zero. Again, the debonded region cannot support shear or tension but can support compression. It is assumed that the tensile and shear forces required to cause debonding are related, i.e. less shear is required to debond a strip of adhesive from a substrate if a tensile force exists between the two. The relationship between these stresses is obtained through peel tests as illustrated in Figure 2-5.

A strip of adhesive with a flexible backing is applied to a rigid substrate. A peel force P is applied to the flexible backing at peel angle ω. The force required to strip the adhesive from the backing is then measured. This is repeated for various peel angles.

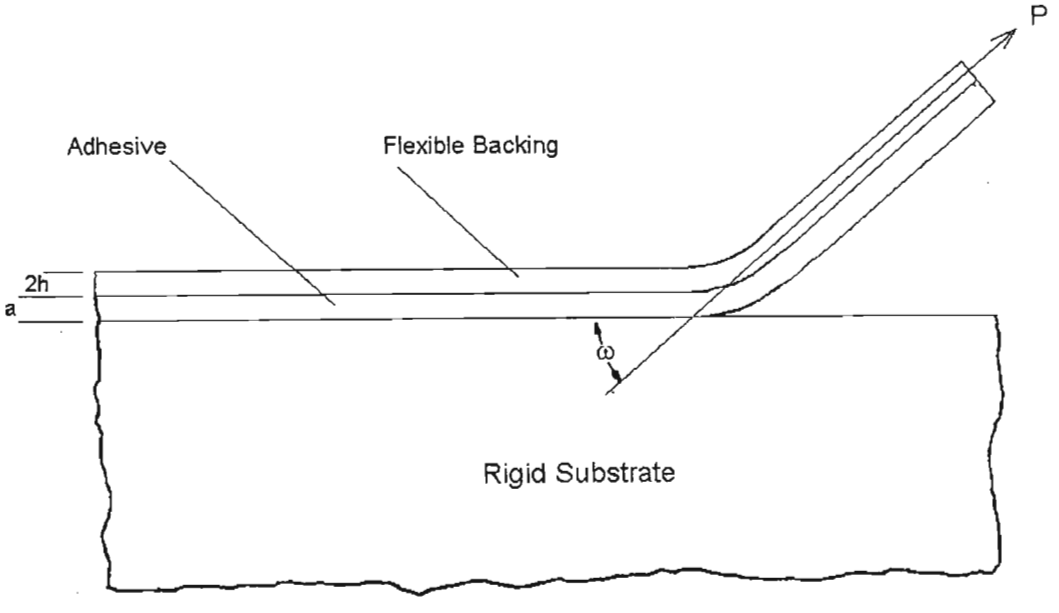

Figure 2-5: Illustration of the plane strain peel test

(after Dharani et. al. : 1998)

If the tensile and shear stresses at the debonding interface are denoted by σ_o and τ_o respectively, then

$$\sigma_o = 2\beta P(\beta m_c + \sin\omega)$$

$$\tau_o = \alpha P \cos\omega$$

Where the terms α, β and m_c are given by

$$\beta = \left(\frac{3Y}{8Eah^3}\right)^{1/4}$$

$$\alpha = \left(\frac{G}{2Eah}\right)^{1/2}$$

$$m_c = \left(\frac{4Eh^3(1-\cos\omega)}{3P}\right)^{1/2} - h\cos\omega$$

Where G and Y are the shear and Young's moduli respectively for the adhesive, E is the Young's modulus of the backing, a is the adhesive thickness and $2h$ is the flexible backing thickness.
If a linear relation exists between the tensile and shear debonding stresses then,

$$\sigma_{cul} \approx \left(\frac{2YP_{90}}{a}\right)^{1/2}$$

and

$$\tau_{cul} \approx P_o\left(\frac{G}{2Eah}\right)^{1/2}$$

Where σ_{cul} denotes the debonding tensile stress when no shear is present and τ_{cul} denotes the debonding shear stress when no tensile stress exists. P_{90} is the debonding force at 90° peel angle and P_o is the debonding force at very low peel angle.

For the finite element code Dharani et. al. (1998) uses a non-reflecting boundary for the clamped sides of the specimen to simulate an infinite body. This is achieved by producing an impedance matching function that cancels incoming stress waves so that none are reflected back from the boundary.

The main energy absorption mechanism for normal composite materials is fragmentation. Matrix failures can occur by tension and compression and fibres failure by tension. Belingardi, Gugliotta and Vadori (1998) compares the results obtained by applying a computational methodology, based on the finite element technique, with experimental results of composite material plates subjected to impact loading. The DYNA-3D finite element code is used for the numerical modelling. A composite material comprising a stack of laminae of unidirectionally reinforced matrices is considered along with the assumption that the material behaves linearly until, under certain load, brittle fracture occurs. Due to the brittle behaviour of such composites, the mechanism of energy dissipation is fracture, i.e. fragmentation of material, fibre breakage and / or matrix breakage. A polynomial expression for the definition of the critical material surface in the stress space is adopted as all the coefficients are easily determined from pure tension or pure shear tests, as opposed to a piecewise continuous surface model to take into account different modes of failure. The model also incorporates the ply-discount approach for failure where some of the load carrying capabilities of the single lamina are lost when fibres or matrix break down. This means that the load carrying capability of the stack of laminae is globally reduced and when all the laminae are broken the material is completely degraded to no mechanical characteristics.

The Young's moduli and Poisson's ratio are obtained from laboratory tests and then used to derive the Lamé constants λ, α_1, β_1, μ and μ_1. These constants are used to calculate the Cauchy stress components from the following equation:

$$\begin{bmatrix} T_{11} \\ T_{22} \\ T_{33} \\ T_{12} \\ T_{23} \\ T_{31} \end{bmatrix} = \begin{bmatrix} \lambda + 2\alpha_1 + \beta_1 + 2\mu + 4\mu_1 & \lambda + \alpha_1 & \lambda + \alpha_1 & 0 & 0 & 0 \\ \lambda + \alpha_1 & \lambda + 2\mu & \lambda & 0 & 0 & 0 \\ \lambda + \alpha_1 & \lambda & \lambda + 2\mu & 0 & 0 & 0 \\ 0 & 0 & 0 & 2(\mu + \mu_1) & 0 & 0 \\ 0 & 0 & 0 & 0 & 2\mu & 0 \\ 0 & 0 & 0 & 0 & 0 & 2(\mu + \mu_1) \end{bmatrix} \begin{bmatrix} E_{11} \\ E_{22} \\ E_{33} \\ E_{12} \\ E_{23} \\ E_{31} \end{bmatrix}$$

Where T_{ij} are the Cauchy stress components and E_{ij} are the Euler-Almansi strain components.

A plane stress state is assumed resulting in T_{23}, T_{31}, T_{33}, E_{23} and E_{31} reducing to zero. Thus, the constitutive law for a single lamina with a single set of unidirectional fibres is defined. The polynomial expression for the critical surface is modified to a piecewise continuous surface in the stress space with failure occurring when one of the stress components satisfies the following conditions:

Fibre mode – Tension

$$\left(\frac{T_{11}}{X_t}\right)^2 + \beta\tau\left(\frac{T_{12}}{S_c}\right)^2 = 1 \quad ; \qquad T_{11} \rangle 0$$

Fibre mode – Compression

$$\left(\frac{T_{11}}{X_c}\right)^2 = 1 \quad ; \qquad T_{11} \leq 0$$

Matrix mode – Cracking

$$\left(\frac{T_{22}}{Y_t}\right)^2 + \tau\left(\frac{T_{12}}{S_c}\right)^2 = 1 \quad ; \qquad T_{22} \geq 0$$

Matrix mode – Crushing

$$\frac{1}{Y_c}\left[\left(\frac{Y_c}{2S_c}\right)^2 - 1\right]T_{22} + \left(\frac{T_{22}}{2S_c}\right)^2 + \tau\left(\frac{T_{12}}{S_c}\right)^2 = 1 \quad ; \qquad T_{22} \leq 0$$

where X_t, X_c, Y_t, Y_c are respectively the tension and compression strength along and perpendicular to the fibre direction while S_c is the shear strength of a single lamina in the 1-2 plane. β is a factor that reduces the too high sensitivity of the fibre breakage collapse mode to the shear effect and τ takes into account the nonlinear effect of the shear stress on the failure surface.

A critical remark made by Belingardi et. al. (1998) is that in tension along the fibre direction, when some mechanical characteristics of a lamina are degraded, dependency between strain and stress ceases to exist; the stress law is imposed in the time domain regardless of the strain state. When the critical surfaces are reached and fibre breakage occurs, the stress state is

$$T_{11} = 0 \quad ; \qquad T_{12} = 0$$

and must hold for every strain state.

For determination of the energy dissipation during the damage phase of the material a co-rotational formulation is used.

$$\left(\frac{dW_{\text{int}}}{dt}\right)_{undamaged} = \int_{\Omega} D_{ij} C_{ijrs} E_{rs} d\Omega$$

where $\left(\frac{dW_{\text{int}}}{dt}\right)_{undamaged}$ is the stored internal energy in an undamaged material, D_{ij} are the components of the velocity strain and C_{ijrs} are the components of the fourth order constitutive tensor.

When the material is subjected to degradation, the stored internal energy is,

$$\left(\frac{dW_{\text{int}}}{dt}\right)_{damaged} = \int_{\Omega} D_{ij} C^{*}_{ijrs} E_{rs} d\Omega$$

Thus, the energy dissipation during the damage phase of the material is

$$\left(\frac{dW_{\text{int}}}{dt}\right)_{undamaged} - \left(\frac{dW_{\text{int}}}{dt}\right)_{damaged} = \int_{\Omega} D_{ij}\left(C_{ijrs} - C^{*}_{ijrs}\right) E_{rs} d\Omega$$

Belingardi et. al. (1998) proceed to present a good case study that has the ability to be used to test an initial model generated for the current investigation, in a general sense.

The issue of impact energy absorption of polymer composite sandwich beams is investigated using a beam in three point bending with roller supports by Mines (1998). The beam was constructed using woven glass, aramid and carbon polyester resin skins with Coremat or foam cores by applying the wet layup technique. Coremat is a proprietary material that consists of a non-woven polyester felt with 50 % micro-spheres. The core is impregnated with resin during the wet layup lamination process resulting in a solid material with isolated pores. Mines (1998) defines the structural behaviour of sandwich structures under impact response to include matrix damage, fibre pullout and failure, delamination and core multiaxial crushing. In the case of the three point bend beam, there are eight possible modes of structural failure depending on material and structural configuration. These failure modes include upper skin compression failure, core shear failure, lower skin tensile failure and upper skin wrinkling. The best mode of failure for energy absorption is upper skin failure and subsequent stable core crushing. The upper skin failure is modelled using standard linear elastic theory and the compression failure stress of the upper skin and the core crushing failure is modelled using a limit analysis assuming global beam deformation in the central plastic hinge. The energy absorption is taken to be the area under the force-displacement graph.

The basic modelling process can be summarised as follows. The upper skin failure is determined using the compression failure stress. The upper skin is then neglected from further computations and stable crushing of the core is assumed. For a given core upper surface strain the position of the neutral axis is calculated using force equilibrium conditions across the central beam section. The beam force and moment distribution is then derived. The force is fed into an empirical multiaxial core crush criterion as a shear stress and the neutral axis is recalculated. The compression stresses due to contact load are neglected due to the high crush strength of the Coremat core. The new

neutral axis gives a revised moment and force that is used to predict the beam deflection for the given core upper surface strain.

Static loading analysis showed good correlation between experiment and theoretical results post upper skin failure. No results of the upper skin failure (theoretical) using compression failure load is given to compare with the experimental results, and impact loading analysis is restricted to low velocity, dropped object problems where the impact resistance of a material is determined largely by its strain rate properties. Force-time results are obtained from accelerometer readings and then the displacement of the impact mass is determined from its acceleration.

The results obtained by Mines (1998) reveal that for the short span beam, the upper skin dynamic failure load is larger than the static load failure as well as that theoretically predicted. The theoretical core crush model (elastic-plastic model with central hinge) also under predicts the experimental forces by approximately 50 %. Further, the theoretical strain-rate dependent model shows little difference to the theoretical strain-rate independent model. For the larger span beam tests the upper skin dynamic failure load is less than that of the static loading conditions. The dynamics of these tests, however, are different as the beam bounces away from the impactor. Comparing these results to those obtained by Harding et. al. (1998) for laminated composites, the obvious difference lies in the damage initiation and propagation in the composite. While the fibre reinforced composite failure initiated in the bottom of the beam and propagated upward, the failure in the sandwich panels is initiated in the upper skin of the beam. The fibre reinforced polymer composite also experienced higher loads and lower displacements than the sandwich panel, though this can be attributed to the lower strength and higher ductility respectively, of the core material of the sandwich structure.

The remainder of the investigation (Mines : 1998) briefly discusses quality of beam manufacture, variation of hinge size with beam span, multiaxial crush criteria for core materials, effects of moving the position of the impact, of using clamped boundary conditions and having beam in-plane loads, effect of low density core materials, effects of geometry and velocity of impactor, other modes of beam failure, beam specific energy absorption and effects of skin reinforcement orientation and type of resin.

The investigation by Charles, Collembet, Jeronimidis, Lalbin and Lataillade (1997) presents a methodology for numerically taking into account the physics of damage events during impact of composite structures. They propose that numerical calculations must be combined with experimental data to account for the three dimensional, multiscaled and coupled characteristics of damage phenomena. Charles et. al. (1997) analysed the impact of circular long fibre glass-epoxy

$0°/90°$ symmetrical laminated plates using a hemispherical impactor of mass 2.3 kg and velocities less than 6 m/s. Only local damage events are observed in transverse matrix cracking and delamination.

Numerically, the time step is linked to the smallest dimension of the mesh to yield a condition of stability in time integration. An averaging technique developed on the scale of a finite element is used to model matrix cracking, i.e. the effect of cracks in the matrix is quantified by calculating elastic characteristics of a homogenised undamaged material equivalent to the initial material containing cracks. Maximum stress criteria are used to initiate numerical cracking and its effects. An extension criterion is added to take into account the stress concentration at the tip of the cracks. Delamination is modelled by assembling the different layers of the structure with double nodes. When the link force (force at the double nodes) in a specific direction exceeds a critical value, separation of the double nodes is effected. This is essentially a contact technique based on Lagrange multipliers and differs from the classical fracture mechanics energy based approach. Collembet, Lalbin and Lataillade (1997) give the conditions for the separation of a double node. At a given interface a double node is numerically authorised to separate if, for the lower layer all adjacent finite elements are cracked and, for the upper layer one adjacent finite element is cracked or one adjacent double node is already separated, as indicated in the example of Figure 2-6.

For the numerical model to be an adequate representation of real life events, physical considerations based on experimental observations need to be integrated with the numerical condition. Thus, a damage chronology based on experimental observations has to be postulated together with critical initiating factors. Crack extension is numerically modelled as equivalent to the creation of a new crack in an element adjacent to a cracked one with the critical extension stress lower in the element receiving the crack than the critical initiation stress in the element originating the crack. The contact projectile/target is simplified as a node and the projectile is represented as a weighted point with initial velocity.

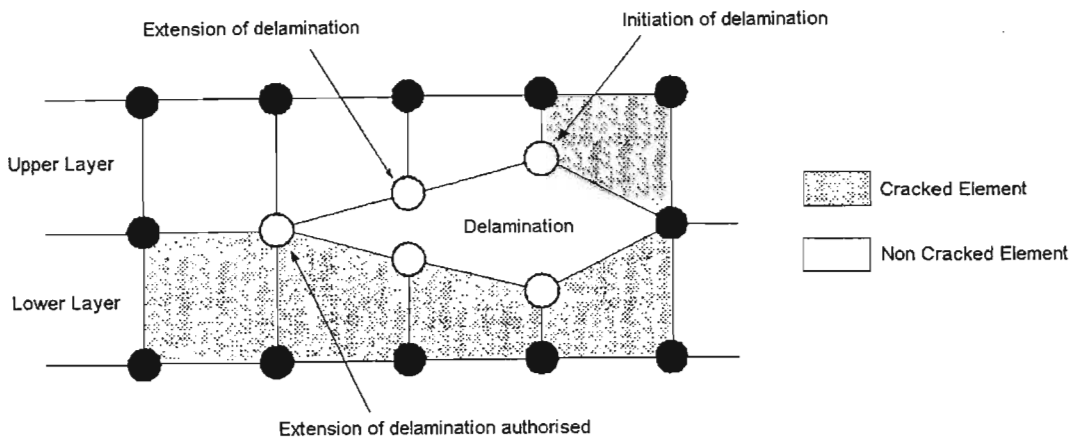

Figure 2-6: Two dimensional representation of delamination conditions between two layers with double nodes (after Collombet et. al. : (1997)

Expanding the issue of crack growth further, Needleman (1997) describes a framework for modelling crack growth based on introducing one or more cohesive surfaces into a continuum. In the traditional approach to fracture mechanics a parameter characterising the crack tip field, e.g. the energy release rate, is assumed to be a material property and is distinguished from stress analysis. Thus, incorporating a model of the fracture process into the initial/boundary value problem formulation provides an alternative approach. Needleman (1997) has chosen for discussion a framework where the failure characteristics are embedded in a phenomenological constitutive relation that describes separation along one or more cohesive surfaces. Within the framework, the continuum is characterised by two constitutive relations; one relates the stress and deformation in the bulk material and the other relates the tension and displacement jump across a cohesive surface. A mathematical analysis is presented using volumetric and cohesive surface internal virtual work with Lagrangian description. The author believes that this is too in-depth modelling for the purposes of the current investigation and is inclined to combine this methodology with that of Charles et. al. (1997) for the numerical scenario.

Lewis (1998) presents a methodology for predicting and modelling material failure in solids subjected to impact loading using classical void growth models in a material point method. However, the author is of the opinion that this is too in-depth an analysis for the modelling requirements of the current investigation. Chandra and Rajendran (1998) present a review of micromechanical and engineering modelling of polymeric matrix composites under high velocity impact. While high velocity impact is outside the scope of the current investigation this paper

describes alternative views to matrix microcracking that the author believes is important. The first view is that when microcracks form in an undamaged composite, the stresses change with all stress components becoming non zero, in general, and that microcracking initiates when the stress in the 90° plies becomes equal to the transverse strength of the unidirectional material. The alternative is that the first microcrack forms when the energy released due to the formation of that microcrack exceeds some critical value, known as the microcracking toughness of the composite material system. According to Chandra et. al. (1998), this energy prediction captures most features of experimental observations and appears to be a significant improvement over strength theories. Also presented in this paper is a useful figure showing the various energy dissipation mechanisms active during an impact event and is used as Figure 2-7 in this thesis to bring to an end the review on impact loading.

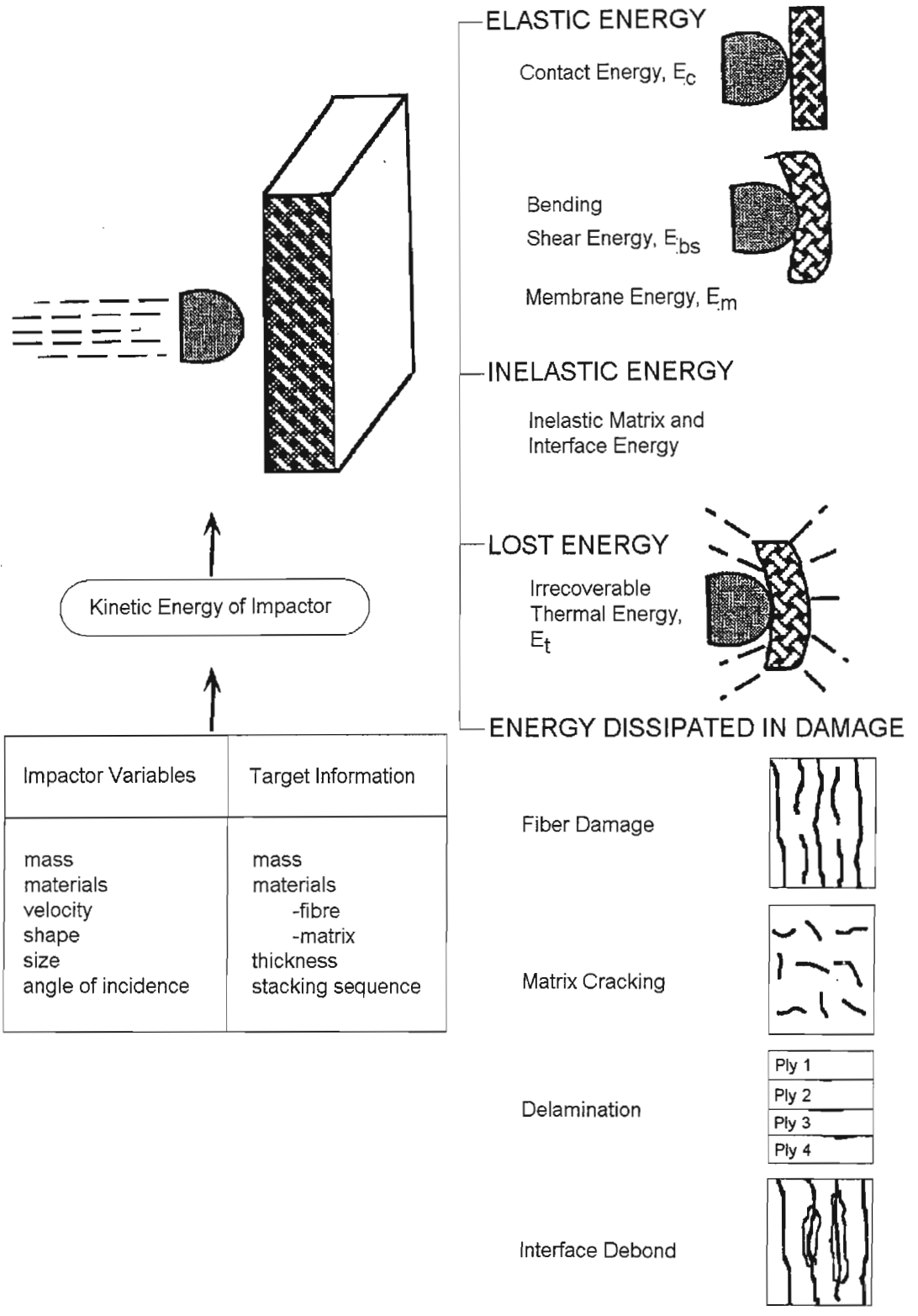

Figure 2-7: Schematic of an energy balance approach in an impact event

(after Chandra et. al. : 1998)

2.2 Shape Memory Materials

The novel performances of shape memory materials include high damping capacity, large recoverable strain and recovery stress and property changes due to thermal or stress induced microstructural transformations. When the material has been transformed to the martensitic phase, it can be subjected to significant plastic deformation under relatively modest load since the yield limit of the material in the martensitic phase is much lower than its counterpart in the austenitic phase. The martensitic transformation represents a diffusionless lattice transformation involving shearing deformations (Funakubo : 1987). Martensitic transformations can involve slip and twinning, but for this transformation to be reversible, deformation by slip should not be involved in the process (Birman : 1997). The term SIM (stress-induced martensite) identifies martensite obtained as a result of mechanical loading. The yield stress of SMA varies greatly dependent on the phase and according to Funakubo (1987) can be an almost linear function of temperature. Table 2-2 illustrates an example of the differences in material properties of the austenitic and martensitic phases.

Table 2-2: Properties of nitinol Ni-44.8wt % Ti

(after Birman : 1997)

Phase	Austenite	Martensite
Modulus of elasticity (GPa)	30.0	13.0
Poisson's ratio	0.33	0.33
Coefficient of thermal expansion (10^{-6}/°C)	12.5	18.5
Start temperature (°C)	29	23
Finish temperature (°C)	51	5

Most analytical constitutive models of SMA rely on a linear relationship between martensitic and austenitic properties with the proportionality coefficient associated with the martensitic fraction, though this should be used with caution, as it still needs to be experimentally verified. To add complexity to the model, stress-strain curves within the range $M_F < T < A_F$ are affected by the formation of stress-induced martensite causing the martensitic fraction to continuously change as a result of increasing or decreasing stress. At the same time, the change of the martensitic fraction is accompanied by changes in the properties of the material. When $T > A_F$ the material is in the

stress-free state and the martensite formed as a result of increasing stress represents a superelastic behaviour (Birman : 1997).

Although the first attempts to mathematically describe the behaviour of shape memory materials are traced back to the 1970s (Birman : 1997), only the more recent contributions are reviewed in this thesis. The Tanaka model (Nagaki and Tanaka : 1982) was originally developed to describe a three dimensional solid but its practical implementation was limited to the one dimensional case. The model has since been described in a number of papers (Tanaka : 1986; Tanaka : 1990; Tanaka : 1991) and is based on the energy balance equation and the Clausius-Duhem inequality. The constitutive equations relate the rate of change of the second Piola-Kirchoff tensor of stresses to those of the Green's strain tensor, temperature and the set of scalar variables, which characterises the extent of a phase transition. In the case of martensitic transformations the scalar variables are reduced to just one parameter, i.e. the martensitic fraction. The coefficients in the tensor constitutive equation are the tensors of elastic and thermoelastic moduli and the material (transformation) tensor that, in general, depends on strain, temperature and martensitic fraction. The elements of the tensors of elastic and thermoelastic moduli are considered linear functions of the martensitic fraction with the other state variables being expressed as a function of the rate of change of martensitic fraction. For the one dimensional model the elastic and thermoelastic moduli are assumed constant. Also, the martensitic fraction in the process of martensitic and reverse transformations is expressed in terms of exponential functions of temperature and stress.

The Liang and Rogers (1990) one dimensional model is derived by modifying the Tanaka model by replacing the finite form exponential transformation kinetics equation with a cosine law. The three dimensional model (Liang and Rogers : 1991) is developed based on the first and second laws of thermodynamics and the concept of the Helmholtz free energy. The theory utilises experimental results that illustrate that the phase transformations are governed by the distortional energy. Thus, the general state variables are defined in terms of just three parameters, viz. the equivalent strain, absolute temperature and martensitic fraction.

The Brinson one dimensional model (Brinson : 1993; Brinson and Lammering : 1993) utilises the rate constitutive equation of Tanaka as well as elements of the Liang and Rogers model. Brinson introduces the sub-division of the martensitic fraction into two components corresponding to the temperature induced and stress induced martensites. Two constitutive relations are considered. The first is based on the assumption that material parameters remain constant and results in a law similar to that in the Tanaka and Liang and Rogers models. The second relation is based on isothermal stress-strain curves and yields the conclusion that only the thermoelastic term associated with the stress-induced martensite has to be retained in the constitutive equation. This form of

constitutive equation is obtained without the assumption of constant material parameters, i.e. the elastic modulus is assumed to be a linear function of the martensitic fraction, the material constant is proportional to the elastic modulus corresponding to the current value of martensitic fraction and the thermoelastic modulus is assumed constant.

The three dimensional model of Boyd and Lagoudas (Birman : 1997) is a modification of the constitutive theories of Liang and Rogers and Tanaka, i.e. the constant material tensor assumption during the transformation process is removed, and the elastic and thermoelastic tensors are calculated in terms of the martensitic fraction according to the rule of mixtures.

The model of Abeyaratne, Knowles and Kim (Birman : 1997) is applicable to one dimensional thermoelastic solids with a tri-linear stress-strain curve. For each temperature, this curve consists of three straight sections corresponding to an initial increase of the stress as the strain increases from zero, a decline to a local minimum and a subsequent increase. Accordingly, even though the stress in a thermoelastic bar remains constant, the strain may be a piecewise function of the local temperature. This one dimensional model accounts for thermo-mechanical coupling and satisfies the Clausius-Clapeyron inequality.

Attempts to incorporate shape memory actuators in composite structures to improve their impact tolerance have been conducted by Paine and Rogers (1994a; 1994b) and Birman et. al. (1996a; 1996b) and have already been discussed in Chapter 1.

In terms of micromechanics modelling of smart composites, Taya (1999) discusses a summary of analytical modelling as applied to piezoelectric composites, shape memory alloy fibre composites and piezoresistive composites and presents models that take into account coupled behaviour between stress, electric field and magnetic field. Table 2-3 summarises various types of coupled behaviour between mechanical, thermal and electromagnetic phenomena. The first five rows denote linear coupling behaviour while the last four are for nonlinear or non-colinear coupling behaviour.

Table 2-3: Coupling behaviour

(after Taya : 1999)

Coupled Behaviour	Flux Vector/Field Vector	Field Vector or Scalar	Coupling Coefficient
Piezoelectric	Stress	Electric field	e
Thermoelastic	Strain	Temperature change	a
Pyroelectric	Electric displacement	Temperature change	p
Piezomagnetic	Stress	Magnetic field	a
Magnetoelectric	Electric displacement	Magnetic field	x
Magnetostrictive	Strain	Magnetisation	Nonlinear
Electrostrictive	Strain	Electric field	Nonlinear
Piezoresistivity	Electric current density	Electric field	s (nonlinear in strain)
Shape-memory effect	Stress, Strain	Temperature change	Nonlinear

The constitutive equation for materials with linear coupling behaviour include the flux vector $\overline{\Sigma}$, field vector $\overline{Z}$ and thermal coupling vector $\overline{\pi}$, in the form of,

$$\overline{\Sigma} = \overline{E}.\overline{Z} + \overline{\pi}\theta$$

where $\overline{E}$ is the coupling coefficient and θ the temperature scalar.

The flux, field and thermal coupling vectors can be expanded to the form,

$$\overline{\Sigma} = \begin{bmatrix} \overline{T} \\ (6x1) \\ \overline{D} \\ (3x1) \\ \overline{B} \\ (3x1) \end{bmatrix}, \qquad \overline{Z} = \begin{bmatrix} \overline{S} \\ (6x1) \\ -\overline{E} \\ (3x1) \\ -\overline{H} \\ (3x1) \end{bmatrix}, \qquad \overline{\pi} = \begin{bmatrix} \overline{\lambda} \\ (6x1) \\ \overline{P} \\ (3x1) \\ \overline{0} \\ (3x1) \end{bmatrix}$$

where $\overline{T}$, $\overline{D}$ and $\overline{B}$ are the flux vectors of stress, electric displacement and magnetic flux respectively; $\overline{S}$, $\overline{E}$ and $\overline{H}$ are the field vectors of strain, electric field and magnetic field respectively; and $\overline{\lambda}$ and $\overline{P}$ are the thermal stress vector, and pyroelectric vector respectively.

The constitutive equation is then inverted to yield

$$\overline{Z} = \overline{F}.\overline{\Sigma} + \overline{\Lambda}.\theta$$

where $\overline{F}$ is the compliance property tensor and $\overline{\Lambda}$ the compliance thermal vector.

Thus, $\overline{E}.\overline{F} = \overline{I}$ *and* $\overline{E}.\overline{\Lambda} + \overline{\pi} = \overline{0}$.

Consider an arbitrary composite that contains numerous fillers made of smart material with linear coupling behaviour. The composite is subjected to an applied field vector on the boundary, $\overline{Z}_o$, where the temperature is assumed constant (Figure 2-8a).

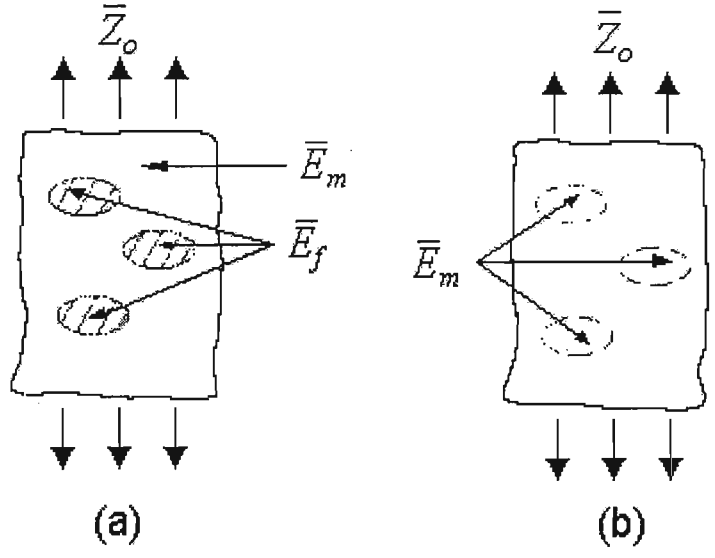

Figure 2-8 : Linear coupled composite with smart material fillers

(after Taya : 1999)

If the volume average of the flux and field vectors in each phase are used to define the flux and field of the composite, then

$$\overline{\Sigma}_c = \left(1 - v_f\right)\overline{\Sigma}_m + v_f\overline{\Sigma}_f$$

where v is the volume fraction and the subscripts c, m and f refer to the composite, matrix and fibre respectively.

Applying the constitutive equation results in (constant temperature)

$$\overline{\Sigma}_i = \overline{E}_i.\overline{Z}_i$$

where $i = c$, m and f.

The averaged field vector in the composite, $\overline{Z}_c$, is equal to the applied field since the disturbance field, $\overline{Z}$, vanishes after integration over the entire composite, i.e.

$$\overline{Z}_c = \overline{Z}_o$$

Thus,

$$\overline{E}_c = \overline{E}_m + v_f\left(\overline{E}_f - \overline{E}_m\right).\overline{A}$$

where $\overline{A}$ is the constraint tensor relating the average field in the filler domain to the applied field, i.e.

$$\overline{Z}_f = \overline{A}\overline{Z}_c = \overline{A}\overline{Z}_o$$

$\overline{A}$ is obtained using Eshelby's model which is given by (Taya : 1999)

$$\overline{\Sigma}_o + \overline{\Sigma} = \overline{E}_f.\left(\overline{Z}_o + \overline{Z}\right) = \overline{E}_m.\left(\overline{Z}_o + \overline{Z} - \overline{Z}^*\right)$$

where $\overline{\Sigma}$ and $\overline{Z}$ are the disturbance of flux and field vectors owing to the existence of fillers and $\overline{Z}^*$ is the equivalent inclusion eigenfield vector replacing the filler (Figure 2-8b).

The uniform flux and field vectors are related by

$$\overline{\Sigma}_o = \overline{E}_m.\overline{Z}_o$$

The disturbance field vector $\overline{Z}$ is linearly related to the eigenfield vector $\overline{Z}^*$ by the Eshelby tensor, $\overline{S}$, for the coupling problem.

$$\overline{Z} = \overline{S}.\overline{Z}^*$$

The Eshelby tensor is a function of the constituent properties and shape of an ellipsoid inclusion since the components of the flux and field vectors of the filler then become uniform. An average Eshelby tensor for non-ellipsoid fillers is defined by Taya (1999).

In terms of nonlinear coupling, Eshelby's model can be used to adequately determine the macroscopic stresses in a composite with SMA fibres. The compressive stress in the matrix at a temperature above the austenite finish temperature, A_f, can be computed using Eshelby's model for elasto-plastic deformation (Taya : 1999).

The stress in the fibre is given by

$$\bar{\sigma}_f = \bar{C}_f.\left(\bar{e} - \bar{e}_T - \bar{e}_p\right) = \bar{C}_m.\left(\bar{e} - \bar{e}^*\right)$$

where $\bar{C}$ is the stiffness tensor, $\bar{e}$ is the strain disturbance, $\bar{e}_T$ is the transformation strain, $\bar{e}_p$ is the plastic strain and $\bar{e}^*$ is the eigenstrain which has a non-zero value in the fibre domain and vanishes in the matrix.

The various strains are given by

$$\bar{e}_T = \left(\upsilon_f \varepsilon_T, \upsilon_f \varepsilon_T, -\varepsilon_T, 0, 0, 0\right)$$

$$\bar{e}_p = \left(-\tfrac{1}{2} e_p, -\tfrac{1}{2} e_p, e_p, 0, 0, 0\right)$$

$$\bar{e} = \bar{S}.\bar{e}^*$$

where υ is the Poisson's ratio, ε_T is the prestrain given to the fibre at room temperature, e_p is the plastic strain of the fibre axis and $\bar{S}$ is Eshelby's tensor.

The above three equations are used to solve for $\bar{e}^*$ as

$$\bar{e}^* = \left[\left(\bar{C}_f - \bar{C}_m\right).\bar{S} + \bar{C}_m\right]^{-1}.\bar{C}_f.\bar{e}_p$$

where the superscript '-1' denotes the inverse of a matrix.

The plastic strain in the fibre, $\bar{e}_p$, is obtained by satisfying the yield condition for the fibre,

$$\left(\sigma_f\right)_{33} - \left(\sigma_f\right)_{11} = \sigma_{yf}$$

where σ_{yf} is the yield stress of the fibre and the numerical subscripts denote the general fibre directions.

Taya (1999) also presents a useful model on piezoresistive materials, but this is left for discussion in the review on piezoelectric materials.

An alternative model is given by Sittner, Takakura, Tokuda and Ye (1998) where a two dimensional mechanical model of polycrystalline SMA based on crystal plasticity and the deformation mechanism of SMA, is described in an attempt to calculate the deformation behaviours of SMA under multiaxial loading conditions. According to Sittner et. al. (1998), the majority of models proposed to describe the thermo-mechanical behaviours of SMA are based on thermodynamics and kinetics whereas all of the SMA in practical applications are polycrystal.

Every grain in the polycrystalline medium has its own orientation with twenty-four potential variants determined by the crystallographic structure of the material. The stress is a symmetric second rank tensor whose number of independent variables is six, though the temperature is a scalar parameter (single variable). According to the loading conditions (magnitude and direction) only in such potential variants that are in the preferred directions in the grains of the polycrystal will the transformation be induced. The relation between stress, τ and the transformation strain γ_T in the process of stress induced martensite transformation and its reverse transformation is shown in Figure 2-9. T is the experimental temperature and $\tau_{MS}(T)$, $\tau_{MF}(T)$, $\tau_{AS}(T)$ and $\tau_{AF}(T)$ are the martensite transformation starting and finishing stresses (critical stress) and the austenite transformation starting and finishing stresses (critical stress) under temperature T respectively. $\gamma_{T\,max}$ is the maximum transformation strain determined by the materials crystallographic structure.

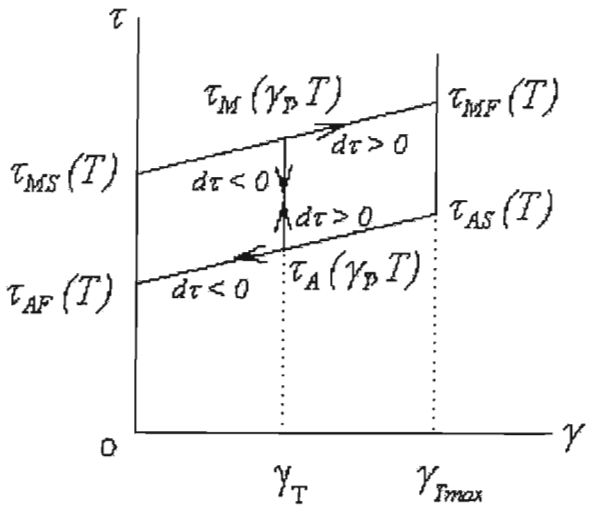

Figure 2-9 : Relation between shear stress and transformation strain in the martensite variant (modified after Sittner et. al. : 1998)

The stress-strain relation in the stress-induced martensite transformation and its reverse austenite transformation can be expressed by the following equations.

$$\tau_M(\gamma_T, T) = \tau_{MS}(T) + H\gamma_T$$

$$\tau_A(\gamma_T, T) = \tau_{AF}(T) + H\gamma_T$$

where H is the hardening coefficient.

Sittner et. al. (1998) assumes a linear relation between the critical stresses $\tau_{MS}(T)$ and $\tau_{AF}(T)$ and temperature, i.e.

$$\tau_{MS}(T) = \tau_{MS_o} + \beta(T - T_o)$$

$$\tau_{AF}(T) = \tau_{AF_o} + \beta(T - T_o)$$

where β is the temperature coefficient and τ_{MS_o} and τ_{AF_o} are the transformation critical stresses under reference temperature T_o.

Thus, all the critical stresses can be obtained by the following expressions,

$$\tau_{MF} = \tau_{MS}(T) + H\gamma_{T\max}$$

$$\tau_{AS} = \tau_{AF}(T) + H\gamma_{T\max}$$

$$\tau_{MF_o} = \tau_{MS_o} + H\gamma_{T\max}$$

$$\tau_{AS_o} = \tau_{AF_o} + H\gamma_{T\max}$$

Taking the differential of the constitutive equation yields

$$d\tau_M(\gamma_T, T) = \beta dT + H d\gamma_T$$
$$d\tau_A(\gamma_T, T) = \beta dT + H d\gamma_T$$

where $d\tau$ is the increment in shear stress, dT is the increment in temperature and $d\gamma_T$ is the increment in transformation strain.

Thus, in the loading ($d\tau > 0$) and unloading ($d\tau < 0$) process under constant temperature ($dT = 0$),

$$d\tau > 0 \ \text{and} \ \tau < \tau_M(\gamma_T, T) : d\gamma_T = 0$$

$$d\tau > 0 \ \text{and} \ \tau = \tau_M(\gamma_T, T) \ \text{and} \ \gamma_T < \gamma_{T\max} : d\gamma_T = \frac{d\tau}{H}$$

$$d\tau > 0 \ \text{and} \ \gamma_T = \gamma_{T\max} : d\gamma_T = 0$$

$$d\tau < 0 \ \text{and} \ \tau > \tau_A(\gamma_T, T) : d\gamma_T = 0$$

$$d\tau < 0 \ \text{and} \ \tau = \tau_A(\gamma_T, T) \ \text{and} \ \gamma_T > 0 : d\gamma_T = \frac{d\tau}{H}$$

$$d\tau < 0 \ \text{and} \ \gamma_T = 0 : d\gamma_T = 0$$

In the temperature cycles under a constant stress ($d\tau = 0$),

$$dT > 0 \ and \ \tau > \tau_A(\gamma_T, T) : d\gamma_T = 0$$

$$dT > 0 \ and \ \tau = \tau_A(\gamma_T, T) \ and \ \gamma_T > 0 : d\gamma_T = -\frac{\beta}{H} dT$$

$$dT > 0 \ and \ \gamma_T = 0 : d\gamma_T = 0$$

$$dT < 0 \ and \ \tau < \tau_M(\gamma_T, T) : d\gamma_T = 0$$

$$dT < 0 \ and \ \tau = \tau_M(\gamma_T, T) \ and \ \gamma_T < \gamma_{T\max} : d\gamma_T = -\frac{\beta}{H} dT$$

$$dT < 0 \ and \ \gamma_T = \gamma_{T\max} : d\gamma_T = 0$$

In the crystal model Sittner et. al. (1998) assumes that the number of potentially twinned martensite variants is K and for the k_{th} transformation system the twinning plane unit vector is $\overline{n}^{(k)} = \left[n_1^{(k)}, n_2^{(k)}, n_3^{(k)}\right]$ and the shear direction unit vectors is $\overline{m}^{(k)} = \left[m_1^{(k)}, m_2^{(k)}, m_3^{(k)}\right]$. So the resolved shear stresses on the k_{th} transformation system can be calculated as,

$$\tau^{(k)} = \sum_{i,j=1}^{3} \alpha_{ij}^{(k)} \sigma_{ij}$$

or

$$d\tau^{(k)} = \sum_{i,j=1}^{3} \alpha_{ij}^{(k)} d\sigma_{ij}$$

where $\alpha_{ij}^{(k)}$ is the generalised Schmid factor defined as

$$\alpha_{ij}^{(k)} = \frac{\left(m_i^{(k)} n_j^{(k)} + n_i^{(k)} m_j^{(k)}\right)}{2}$$

and σ_{ij} is the stress tensor of a single crystal grain.

Thus, when the increments of stress tensor $d\sigma_{ij}$ is given, the resolved shear stress increment $d\tau$ in the transformation system can be calculated.

To consider the effect of the interactions among transformation systems, the model is modified by using the isotropic hardening model.

$$\tau_M^{(k)}\left(\gamma_T^{(i)},T\right)=\tau_{MS}(T)+H\sum_{i=1}^{k}\gamma_T^{(i)}$$

or

$$d\tau_M^{(k)}\left(\gamma_T^{(i)},T\right)=\beta dT+H\sum_{i=1}^{k}d\gamma_T^{(i)}$$

and

$$\tau_A^{(k)}\left(\gamma_T^{(i)},T\right)=\tau_{AF}(T)+H\sum_{i=1}^{k}\gamma_T^{(i)}$$

or

$$d\tau_A^{(k)}\left(\gamma_T^{(i)},T\right)=\beta dT+H\sum_{i=1}^{k}d\gamma_T^{(i)}$$

Also, the transformation is assumed to finish when the sum of volume fractions of the variants in the crystal is equal to unity, which manipulates by Sittner et. al. (1998) to,

$$\gamma_T^{(1)}+\gamma_T^{(2)}+\cdots+\gamma_T^{(k)}+\cdots+\gamma_T^{(K)}\le\gamma_{T\max}$$

Once $d\gamma_T^{(k)}$ is calculated in this process, the transformation strain increment $d\varepsilon_{T_{ij}}$ of crystal grain component can be calculated as,

$$d\varepsilon_{T_{ij}}=\sum_{k=1}^{K}\alpha_{ij}^{(k)}d\gamma_T^{(k)}$$

and then the total strain increment in the crystal is calculated as,

$$d\varepsilon_{ij}=d\varepsilon_{T_{ij}}+d\varepsilon_{e_{ij}}$$

where $d\varepsilon_{e_{ij}}$ is the elastic strain increment calculated by Hooke's law in the crystal.

For the polycrystalline model, the interaction among grains are incorporated by using the stress constant idea (Sittner et. al. : 1998), i.e. the stress of the grain is the same as the macroscopic stress in the material and the macroscopic strain is the average of the strains of every grain.

The calculation process is schematically represented in the flowchart of Figure 2-10.

Closely related to the strain of a material is its Poisson's ratio. By strict definition, the Poisson's ratio of a material is only valid for small strain linear elastic behaviour and thus, it becomes necessary to define a strain varying Poisson's ratio for highly nonlinear elastic materials such as biomaterials and smart materials. Evans, Smith and Wootton (1999) discuss the importance of the use of a Poisson's function in appropriate circumstances.

The usual strain quoted is the engineering strain, e (sometimes called the nominal or Cauchy strain), which is a measure of extension to initial length, l_o.

$$e = \frac{l_i - l_o}{l_o}$$

where l_i is the current length of the specimen.

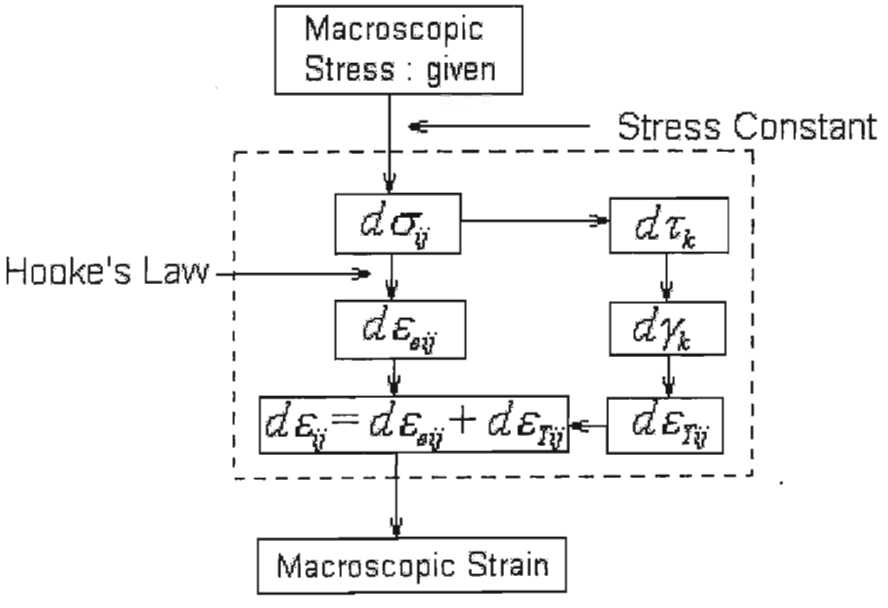

Figure 2-10 : Flowchart of strain calculation process

(modified after Sittner et. al. : 1998)

When dealing with larger extensions, it is common to refer to the true strain or Hencky strain. Most textbooks state in words that the true strain is the ratio of extension to instantaneous length, that is $(\delta l)/l_i$, but then go on to define true strain as a summation of these (Evans et. al. : 1999),

$$\varepsilon_{\log} = \int_{l_o}^{l_i} \frac{\delta l}{l_i} = \ln(1+e)$$

Thus, the true strain is sometimes referred to as the log true strain ε_{log}. The disadvantage is that this integral returns a secant value of the extension and not a localised tangent value. Thus, if the deformation is nonlinear this true strain may not accurately reflect instantaneous conditions, but more those relative to starting conditions. The simple ratio between extension and instantaneous length does return a tangent value of the deformation and is referred to as instantaneous true strain.

$$\varepsilon_{\text{int}} = \frac{\delta l}{l_i}$$

ε_{int} can be calculated with sequential experimental data as,

$$\varepsilon_{\text{int}} = \frac{l_i - l_{i-1}}{l_{i-1}},$$

for $l_i - l_{i-1}$ small enough (Evans et. al. : 1999).

The summation of ε_{int} is equivalent to ε_{log} if the step size between data points is sufficiently small. The summation of the instantaneous true strains is referred to as the total instantaneous true strain ε_{tot},

$$\varepsilon_{tot} = \sum_{1}^{i} \frac{l_i - l_{i-1}}{l_{i-1}}$$

In the limit of infinitesimal strains, engineering strain e, log transform true strain ε_{log} and total instantaneous true strain ε_{tot} are identical, and as the value of e increases, the ε_{log} and ε_{tot} diverge from e. The engineering, log transform and total instantaneous true strain are essentially summations and thus, initial changes in dimension have far greater effects on these summative strains than later changes. The instantaneous true strain, ε_{int}, does not do this. Similar functional changes in length produce similar changes in ε_{int} at any overall strain.

The standard definition of the Poisson's ratio is,

$$\upsilon_{xy} = \frac{-\varepsilon_{\log_y}}{\varepsilon_{\log_x}}$$

where x is the direction of the applied strain and y is the orthogonal direction.

Using either e, ε_{log} or ε_{tot} strains to calculate Poisson's ratio gives respectively,

$$\upsilon_{eng_{xy}} = \frac{-e_y}{e_x}$$

$$\upsilon_{\log_{xy}} = \frac{-\varepsilon_{\log_y}}{\varepsilon_{\log_x}}$$

$$\upsilon_{tot_{xy}} = \frac{-\varepsilon_{tot_y}}{\varepsilon_{tot_x}}$$

and, as with e, ε_{log} and ε_{tot} strains, if the step size is sufficiently small, they are all equivalent.

The Poisson's function $\upsilon_{\text{int}_{xy}}$ is defined as,

$$\upsilon_{\text{int}_{xy}} = \frac{-\varepsilon_{\text{int}_y}}{\varepsilon_{\text{int}_x}}$$

If experimental conditions do not allow the rapid collection of dimension data, the Poisson's function can be calculated using the graphical method or one of the numerical methods described by Alderson, Alderson and Evans (1997). Evans et. al. (1999) also present their findings on various methods available for smoothing of experimental data. The author believes that this is useful information and the reader is referred to the preliminary literature review, presented in Appendix A, for a summary.

Casciati, Faravelli and Petrini (1998) discuss energy dissipation in SMA, specifically dissipation by hysteretic plastic cycles in structural bars of significant diameter. Thermal transformations follow the plasticity process and hence classical mechanical models of constitutive law can be adopted in the energy dissipation analysis such as the material plasticity law (a simple Von Mises

scheme), though an associated hardening rule needs to be selected. Casciati et. al. (1998) uses a three dimensional Von Mises plastic model with isotropic hardening because it is offered by commercial finite element codes. The extension of the Mróz multi-surface hardening model to SMAs is also given consideration. The model further incorporates the commonly used concept of back-stress tensor for plastic hardening that provides the centre of the yield surface and varies with isotropic hardening. The back stress depends on the maximum prestress and the asymptotic value of the yield stress depends on the strain amplitude. In terms of the modelling process, two key items are identified viz. the sequence of the transformation temperatures; the differential scanning calorimeter (DSC) test estimates the temperature of phase transition, and the degree of heterogeneity of the material which is mainly due to its production technique; plasma technology offers good homogeneity while standard production processes give rise to finite levels of heterogeneity.

Once all the discussed variables are taken into account in the model, the energy dissipation appears to be obtained from the conventional load-displacement method.

2.3 Magnetostrictive Materials

An ideal smart material will develop large strokes under precise and rapid control. Piezoelectric and magnetostrictive materials exhibit rapid responses but have small strokes while SMA have large strokes, but their control is slow due to thermomechanical control.

The constitutive equations for magnetostriction in the one-dimensional case are,

$$\varepsilon = S\,\sigma + d\,H$$

and

$$B = d\,\sigma + \mu\,H$$

Where ε is the strain, B the flux density, S the compliance, σ the stress, d the magnetomechanical cross coupling coefficient, H the magnetic field intensity and μ the permeability at the nominal operating stress.

For three-dimensional analysis, these equations transform to,

$$\begin{bmatrix} \varepsilon \\ B \end{bmatrix} = \begin{bmatrix} \boldsymbol{S} & \boldsymbol{M} \\ \boldsymbol{M}^{tr} & \mu \end{bmatrix} \begin{bmatrix} \sigma \\ H \end{bmatrix}$$

where

$$[\varepsilon] = \begin{bmatrix} \varepsilon_x \\ \varepsilon_y \\ \varepsilon_z \\ \gamma_{yz} \\ \gamma_{xz} \\ \gamma_{xy} \end{bmatrix} \quad \text{and} \quad [\sigma] = \begin{bmatrix} \sigma_x \\ \sigma_y \\ \sigma_z \\ \tau_{yz} \\ \tau_{xz} \\ \tau_{xy} \end{bmatrix}$$

S is the 6 X 6 compliance matrix and the magnetostrictive tensor M is,

$$[M] = \begin{bmatrix} m_x & m_{xy} & m_{xz} \\ m_{xy} & m_y & m_{yz} \\ m_{xz} & m_{yz} & m_z \\ 0 & 0 & 0 \\ 0 & 0 & 0 \\ 0 & 0 & 0 \end{bmatrix}$$

μ is the 3 x 3 matrix of permeabilities of the magnetostrictive material and the flux density and magnetic field are given by,

$$[B] = \begin{bmatrix} B_x \\ B_y \\ B_z \end{bmatrix} \text{ and } [H] = \begin{bmatrix} H_x \\ H_y \\ H_z \end{bmatrix} \text{ respectively.}$$

Ullakko (1996) suggests the magnetic control of SMA in an attempt to overcome the current drawbacks of smart materials by investigating an Fe-33.5Ni alloy. The advantage of the magnetostrictive route is that commercially available materials such as Terfenol, offer strains that are an order of magnitude higher than those of the current piezoceramic materials. Further, forces developed by Terfenol are approximately twenty times higher than those of piezoceramics, and energy densities of magnetostrictive materials can be ten times higher than those attained in hydraulic machines. Actuation of magnetically controlled SMA is based on the control of the shape memory effect by the reorientation of martensite unit cells in an applied magnetic field that is analogous to their conventional thermomechanical control. In conventional SMA, the martensite must exhibit a twinned substructure in order for the shape memory effect to occur. The twin structures reorientate themselves in an external stress field to achieve a shape change, as shown in Figure 2-11b.

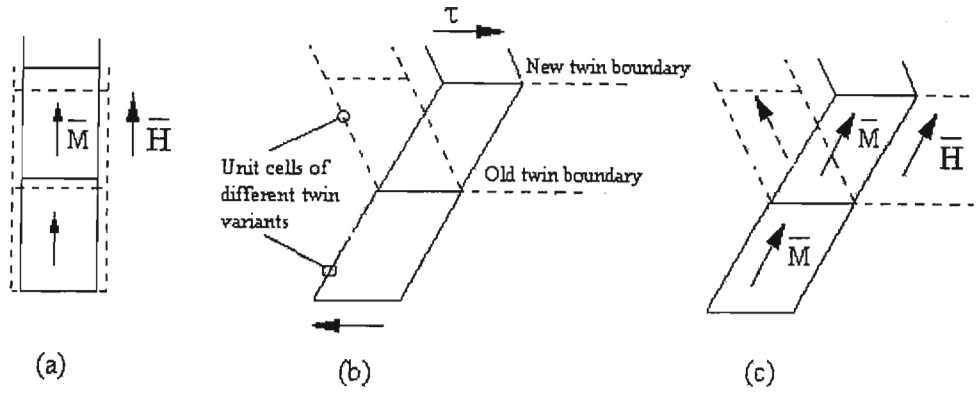

Figure 2-11: Shape changes that cause the strokes in (a) magnetostrictive, (b) shape memory and (c) magnetically driven SMA (after Ullakko : 1996)

When stress is applied, some twin variants grow and some shrink to accommodate the shape change resulting in the eventual establishment of only one twin variant orientated to the applied stress. The principle of magnetically controlled shape memory materials, called magneto shape memory (MSM) alloys, is analogous to this method of conventional shape change. The essential difference is that the motion of the twin boundaries or the interfaces between martensite and austenite in MSM materials is driven by an applied magnetic field instead of a stress field.

In crystalline ferromagnetic materials, magnetisation vectors lie along definite crystallographic axes called directions of easy magnetisation and the energy that directs the magnetisation along these directions is called crystal anisotropy energy. On the application of an external magnetic field the magnetisation tends to turn away from the easy direction of the unit cell and align in the direction of the external field (Figure 2-11a). A high anisotropy energy requires a high external magnetic field to realign the magnetisation direction.

If the energy of motion of twin boundaries is low enough at the same time, magnetisation can turn the unit cells as it turns to the direction of the external field to keep magnetisation in the original easy direction as depicted in Figure 2-11c. As a result, twins in favourable orientation to the magnetic field grow at the expense of other twins causing the twin boundary motion and shape change of the material. The condition that makes possible the turning of the unit cells of one twin variant into another is expressed as,

$$U_k > E_t + W + E_o$$

where U_k is the anisotropy energy, E_t is the energy of twin boundary motion, W is the work done by the actuator material (W is negative if turning is assisted by external stress) and E_o includes internal strain and other energy terms.

If the energy terms on the right hand side of the equation are small, applied magnetic fields of only tens of millitesla (mT) can cause strokes of a few percent, which are more than an order of magnitude larger than those attained in high-magnetostrictive Terfenol (Ullakko : 1996). If the magnetic straining of the MSM material is opposed by a high mechanical stress, the magnetically orientated twin structure can be recovered to the original structure. The magnetisation may, however, remain in the direction of the external field under the load. As the external stress is removed, the twin variants turn again in such a way that their easy direction of magnetisation is close to the external field . This recoverable strain is called magnetosuperelasticity.

Experimental analysis was conducted on the magnetic control of the motion of austenite-martensite interfaces in a Fe-33.5%Ni alloy (mass %) (Ullakko : 1996). The results, presented in Figure 2-12, showed a decrease in resistivity of the alloy and a 3.7 % martensitic phase transformation when a 230 mT perpendicular magnetic field was applied at 77 K. Further testing using a strain gauge showed that the strain increased (due to the formation of martensite) when the magnetic field was parallel with the direction in which the strain was measured. The strain decreased (due to reorientation of the martensitic structure in the applied magnetic field) when the magnetic field was turned perpendicular to the strain gauge.

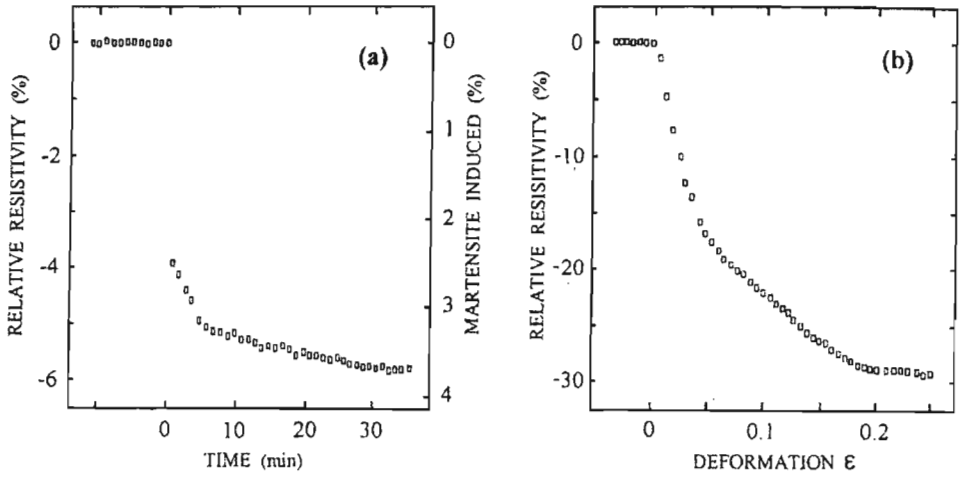

Figure 2-12: Experimental results obtained by Ullakko (after Ullakko : 1996)

Livingston (1982) presents a simple model of magnetomechanical coupling in amorphous metal ribbons (amorphous metals have superior magnetomechanical properties to crystalline magnetostrictive materials, in general). The major source of magnetic anisotropy in amorphous metals are structural anisotropies induced by annealing under a magnetic field (and/or applied stress) and magnetostrictive anisotropies produced by the interaction between magnetostrictive strain and applied or residual stress.

An amorphous metal ribbon with a width-wise magnetic easy axis is considered. This can be accomplished by annealing in a large magnetic field parallel to the ribbon width. The resulting domain structure with no applied field and no applied stress is shown in Figure 2-13a while Figure 2-13b shows the rotation of the magnetisation towards the length direction due to the application of a longitudinal magnetic field H.

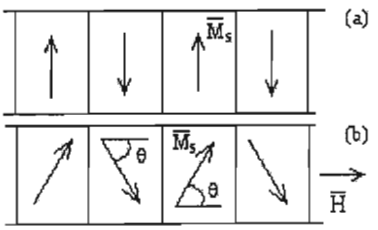

Figure 2-13 : Domain structure of a transverse annealed amorphous ribbon under (a) zero magnetic field and (b) longitudinal magnetic field (after Livingston : 1982)

The contribution of the applied field to the energy density is,

$$- M_s H \cos\theta$$

where M_s is the domain magnetisation per unit volume.

Finding the angle θ for minimum energy yields, for the longitudinal component of magnetisation,

$$M = M_s \cos\theta = M_s \frac{H}{H_A} \qquad \left(H \leq H_A\right)$$

where $H_A = \frac{2k_u}{M_s}$ is the anisotropy field and k_u is the induced anisotropy constant. θ is the angle between the magnetisation (assumed to remain in the ribbon plane) and the ribbon length.

The spontaneous magnetostrictive strain in each domain is λ_s in the direction of magnetisation and $-\lambda_s/2$ in the orthogonal directions. Thus, as the magnetisation rotates from the width to the length direction, the longitudinal strain, ε, changes from $-\lambda_s/2$ to λ_s, a change of $3\lambda_s/2$. The longitudinal strain is given by,

$$\varepsilon = \frac{3\lambda_s}{2}\left(\cos^2\theta - \frac{1}{3}\right) = \frac{3\lambda_s}{2}\left(\frac{H^2}{H_A{}^2} - \frac{1}{3}\right)$$

Hence, a measure of magnetomechanical coupling is,

$$d = \frac{d\varepsilon}{dH} = \frac{3\lambda_s H}{H_A{}^2}$$

and reaches a maximum at $H=H_A$.

The longitudinal strain due to the application of stress σ is,

$$\varepsilon = \frac{\sigma}{E_m} + \frac{3\lambda_s}{2}\left(\frac{H^2}{H_{A\sigma}{}^2} - \frac{1}{3}\right)$$

where the term $\frac{\sigma}{E_m}$ is the Hooke's law term (E_m is the Young's modulus at constant magnetisation) and $H_{A\sigma}$ is a reduced anisotropy field given by

$$H_{A\sigma} = \frac{2k_u - 3\lambda_s\sigma}{M_s}$$

However, this characterisation is only if the magnetic easy axis remains in the width direction, i.e. if $\sigma < \sigma_c = 2k_u/3\lambda_s$. If σ exceeds σ_c, the magnetic easy axis abruptly switches to the length direction.

The magnetomechanical coupling factor, k, is related to the fractional energy transfer between magnetic and mechanical energy and is given by,

$$k = \left[1 + \frac{M_s H_{A\sigma}{}^3}{9\lambda_s{}^2 E_m H^2} \right]^{-1/2} \leq 1$$

The magnetomechanical coupling factor reaches a maximum at $H = H_{A\sigma}$.

To facilitate rotation of the magnetisation and accompanying magnetostrictive strain, the desired properties are high λ_s, M_s and E_m and low k_u, H_A and σ_c.

Dapino, Flatau and Smith (1998) characterise the resultant strain due to the rotation of magnetic moments within the material through consideration of the Jiles-Atherton mean field theory for ferromagnetic hysteresis in combination with a quadratic moment rotation model for magnetostriction. The internal dynamics of the magnetostrictive rod as it vibrates is modelled through force balancing that yields a wave equation with magnetostrictive inputs.

A typical current control transducer is considered (Figure 2-14). It consists primarily of a cylindrical magnetostrictive rod actuator, a wound wire solenoid, an enclosing permanent magnet and a prestress mechanism.

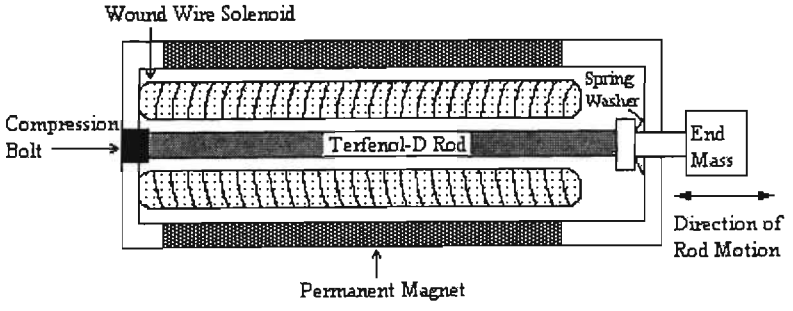

Figure 2-14: Cross section of a Terfenol-D magnetostrictive transducer

(after Dapino et. al. : 1998)

The magnetic moments in the rod have a primary orientation perpendicular to the longitudinal axis. When current is applied to the solenoid, a magnetic field is produced that causes the moments to

rotate to align with the field, and the resulting forces and strains provide the actuator capabilities of the transducer. The permanent magnets are used to attain bi-directional strains and forces in the rod.

The active strain that is generated due to moment rotation and alignment is modelled in two steps. First an energy based relationship between the current, I, applied to the solenoid and the resulting magnetisation, M, is derived using a modified Jiles-Atherton field theory for ferromagnetic hysteresis. A quadratic moment rotation model is then applied to yield the output magnetostriction, λ. The Jiles-Atherton theory is based upon the observation that moments in ferromagnetic materials, such as Terfenol-D, are highly aligned in domains at temperatures below the Curie point. The reorientation of these moments within the domains produces anhysteretic magnetisation, M_{an}, that is completely reversible. However, due to the presence of defects or second phase materials, such magnetisation curves are rarely observed in commercial materials and the Jiles-Atherton theory quantifies the observed magnetisation in terms of reversible, M_{rev}, and irreversible, M_{irr}, components.

To quantify the various magnetisation concepts described above, it is first necessary to determine the effective field, H_{eff}, that acts upon the magnetic moments in the Terfenol rod. Atherton and Jiles (1986) and Jiles (1991) show that H_{eff} is dependent on the magnetic field generated by the solenoid, magnetic moment interactions, crystal and stress anisotropies, temperature and geometry of the transducer. For this model, the crystalline anisotropies are ignored as they are assumed negligible under large prestress conditions.

Thus, under the further assumption of fixed temperature and quasi-static operating conditions, H_{eff} is modelled by,

$$H_{eff}(t,x) = H(t,x) + \alpha M(t,x) + H_{\sigma}(t,x)$$

where x denotes the longitudinal coordinate, H is the field generated by a solenoid with n turns per unit length, αM quantifies the field due to magnetic interactions between moments and H_{σ} is the field due to magnetoelastic domain interactions. The parameter α quantifies the amount of domain interaction.

A reasonable approximation to the effective field under a variety of operating conditions is given by,

$$H_{eff}(t,x) = nI(t)\varphi(x) + \tilde{\alpha}M(t)$$

where I is the current to the solenoid, $\varphi(x)$ is an empirically determined function and $\tilde{\alpha}$ is given by,

$$\tilde{\alpha} = \alpha + \frac{9}{2}\frac{\lambda_s \sigma_o}{\mu_o M_s^2}$$

where λ_s is the saturation magnetostriction, M_s is the saturation magnetisation and μ_o is the free space permeability.

The approximate H_{eff} expression is limited to low frequencies because ac losses are not incorporated in the model. The anhysteretic magnetisation is now written in terms of the Langevin function as,

$$M_{an}(t,x) = M_s\left[\coth\left(\frac{H_{eff}(t,x)}{a}\right) - \frac{a}{H_{eff}(t,x)}\right]$$

where the constant $a = \frac{Nk_BT}{\mu_o M_s}$, k_B is Boltzmann's constant, N is the domain density and k_BT represents the Boltzmann thermal energy.

The irreversible magnetisation is a partial differential given by,

$$\frac{\partial M_{irr}}{\partial t}(t,x) = \frac{dI}{dt}\varphi(x).\frac{M_{an}(t,x) - M_{irr}(t,x)}{k\delta - \tilde{\alpha}\left[M_{an}(t,x) - M_{irr}(t,x)\right]\frac{dM_{irr}}{dM}}$$

where $k = \frac{\langle p\rangle\langle \varepsilon_\pi \rangle}{2m\mu_o(1-c)}$, $\langle p\rangle$ is the average density of pinning stresses, $\langle \varepsilon_\pi \rangle$ is the average density for 180° walls, c is a reversibility coefficient, m is the magnetic moment of a typical domain and δ is defined to have the value +1 when $\frac{dH}{dt} > 0$ and –1 when $\frac{dH}{dt} < 0$ to guarantee that pinning always opposes changes in magnetisation.

A major disadvantage of this model is that many of the parameters are unknown and have to be estimated based on average energy requirements for the breakage of pinning sites. The reversible magnetisation quantifies the degree to which domain walls bulge before attaining the energy necessary to break the pinning sites, and is given by,

$$M_{rev}(t,x) = c\left[M_{an}(t,x) - M_{irr}(t,x)\right]$$

with the total magnetisation deriving to,

$$M(t,x) = M_{rev}(t,x) + M_{irr}(t,x)$$

The characterisation of the magnetostriction, $\lambda \equiv \frac{dL}{L}$, in terms of magnetisation, M, remains as the final aspect of the model. Magnetostriction provides a measure of the active strains generated by the material because it indicates the relative change in length from the ordered but unaligned state to the state in which domains are aligned. Consideration of the potential energy of the system yields,

$$\lambda(t,x) = \tfrac{3}{2}\frac{\lambda_s}{M_s^2} M^2(t,x)$$

2.4 Piezoelectric Materials

Piezoelectric materials can be used as sensors and actuators in a smart structure because of its unique electric properties; piezoelectric materials create an electric field when strained, and conversely, strain under an electric field. As a consequence of this characteristic, researchers have begun investigating the use of piezoelectric materials to counteract impact loads.

Rao and Sunar (1999) present a survey article that collects recent research studies on sensing and control of flexible structures via piezoelectric materials. Piezoelectricity basically defines a relation between an applied electric field and strain, or an applied strain and electric field in certain crystals, ceramics and films. Piezoelectric materials can be bonded to the surface of host structures or embedded into laminates. Instead of directly bonding piezoelectric actuators to the surfaces of host structures, they can also be bonded to host structures by thin viscoelastic layers or they can be bonded to stiff constraining layers that are in turn bonded to host structures by thin viscoelastic layers.

In piezoelectric theory, the linear theory deals with small displacement and structural vibrations, and assumes quasi-static motion indicating that the mechanical and electrical forces are balanced at any given instant. The non-linear theory deals with the dynamics of anisotropic piezoelectric shells undergoing large displacements. The linear equations of piezoelectricity in matrix form are written as

$$\overline{D} = \overline{e}\hat{\varepsilon} + \overline{P}E$$

for the direct piezoelectric effect, and for the converse piezoelectric effect as

$$\hat{\sigma} = \overline{Q}\hat{\varepsilon} - \overline{e}^{T}E$$

where $\hat{\sigma}$ and $\hat{\varepsilon}$ denote stress and elastic strain in the material co-ordinates respectively, $\overline{Q}$ is the elastic stiffness matrix, $\overline{e}$ is the piezoelectric stress coefficient matrix, E is the electric field intensity, $\overline{D}$ is the electric displacement and $\overline{P}$ is the dielectric permitivity matrix.

The expanded form of these constitutive equations are given as,

$$\begin{Bmatrix} D_1 \\ D_2 \\ D_3 \end{Bmatrix} = \begin{bmatrix} 0 & 0 & 0 & 0 & e_{51} & 0 \\ 0 & 0 & 0 & e_{42} & 0 & 0 \\ e_{13} & e_{23} & e_{33} & 0 & 0 & 0 \end{bmatrix} \begin{Bmatrix} \varepsilon_{11} \\ \varepsilon_{22} \\ \varepsilon_{33} \\ \gamma_{23} \\ \gamma_{13} \\ \gamma_{12} \end{Bmatrix} + \begin{bmatrix} P_{11} & 0 & 0 \\ 0 & P_{22} & 0 \\ 0 & 0 & P_{33} \end{bmatrix} \begin{Bmatrix} E_1 \\ E_2 \\ E_3 \end{Bmatrix}$$

for the direct piezoelectric effect, and for the converse piezoelectric effect as,

$$\begin{Bmatrix} \sigma_{11} \\ \sigma_{22} \\ \sigma_{33} \\ \tau_{23} \\ \tau_{13} \\ \tau_{12} \end{Bmatrix} = \begin{bmatrix} C_{11} & C_{12} & C_{13} & 0 & 0 & 0 \\ C_{21} & C_{22} & C_{23} & 0 & 0 & 0 \\ C_{31} & C_{32} & C_{33} & 0 & 0 & 0 \\ 0 & 0 & 0 & C_{44} & 0 & 0 \\ 0 & 0 & 0 & 0 & C_{55} & 0 \\ 0 & 0 & 0 & 0 & 0 & C_{66} \end{bmatrix} \begin{Bmatrix} \varepsilon_{11} \\ \varepsilon_{22} \\ \varepsilon_{33} \\ \gamma_{23} \\ \gamma_{13} \\ \gamma_{12} \end{Bmatrix} - \begin{bmatrix} 0 & 0 & e_{13} \\ 0 & 0 & e_{23} \\ 0 & 0 & e_{33} \\ 0 & e_{42} & 0 \\ e_{51} & 0 & 0 \\ 0 & 0 & 0 \end{bmatrix} \begin{Bmatrix} E_1 \\ E_2 \\ E_3 \end{Bmatrix}$$

Some important piezoelectric materials that are in use today are lithium niobate ($LiNbO_3$), zinc oxide (ZnO), aluminium nitride (AlN), lead zirconate titanate (PZT), polarised fluoropolymers, odd nylons, polyurea, vinylidene cyanide copolymers and polyvinylidene fluoride (PVDF or PVF_2). $LiNbO_3$ is a crystal with high electromechanical coupling and very low acoustical attenuation. ZnO has a high piezoelectric coupling compared to non-ceramic materials, pyroelectric properties and great stability of its hexagonal phase. AlN is a thin film piezoelectric material that has a high acoustic velocity and endurance in humidity and high temperatures. PZT is a piezoceramic with high piezoelectric, dielectric and elasticity coefficients together with a large pyroelectric response and spontaneous polarisation. Finally, PVDF and other piezopolymers are known for their flexibility, durability, lightweight and relatively low acoustic impedance. They also have strong piezoelectric and pyroelectric properties.

An important consideration in the sensing and control of flexible structures is the choice of appropriate piezoelectric sensors and actuators. Piezoelectric sensors can be chosen from the types of displacement, velocity or acceleration, slope, slope rate or slope acceleration and strain, strain rate or strain acceleration. Piezoelectric actuators are selected from the types of applied force, applied moment or applied strain. Combining the sensing and actuating characteristics of a piezoelectric material into one single device is also possible and extremely useful. Important parameters for the performance of actuators are stroke or strain, stiffness, bandwidth, linearity, temperature sensitivity, strength density and efficiency while important parameters for the

performance of piezoelectric sensors include the sensitivity to strain/displacement, spatial resolution, frequency bandwidth, temperature sensitivity, linearity and hysteresis.

Work conducted by Joshi and Mannas (1993) focuses on smart laminated plates under impact and the electric field created by piezoelectric patches in the structure. Several studies are made comparing the electric field generated by piezoelectric patches of varying size, shape and location within the plate. In terms of patch location, the elastic waves created by the impact take a finite amount of time to travel between the impact point and the piezoelectric patch. The flexural waves created by the impact are also dispersive. Thus, the closer the patch is to the impact point the sooner the electric field is generated and the greater the magnitude of the electric field. The trend in the effects of patch size to electric field is that as the size of the piezoelectric patch increases, the average electric field it generates decreases. This is due to the averaging out of positive and negative oscillating waves of electric field. Larger piezoelectric elements are able to average more oscillations at the same time and thereby reduce the average electric field generated. The shape of the piezoelectric patch does not affect the impact force so long as the different shape patches cover approximately the same area. Patches, however, which are short in the longitudinal direction of the plate tend to produce higher average electric field values than longer patches that average out electric field oscillations. A summary of the results obtained by Joshi and Mannas for the effect of distance from the impact point on electric field generation is presented in Figure 2-15.

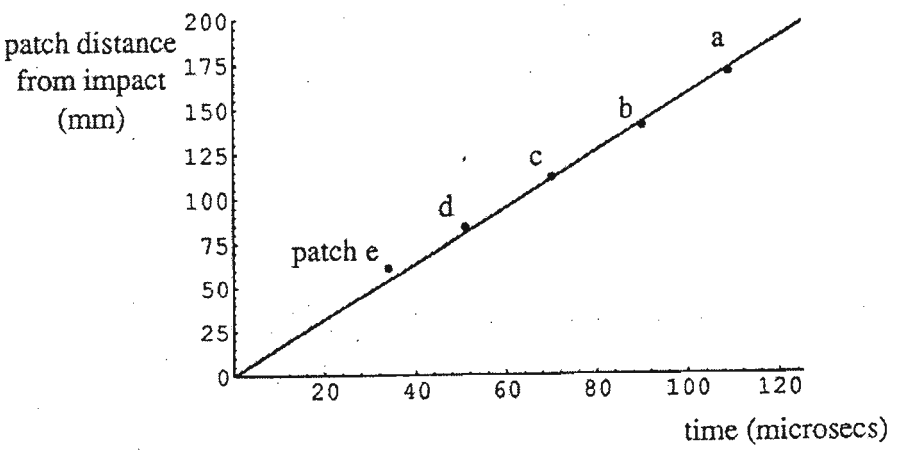

Figure 2-15: Time between impact and generation of 0.002 V/cm average electric field (after Joshi and Mannas : 1993)

As a step further, to piezoelectric patches, Agbossou, Mahut and Pastor (1998) investigate the use of piezoelectric fibre composite elements in structural vibration systems. Similar to normal composites, there are two kinds of information that characterise the properties of a piezoelectric

fibre composite, viz. the internal phase geometry and the physical properties of the phases. Several micromechanical models of effective electroelastic properties in piezoelectric composites define Representative Volume Element (RVE) dimensions. The dimension of the RVE is large compared to typical phase region dimensions and represents the structural homogeneity of the composite material. For a piezoelectric composite body the homogenous boundary conditions are either,

$$u_i(S) = \varepsilon_{ij}^o x_j \quad and \quad \Phi(S) = G_j^o x_j$$

or

$$T_i(S) = \sigma_{ij}^o n_j \quad and \quad D_i n_i = D_i^o n_i$$

where $u_i(S)$ and $\phi(S)$ denote the displacements and the electric potential on the outside boundary S, ε^o, σ^o and G^o are constant strain, stress and electric potential gradient respectively and U, G, T and x denote the mechanical displacement, electric potential gradient, stress vector and location vector respectively.

The effective electroelastic properties are defined by considering the volume average of the piezoelectric field variables (ε_{ij}, σ_{ij}, ϕ_i) and the relations,

$$\left\langle \sigma_{ij} \right\rangle = C_{ijkl}^{\text{hom}} \left\langle \varepsilon_{kl} \right\rangle + e_{mij}^{\text{hom}} \left\langle G_m \right\rangle$$

and

$$\left\langle D_i \right\rangle = e_{ikl}^{\text{hom}} \left\langle \varepsilon_{kl} \right\rangle - \epsilon_{ij}^{\text{hom}} \left\langle G_j \right\rangle$$

where the symbol <> denotes the volume average, σ_{ij}, ε_{ij} and C_{ijkl} are the components of stress, strain and elasticity tensors respectively, D_i, G_i, ϵ_{ij} and e_{ikl} are the components of electric displacement, electric potential gradient, dielectric and piezoelectric tensors respectively.

Using the previous concept of homogeneity, Wang (1992) used a Green's function technique to develop a solution for an ellipsoid inclusion in a piezoelectric medium while Schulgasser (1992) demonstrated that five universal relationships, which are independent of geometry at given volume fractions, connect six of the effective physical constants. In 1995, Yu developed the Periodic

Microstructural Model to estimate the electro-thermo-elastic response of piezoelectric composites. This model used Fourier series to include the constituent properties and shapes, and provided analytical estimates for some effective electro-thermo-elastic moduli of two-phase piezoelectric composites.

Figure 2-16 displays the method used by Agbossou et. al. (1998) for dynamic analyses of a piezoelectric fibre composite in an active beam using homogenisation and finite elements.

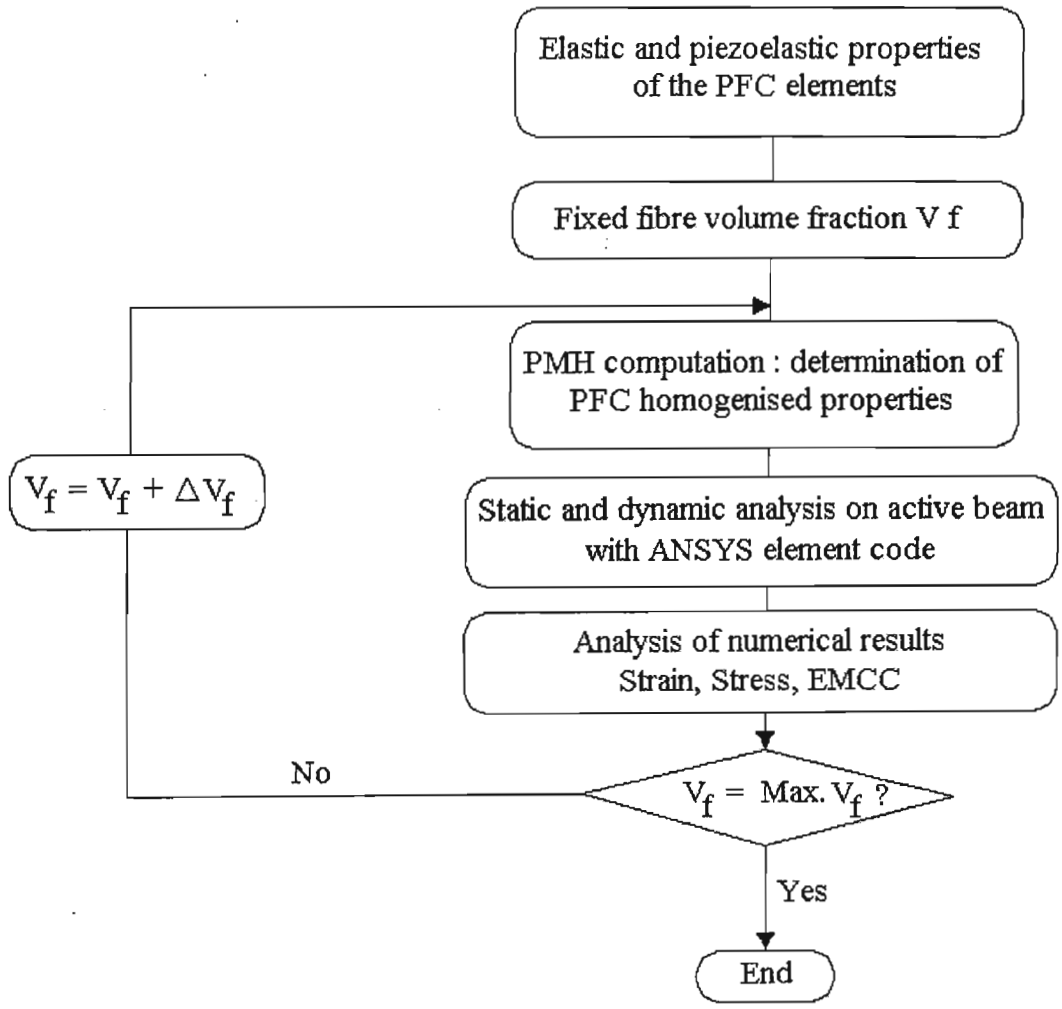

Figure 2-16: Computation scheme of dynamic behaviour of piezoelectric fibre composites (after Agbossou et. al. : 1998)

The electromechanical coupling coefficient (EMCC) governs the energy transformation and is a fundamental property of a piezoelectric medium. It gives the ratio of electrical (mechanical) energy stored in the volume of a piezoelectric body and capable of conversion to the total mechanical (electrical) energy supplied to the body. Agbossou et. al. (1998) use the dynamic EMCC as,

$$k_d = \sqrt{\frac{\left(F_p^{\,2} - F_s^{\,2}\right)}{F_p^{\,2}}}$$

where k_d is the EMCC and F_s and F_p are the resonance frequencies of the equivalent electrical series and parallel schemes respectively.

Two main conclusions were derived from Agbossou et. al. (1998). Firstly, with the piezoelectric fibre composite, the EMCC can be adapted by changing the fibre content and secondly, the variation of the EMCC peaks at 35 % fibre volume fraction.

The phenomenon of piezoresistivity can be observed in any conductive or semi-conductive material that can undergo large elongation. Taya (1999) considers for investigation a cylindrical rod of length L and cross sectional area S with resistivity ρ. The resistance of the rod, R, is given by,

$$R = \rho G$$

where G is a geometrical factor given by $G = \frac{L}{S}$.

Under applied stress, σ, R can be changed by dR resulting in,

$$\frac{dR}{R} = \left(\frac{1}{\rho}\frac{d\rho}{d\sigma} + \frac{1}{G}\frac{dG}{d\sigma}\right)d\sigma$$

where the first and second terms denote the effect of piezoresistivity and the geometric factor respectively, on the overall resistance R.

For a composite that contains numerous conductive short fibres embedded in an insulating matrix and subjected to applied strain, e, the electrical conductivity of the i-th percolating network along the x-axis (Figure 2-17) can be computed from the following power law,

$$\sigma_{xi} = \sigma_f (p - p_c)^t$$

where p is the probability of bonds, σ_f is the conductivity of the fibres, t is a critical exponent dependent only on dimensionality and type of microstructure and p_c is the critical probability of bonds at the percolation threshold, at and above which the composite becomes conductive. p is given by,

$$p = \frac{N_f + 2N_i}{4N_f + 2N_i}$$

where N_f and N_i are the number of fibres and the number of intersecting points respectively.

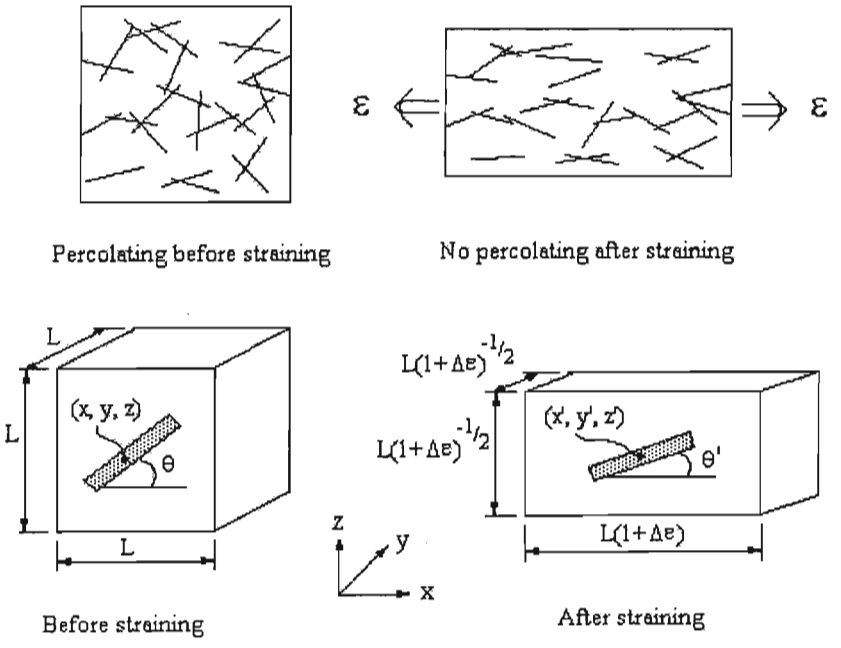

Figure 2-17: Expected microstructure change under straining of a conductive short fibre matrix composite (after Taya : 1999)

The effective electrical conductivity along the x-axis is then given by,

$$\sigma_x = \sum_{i=1}^{m} b_{yi} b_{zi} \sigma_{xi}$$

where m is the number of percolating clusters and b_{yi} (b_{zi}) is the width of the i-th percolating network along the y (z) axis.

Unfortunately, while the probability theory is accurate for small strains, up to 0.1, with substantial experimental results presented by Taya (1999) as verification, no results (experimental) are presented for larger strain values.

Piezoelectric solids exhibit a first order coupling between mechanical stress and electrical potential with the properties of piezoceramics being sensitive to the presence of impurities and microstructural features such as grain size and porosity as well as the processing methodology. Typically, resonant techniques are used along with static and quasi-static tests to determine the properties of piezoelectric materials, however in some cases, such as thin films and heat sensitive piezoelectric materials, these techniques can be unusable and one has to resort to instrumented indentation methods. Giannakopoulos, Ramamurty, Sridhar and Suresh (1999) investigate the response of lead zirconate titanate piezoelectric ceramics to spherical microindentation. In the instrumented indentation tests, the indentor load is continuously recorded as a function of the depth of penetration of the indentor into the material and the information is used to determine material properties such as Young's modulus, yield strength and the strain hardening exponent for metallic materials, and strength and fracture toughness for brittle materials.

Theoretical and finite element analysis reveals that the functional relationships between indentor load and the depth of penetration for the fully coupled problem have the same structure as the uncoupled mechanical problem. Further, the resistance of the material to penetration by the indentor depends on the electrical conductivity (i.e. whether open circuit or closed circuit conditions prevail). Spherical indentors offer the advantage of less complex testing and analysis over other shapes of indentors because they produce a non-singular stress field (Giannakopoulos et. al. : 1999).

In the theoretical analysis the piezoelectric material is considered to be transversely isotropic and the interface between the spherical indentor and the flat surface of the piezoelectric substrate is assumed to be frictionless. There are five elastic, two dielectric and three piezoelectric constants (independent) for a transversely isotropic piezoelectric solid. If the indenting sphere is a perfect

electrical conductor with constant electric potential $\phi = \phi_o$ and radius R, then the boundary conditions at the indented surface are,

$$\phi(r,0) = \phi_o ; \quad 0 \le r \le a, \; z = 0$$

$$D_z(r,0) = 0, \quad r > a, \; z = 0$$

where r and z are the radial and normal co-ordinate directions schematically shown in Figure 2-18, D is the electrical charge distribution and a is the radius of the contact area.

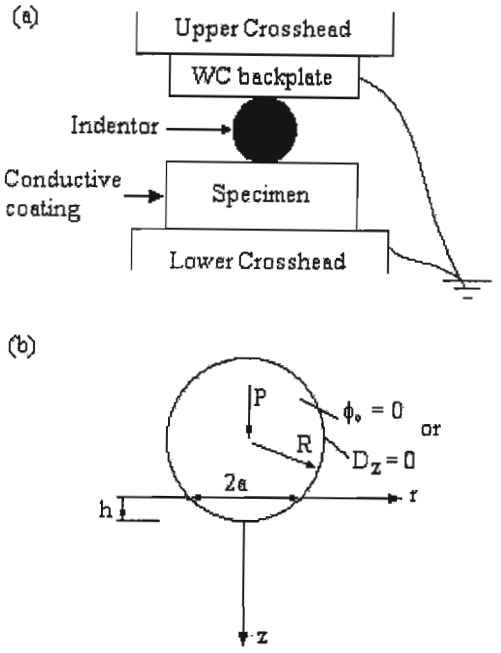

Figure 2-18: Schematic representation of the experimental indentation system (after Giannakopoulos et. al. : 1999)

The first of these equations indicate that the potential of the sphere is also the potential of the contact area, while the second equation shows that the electric charge distribution outside the contact area is zero (external charges are absorbed by the surface or by the use of electrodes). When $\phi_o = 0$, the relation between indentor load, P, and indentation depth, h, is given by,

$$P = \frac{8\sqrt{R}M_4M_5 - M_3M_6}{3M_1M_4 - M_2M_3}h^{3/2}$$

where M_1 through to M_8 are related to the material constants (algebraic relationships given in Giannakopoulos et. al. : 1999).

If the indentor is a perfect insulator with zero electric charge distribution, the boundary condition is,

$$D_z(r,0) = 0, \qquad r \geq 0$$

and the *P-h* relationship is expressed as,

$$P = \frac{8\sqrt{R}M_8M_5 - M_7M_6}{3M_1M_8 - M_2M_7}h^{3/2}$$

If the indented material is electrically rigid, i.e. all the coupling constants are equal to zero, then the constants M_3 and M_7 reduce to zero. In the case of purely elastic Hertzian spherical contact, the *P-h* relation is given by,

$$P = S_1h^{3/2}$$

where $S_1 = \frac{4}{3}\left(\frac{1-\nu_1^2}{E_1} + \frac{1-\nu_2^2}{E_2}\right)^{-1} R^{1/2}$ and is referred to as the contact compliance. E_1 and E_2 are Young's moduli and ν_1 and ν_2 are Poisson's ratio of the specimen and indentor respectively.

To take into account the possibility of deformation at the back face of the indentor, the contact compliance can be redefined as,

$$S = \left[\left(\frac{1}{S_1}\right)^{2/3} + \left(\frac{1}{S_2}\right)^{2/3}\right]^{-3/2}$$

where S is the total contact compliance and S_2 is the contact compliance between the back surface and the indentor.

The results obtained by Giannakopoulos et. al. (1999) showed that the elastic modulus of piezoelectric materials depends on the experimental condition of electrical connectivity between the two opposite faces upon which external loading is applied. The modulus measured with both the ends of the specimen electrically connected is generally lower than that measured with an open circuit. The change in stiffness can be attributed to the additional mechanical resistances offered by the undissipated potential generated due to the mechanical deformation of the piezoelectric solid. Although the charge distribution under the indentor cannot be sustained if the contact area is fixed, the charge build-up increases during the quasi-static advance of the contact area under a steadily increasing indentation load. If the indentor is conducting and grounded, a charge builds up in the indentor opposing that developing in the specimen. This distribution of charge, which changes with time, manifests as a quasi-static electric current.

The majority of analyses characterising piezoelectric actuation of laminates are based on classical laminate theory that assumes a linear strain distribution through the thickness and zero transverse shear stresses. This theory is restricted to thin plate applications, and to address moderately thick and thick laminate constructions the effects of transverse shearing stresses need to be taken into account. Chattopadhyay and Seeley (1997) use a higher order refined displacement field theory to take into account transverse shear stresses through the thickness to analyse smart materials surface bonded or embedded in composite laminates. While higher order laminate theories provide an effective tool to predict the deformation behaviour of composite laminates subjected to bending loads, the difficulty arises in satisfying the stress free boundary conditions at the free surfaces while maintaining continuity of strains through the thickness. Further, the electromechanical coupling coefficients for piezoelectric materials are dependent upon the actual strain in the actuators and this needs to be taken into account.

If it is assumed that there are no defects in the composite material, such as voids or delaminations, then the displacement field is continuous. A further assumption is that the in-plane displacements vary as cubic functions of the thickness z, and the transverse displacement is independent of z (Figure 2-19).

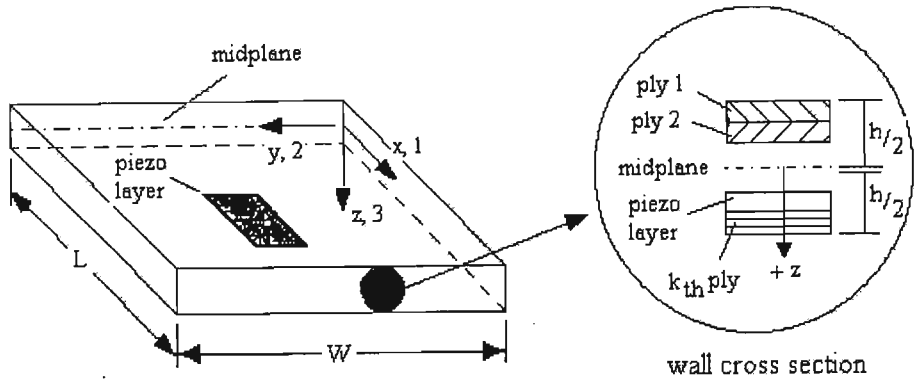

Figure 2-19 : Orientation of composite plate with piezoelectric actuator

(after Chattopadhyay et. al. : 1997)

The general displacement field is defined as,

$$U_1(x,y,z) = u_{10}(x,y) + z\left(-\frac{\partial}{\partial x}u_{30}(x,y) + u_{11}(x,y)\right) + z^2u_{12}(x,y) + z^3u_{13}(x,y)$$

$$U_2(x,y,z) = u_{20}(x,y) + z\left(-\frac{\partial}{\partial y}u_{30}(x,y) + u_{21}(x,y)\right) + z^2u_{22}(x,y) + z^3u_{23}(x,y)$$

$$U_3(x,y,z) = u_{30}(x,y)$$

where U_1, U_2 and U_3 are the total displacements and u_{10}, u_{20} and u_{30} denote the mid-plane displacements of a point (x,y). The partial derivatives of u_{30} represent the rotations of normals to the mid-plane corresponding to the slope of the laminate and u_{11} and u_{21} represent the additional rotations due to shear deformation about the y and x axes respectively. The quantities u_{12}, u_{13}, u_{22} and u_{23} represent higher order functions. Note that if the higher order functions are eliminated, the displacement field reduces to the classical theory.

The displacements and rotations are assumed small and a linear relationship for the kinematic equation is used.

$$\varepsilon_1 = \frac{\partial}{\partial x}U_1,\ \varepsilon_2 = \frac{\partial}{\partial y}U_2,\ \varepsilon_3 = 0$$

$$\varepsilon_4 = \frac{\partial}{\partial z}U_2 + \frac{\partial}{\partial y}U_3$$

$$\varepsilon_5 = \frac{\partial}{\partial z}U_1 + \frac{\partial}{\partial x}U_3$$

$$\varepsilon_6 = \frac{\partial}{\partial y}U_1 + \frac{\partial}{\partial x}U_2$$

where $\varepsilon_{1\text{-}6}$ represent the linear strains.

The forces and moments produced as a result of piezoelectric actuation are also discussed by Chattopadhyay and Seeley (1997) and the results conclude that for moderately thick and thick laminates, the higher order theory efficiently captures the localised nature of the stresses near the actuators while the classical laminate theory showed significant deviations.

Finally, Anderson, Calvert, Denham and Madenci (1997) discuss the sensor response of polyvinylideneflouride films (PVF2) embedded between layers of composite laminates. Piezoelectric PVF2 films retain much of their piezoelectric response upon cooling from curing temperatures up to 200°C, even though the cure temperature exceeds the melting point of the film. Further, ceramic piezoelectric sheets (e.g. PZT) are available down to a thickness of 250 microns but are very fragile, with fracture strains of only 0.1 %. They are also susceptible to loss of poling above the cure temperature, 300 °C to 400 °C for PZT, and can depole at stresses of 10 MPa to 100 MPa. Polymer piezoelectric materials (PVF2 and several nylons and copolymers of vinylidene cyanide) are thinner and tougher but raise concerns about temperature range and the piezoelectric coefficients are much less than those of the ceramics. Anderson et. al. (1997) monitored the sensor response during the cure cycle. The sensor response decreased with increasing temperature and goes to zero in the region of the melting point. The sensor does not respond to stimulus during the rest of the cure, but does exhibit a reduced piezoelectric response once cooled. This is attributed to the constraining of the sample during cure. An unconstrained sample subjected to a similar cycle showed a more rapid loss of response with no return on cooling. The effect of constraint is to raise the melting temperature of the PVF2 and cause recrystallisation in the piezoelectric beta phase instead of the non-piezoelectric alpha phase. Load is shared between the embedded PVF2 sensor and the epoxy matrix on the basis of equal strain.

CHAPTER 3

3 ANALYTICAL DESCRIPTION

The sole objective of this chapter is to develop an analytical model that can be used for numerical simulation, to describe the low velocity impact scenario investigated in this thesis. The scenario considered is a simply supported beam, of rectangular cross-section, subjected to a falling mass impact at midspan. The chapter is divided into four subsections in order of increasing material complexity, i.e. a beam consisting only of matrix material is first considered, then the same beam with shape memory alloy reinforcement is evaluated, followed by the addition of magnetostrictive inclusions and finally a short write-up on piezoelectric control. Another important output of this chapter is the derivation of the geometric relationship between the beam displacement and strain. The implementation of the outputs of this chapter into numeric code is presented in Appendix B.

3.1 Impact of Aluminium Host Structure

Consider the initial problem of the simply supported homogenous aluminium beam subjected to a falling mass impact at midspan, depicted in Figure 3-1 below. The cross-section of the beam is considered to have a width of b and a depth of d.

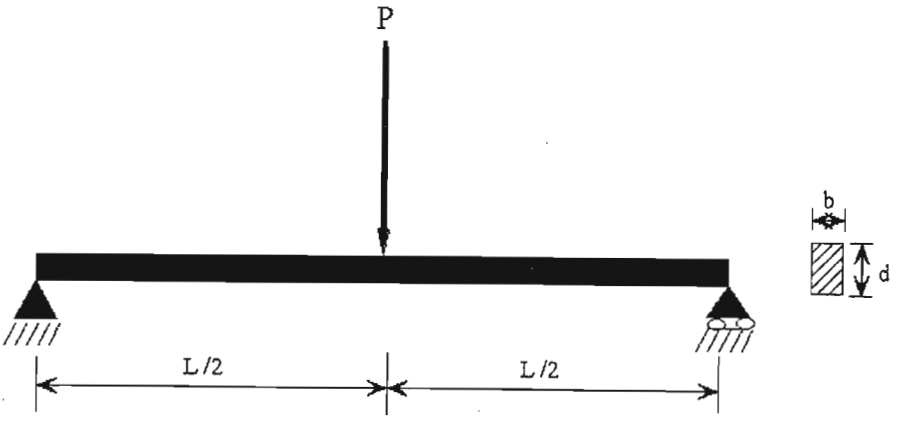

Figure 3-1 : Schematic of beam impact conditions

The conventional average shear and bending stresses for a simply supported beam with a static load at mid-span are given by,

$$\tau = \frac{P}{A}$$
$$= \frac{P}{bd}$$

and

$$\sigma = \frac{M\bar{y}}{I}$$
$$= \frac{\frac{PL}{4}\frac{d}{2}}{\frac{bd^3}{12}}$$
$$= \frac{3PL}{2bd^2}$$

respectively, where P is the load, A is the cross-sectional area, M is the bending moment, I is the second moment of area and L is the length of the beam. $\bar{y}$ is the distance from the neutral axis of the beam to the outermost point. Note that these average stresses are presented for information only and are not used in any calculations. Stresses based on actual displacements and instantaneous modulus are used when required.

From conventional beam theory, the deflection is given by,

$$\delta = \frac{PL^3}{48EI}$$

where E is Young' modulus.

To facilitate numerical modelling, the ability to transform from the force-displacement domain to the stress-strain domain is crucial. Thus, the transformation equation, in the form of the geometric relationship between the displacement, δ, and the strain, ε, needs to be established. Figure 3-2 presents a schematic of the resultant beam behaviour to the problem depicted in Figure 3-1.

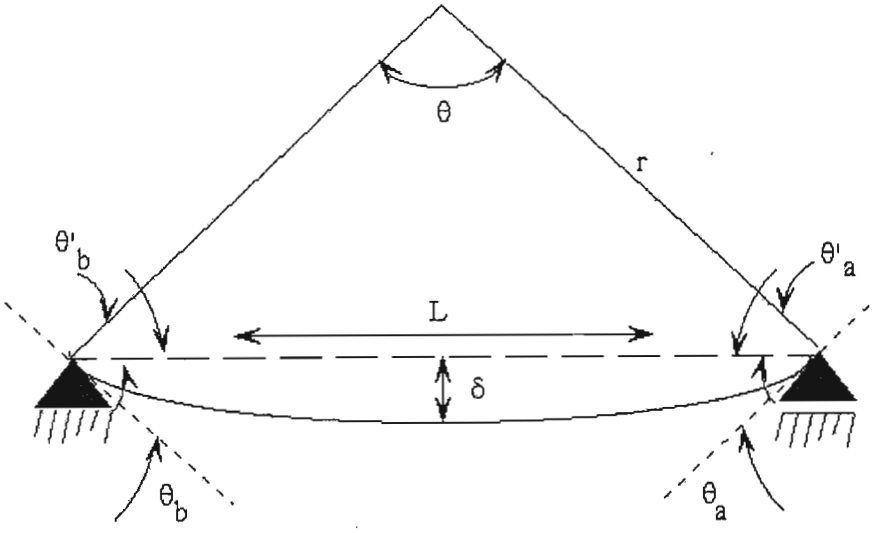

Figure 3-2 : Graphical analysis of the deflection of a beam

The angles of the tangents to the beam at the supports are,

$$\theta_a = \theta_b = \frac{PL^2}{16EI}$$

and as a result,

$$\theta_a' = \theta_b' = \frac{\pi}{2} - \theta_b$$

Using the geometric equations for a triangle, the subtended angle, θ, derives as,

$$\begin{aligned}\theta &= \pi - 2\left(\frac{\pi}{2} - \theta_b\right) \\ &= \pi - 2\left(\frac{\pi}{2} - \frac{PL^2}{16EI}\right) \\ &= \pi - \pi + \frac{PL^2}{8EI} \\ &= \frac{PL^2}{8EI}\end{aligned}$$

and by the sine rule the radius of curvature, r, of the deflected beam is,

$$r = L\frac{\sin\left(\frac{\pi}{2} - \frac{PL^2}{16EI}\right)}{\sin\left(\frac{PL^2}{8EI}\right)}$$

The strain of the beam is defined as the ratio of the change in length to the original length and is given by,

$$\begin{aligned}\varepsilon &= \frac{\Delta L}{L} \\ &= \frac{r\theta - L}{L} \\ &= \frac{PL^2 \sin\left(\frac{\pi}{2} - \frac{PL^2}{16EI}\right)}{8EI \sin\left(\frac{PL^2}{8EI}\right)} - 1\end{aligned}$$

Solving this equation in terms of δ yields,

$$\varepsilon = \frac{\left(\frac{6\delta}{L}\right)\sin\left(\frac{\pi}{2} - \frac{3\delta}{L}\right)}{\sin\left(\frac{6\delta}{L}\right)} - 1$$

where

$$\delta = \frac{PL^3}{48EI}$$

It should be noted at this point that this is the strain-displacement relationship for the beam as a whole and is not representative of the contact area under the impactor. The area directly below the impacting mass (or in the case of a Charpy test, the area at the notch) experiences a larger value of localised strain, and it is this higher strain that is responsible for initiating material failure. Thus, a strain factor is introduced that takes into account this localised strain. The strain factor, ε_{factor}, is considered to be a physical quantity dependent on the length of the beam, the beam cross-section (second moment of area), the contact area of the impactor and the impacting energy. Thus,

$$\varepsilon_{factor} = k\frac{I}{LA^3}mv^2$$

where k is the proportionality constant, I is the second moment of area, L is the beam length, A is the contact area, m is the mass and v is the impact velocity.

Since the strain factor is dependent only on the physics of the system and not on the material, once the value has been determined, it can be fixed for a particular set-up. This is useful for the current investigation since the test set-up remains unchanged from the normal composite to the smart composite analysis.

Also, it is important to remember at this point that in current theory, aluminium does not have a definable yield point (see Figure 3-3) and hence, the conventional strain value of 0.2 % is used to distinguish between the elastic and plastic regions of deformation. This assumption is not necessary when using the damage modulus method of analysis described earlier.

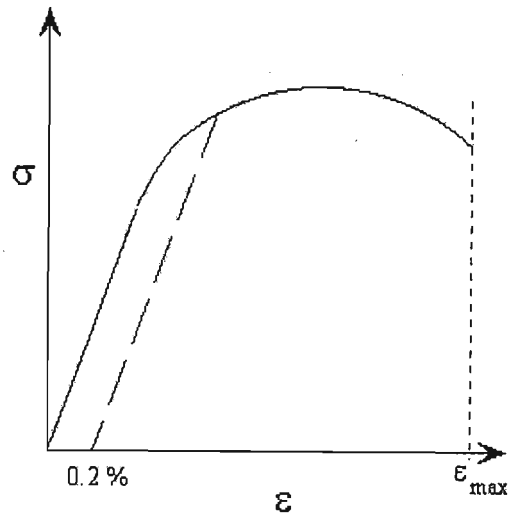

Figure 3-3 : Typical stress-strain curve for aluminium

Now, given the impact velocity of a free-falling projectile of mass, m, the height, h, through which the mass has to fall can easily be calculated as (Figure 3-4),

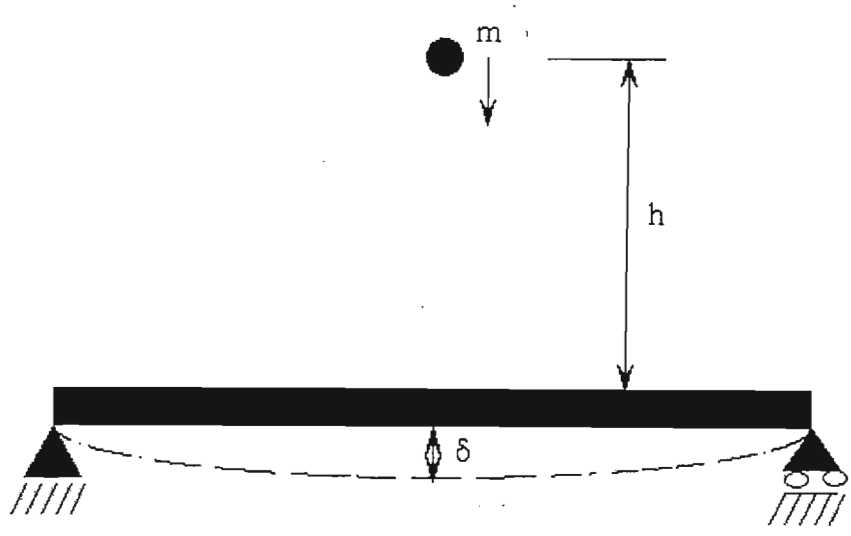

Figure 3-4 : Schematic of impact due to falling mass

$$h = \frac{v^2}{2g}$$

In considering the energy absorption of the beam, the analysis is separated into an elastic component and a plastic component. For the elastic component, the time $t = 0$ is when the mass contacts with the beam.

For now, the assumption is made that the mass does not slow down once it impacts the beam and hence the displacement of the beam is given as,

$$\begin{aligned} \delta &= vt \\ &= \sqrt{2gh}\,t \end{aligned}$$

The time for the beam to reach a state of plasticity is determined by using the plasticity strain and rate of displacement given in the preceding equations.

$$\varepsilon = \frac{\left(\frac{6\delta}{L}\right)\sin\left(\frac{\pi}{2} - \frac{3\delta}{L}\right)}{\sin\left(\frac{6\delta}{L}\right)} - 1$$

If plasticity strain = ε_p, then

$$\varepsilon_p = \frac{\left(\frac{6\delta_p}{L}\right)\sin\left(\frac{\pi}{2} - \frac{3\delta_p}{L}\right)}{\sin\left(\frac{6\delta_p}{L}\right)} - 1$$

where δ_p is the displacement to form a plastic hinge at the midpoint of the beam along its length.

Time to plasticity, t_p, is then,

$$\delta_p = vt_p$$

The simplest way to determine the energy absorbed is to consider the strain energy of the beam. Consider Figure 3-5.

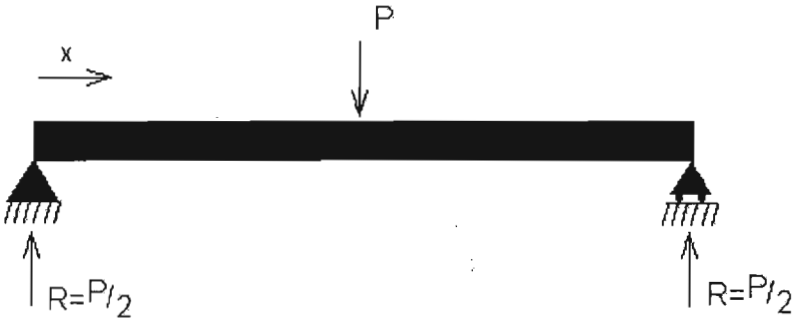

Figure 3-5 : Description of a simply supported beam for strain energy calculation

$$beam\ strain\ energy = 2\int_0^{L/2} \frac{M^2}{2EI}dx$$

where M is the bending moment and x is the distance along the length of the beam.

$$beam\ strain\ energy = 2\int_0^{1/2}\frac{(Rx)^2}{2EI}dx$$

$$= \frac{2R^2}{2EI}\frac{x^3}{3}\Big|_0^{1/2}$$

$$= R\frac{2RL^3}{48EI}$$

$$= \frac{P}{2}\delta$$

since $R = \frac{P}{2}$.

However, this is only representative of the elastic deformation of the beam, and in a Charpy test, around which this theory is developed, the beam is stressed to beyond its elastic limit to ultimate failure. Thus, it is not enough to simply use the elastic strain energy of the beam, and the entire work done on the beam needs to be considered, i.e.

$$Energy = Work = \int_{\delta=0}^{\delta @ ultimate\ failure} P d\delta$$

Further, to achieve a more realistic characterisation of the energy absorption, the beam resistance and decrease in the velocity of the mass need to be taken into account. Consider an arbitrary time t, during the elastic range of deformation. The mass has a velocity of v and an associated energy of $\frac{1}{2}mv^2$. After time interval dt, and ignoring the effects of potential energy due to the change in δ, to simplify the analysis, the energy state of the mass is,

$$Energy_{mass} = \tfrac{1}{2}mv^2 - \Delta Work\ done\ on\ beam$$

$$= \tfrac{1}{2}mv^2 - P\delta_{dt}$$

$$= \tfrac{1}{2}mv^2 - Pvdt$$

Note that the energy balance equation excludes contact energy dissipation, as it was not measured in the experimental work on which the model is based. This has been done to enable model verification and a more accurate comparison between energy absorption capacities.

This energy must now be associated with its new velocity, v_1, to comply with the conservation of energy law. Thus,

$$\tfrac{1}{2}mv_1^2 = \tfrac{1}{2}mv^2 - Pvdt$$

$$v_1^2 = v^2 - \frac{2P}{m}vdt$$

$$\frac{v_1^2 - v^2}{v} = -\frac{2P}{m}dt$$

Solving for the characteristics of velocity yields,

$$\frac{v_1^2 - v^2}{v} = -\frac{2P}{m}dt$$

$$= -\frac{(2)(48)EI}{mL^3}\delta dt$$

$$= -\frac{(2)(48)EI}{mL^3}vtdt$$

$$\frac{v_1^2 - v^2}{v^2} = -\frac{(2)(48)EI}{mL^3}tdt$$

$$\frac{1}{v^2}dv^2 = -\frac{2k}{m}tdt$$

Integrating both sides,

$$\ln v^2 = -\frac{2k}{m}\frac{t^2}{2} + c$$

$$v^2 = Ae^{-\frac{k}{m}t^2}$$

where $A=e^c$.

@ $t=0$, $v=v_o$ (impact velocity) and $A=v_o^2$. Thus,

$$v^2 = v_o^2 e^{-\frac{k}{m}t^2}$$

$$v = \sqrt{v_o^2 e^{-\frac{k}{m}t^2}}$$

The displacement of the beam, taking into account strain energy absorption, is given by,

$$\delta = vt$$
$$= \sqrt{v_o^2 e^{-\frac{k}{m}t^2}}\, t$$

The energy during the elastic range now assumes the form of,

$$Energy = \int P d\delta$$
$$= \int \frac{48EI}{L^3} \delta d\delta$$
$$= \int \frac{48EI}{L^3} \sqrt{v_o^2 e^{-\frac{k}{m}t^2}}\, t\, v dt$$
$$= \int \frac{48EI}{L^3} \sqrt{v_o^2 e^{-\frac{k}{m}t^2}}\, t \sqrt{v_o^2 e^{-\frac{k}{m}t^2}}\, dt$$
$$= \int \frac{48EI}{L^3} v_o^2 e^{-\frac{k}{m}t^2} t\, dt$$

Further, the load P, can be calculated from the stress in the beam as,

$$\sigma = \frac{M\bar{y}}{I}$$
$$M = \frac{PL}{4}$$
$$P = \frac{4\sigma I}{\bar{y}L}$$

Assuming that the changes in L and b are negligible,

$$P = \frac{2\sigma b d^2}{3L}$$

It is important to note that when the elastic point is exceeded and plasticity commences, the beam no longer offers resistance to the load and the energy absorption increases as the beam deforms plastically to the breaking point. At this stage, there are two important considerations. Firstly, if the shape of the stress-strain curve, Figure 3-3, is considered, it is evident that the energy absorbed in the plastic region is greater than the energy absorbed in the elastic region of deformation, i.e. the area under the elastic portion of the curve is less than that under the plastic portion of the curve.

Secondly, from the onset of plastic deformation, the depth of the beam is no longer constant and decreases until the remaining cross-sectional area is no longer sufficient to support the external load in shear. Thus, the final depth of the beam before ultimate failure is given by,

$$depth_{final} = \frac{Load}{(Beam\ Strength)(Width)}$$

Combining the elastic and plastic regions results in the total energy absorption of equation form below.

$$Energy = \int P\delta_{t=0}^{t=t_p} + \int P\delta\Big|_{t=t_p}^{t=t_f}$$

3.2 SMA Unidirectional Reinforced Aluminium

In modelling a unidirectional composite, several assumptions have to be made. Fibres are assumed to be unidirectionally distributed throughout the composite, have uniform properties and diameters and be perfectly bonded to the matrix. Perfect bonding implies that the fibre strains, matrix strains and composite strains are all equal.

Thus,

$$\varepsilon_c = \varepsilon_m = \varepsilon_f$$

where the subscripts c, m and f refer to the composite, matrix and fibre respectively.

Further, to ensure a fibre controlled composite failure the fibre volume fraction, v_f, must be equal to or greater than,

$$v_f = \frac{\sigma_{mu} - (\sigma_m)_{\varepsilon_f^*}}{\sigma_{fu} + \sigma_{mu} - (\sigma_m)_{\varepsilon_f^*}}$$

where σ_{mu} is the matrix ultimate strength, σ_{fu} is the fibre ultimate strength and $(\sigma_m)_{\varepsilon_f^*}$ is the matrix stress at fibre fracture strain.

Assume for the moment that the velocity on impact remains constant through the region of strain from zero to the SMA transformation strain. Once again, the velocity on impact is,

$$v_o = \sqrt{2gh}$$

and the displacement of the beam is given by,

$$\begin{aligned}\delta &= vt \\ &= \sqrt{2ght} = \frac{PL^3}{48EI}\end{aligned}$$

The load is obtained from,

$$\begin{aligned}\sigma_c &= \frac{M\bar{y}}{I} \\ &= \frac{PLd}{8I}\end{aligned}$$

where d is defined earlier as the depth of the beam.

Using the assumption of perfect bonding, the stress in the fibre is solved for as follows,

$$\frac{\sigma_c}{E_c} = \frac{\sigma_m}{E_m} = \frac{\sigma_f}{E_f} \Rightarrow \sigma_f = \frac{\sigma_c E_f}{E_c}$$

or $\sigma_f = \varepsilon E_f$ where ε is determined from the displacement of the beam. When the fibre strain equals the transformation strain, γ_T, the stress in the composite is,

$$\sigma_{c_T} = \varepsilon_f E_c$$

where σ_{c_T} is the stress in the composite at the transformation point.

Once the composite transformation stress is obtained, the transformation load can be solved from,

$$P_T = \frac{8I\sigma_{c_T}}{Ld}$$

The energy absorption of the beam up to the point of transformation is,

$$\begin{aligned} Energy &= \int P d\delta \\ &= \int \frac{48EI\left(\sqrt{2gh}\right)^2}{L^3} t dt \Bigg|_{t=0}^{t=t_T} \end{aligned}$$

If the decreasing velocity of the mass is taken into account then,

$$v = \sqrt{v_o^2 e^{-\frac{k}{m}t^2}}$$

and the energy absorption becomes,

$$\begin{aligned} Energy &= \int P d\delta \\ &= \int \frac{48EI}{L^3} \delta d\delta \\ &= \int \frac{48EI}{L^3} \sqrt{v_o^2 e^{-\frac{k}{m}t^2}}\, t\, v dt \\ &= \int \frac{48EI}{L^3} \sqrt{v_o^2 e^{-\frac{k}{m}t^2}}\, t \sqrt{v_o^2 e^{-\frac{k}{m}t^2}}\, dt \\ &= \int_{t=0}^{t=t_T} \frac{48EI}{L^3} v_o^2 e^{-\frac{k}{m}t^2} t\, dt \end{aligned}$$

This is similar to the energy absorption of the un-reinforced aluminium host beam derived earlier.

For the energy absorption characteristics in the transformation environment, i.e. $\gamma_T \leq \varepsilon \leq \gamma_{T\max}$, (where γ_T is the transformation strain and $\gamma_{T\,max}$ is the maximum transformation strain), the physical properties of the composite is based on the martensitic fraction which in turn is based on the strain of the SMA fibres. The general description of the martensitic transformation in SMA is depicted in Figure 3-6.

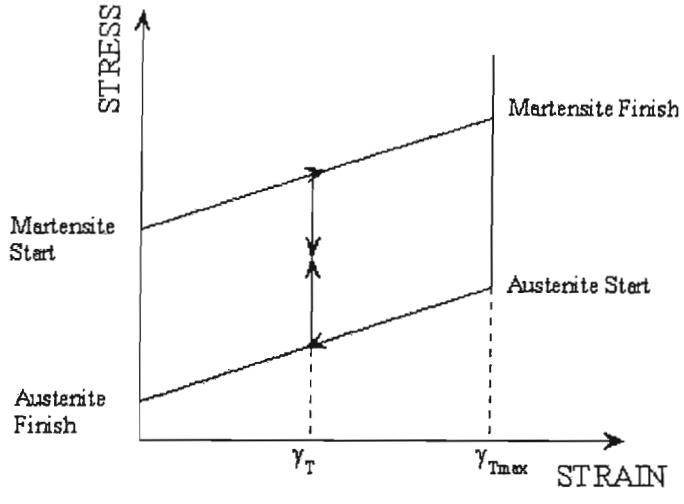

Figure 3-6 : General description of the SMA transformation process

Since it is evident from Figure 3-6 that the strain is linear from γ_T to $\gamma_{T\,max}$, the martensitic fraction is also assumed linear from 0 % to 100 %. Thus,

$$F_M = \frac{\varepsilon - \gamma_T}{\gamma_{T\,\max} - \gamma_T}$$

where F_M is the martensitic fraction.

If it is further assumed that the properties of the SMA fibres vary linearly from the austenitic phase to the martensitic phase according to the martensitic fraction then,

$$E_{fM} = E_{fA} - F_M\left(E_{fA} - E_{fM}\right)$$

where E_{fM} is the modulus of the fibre in the martensitic phase and E_{fA} is the modulus of the fibre in the austenitic phase.

The velocity of the transformation point is,

$$v_T = \sqrt{v_o^2 e^{-\frac{k}{m} t_T^2}}$$

and applying the energy balance equation for strain energy results in,

$$Energy = \tfrac{1}{2}mv^2 - Pd\delta$$
$$= \tfrac{1}{2}mv^2 - \frac{48E_cI\delta}{L^3}d\delta$$

The displacement is given by $\delta = vt$ and the modulus of the composite by,

$$E_c = \upsilon_f E_f + \left(1-\upsilon_f\right)E_m$$
$$= \upsilon_f\left[E_{fA} - F_M\left(E_{fA} - E_{fM}\right)\right] + \left(1-\upsilon_f\right)E_m$$
$$= \upsilon_f\left[E_{fA} - \frac{\varepsilon - \gamma_T}{\gamma_{T\max} - \gamma_T}\left(E_{fA} - E_{fM}\right)\right] + \left(1-\upsilon_f\right)E_m$$

An analysis of the energy absorption yields,

$$Energy = \tfrac{1}{2}mv^2 - \frac{48I}{L^3}\delta\left\{\upsilon_f\left[E_{fA} - \frac{g(\delta)-\gamma_T}{\gamma_{T\max}-\gamma_T}\left(E_{fA}-E_{fM}\right)\right] + \left(1-\upsilon_f\right)E_m\right\}d\delta = \tfrac{1}{2}mv_1^2$$

$$\tfrac{1}{2}mv^2 - \frac{48I}{L^3}vt\left\{\upsilon_f\left[E_{fA} - \frac{g(vt)-\gamma_T}{\gamma_{T\max}-\gamma_T}\left(E_{fA}-E_{fM}\right)\right] + \left(1-\upsilon_f\right)E_m\right\}vdt = \tfrac{1}{2}mv_1^2$$

$$\tfrac{1}{2}m\left(v_1^2 - v^2\right) = \frac{48I}{L^3}v^2\left\{\upsilon_f\left[E_{fA} - \frac{g(vt)-\gamma_T}{\gamma_{T\max}-\gamma_T}\left(E_{fA}-E_{fM}\right)\right] + \left(1-\upsilon_f\right)E_m\right\}tdt$$

$$\frac{1}{v^2}dv^2 = \frac{(2)(48)I}{mL^3}\left\{\upsilon_f\left[E_{fA} - \frac{g(vt)-\gamma_T}{\gamma_{T\max}-\gamma_T}\left(E_{fA}-E_{fM}\right)\right] + \left(1-\upsilon_f\right)E_m\right\}tdt$$

Integrating this expression and solving for v results in $v = f(t) + D$, where D is a constant. The energy absorbed during this transformation stage is thus,

$$Energy = \int\frac{48E_cI}{L^3}\delta d\delta$$

where $\delta = vt$.

If, during transformation, the displacement is kept constant, the force increases to account for the energy required for martensitic conversion. Thus, the energy graph during this stage should be similar to the pure aluminium beam, only greater in magnitude, i.e., Figure 3-7, for example,

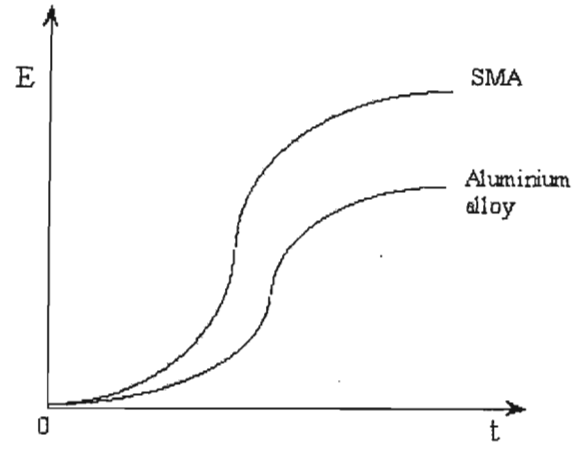

Figure 3-7 : Energy of SMA reinforced aluminium during the transformation stage

After the martensitic transformation, ($\gamma_{T\max} \leq \varepsilon \leq \varepsilon_{fail}$ where ε_{fail} is the failure strain), since the composite is governed by a fibre controlled failure, the material continues to bear load until the strain in the fibre reaches the ultimate martensitic fracture strain, at which point the material fails.

The velocity at the end of transformation is $v = f(t)$ at $F_M = 1$. The material has a new Young's modulus and is assumed to react in a conventional manner once again. The analysis for post-transformation is thus similar to the pre-transformation analysis, i.e.,

$$P = \frac{8I\sigma}{Ld}$$

and

$$Energy = \int P d\delta$$

with $\delta = vt$, where $v = \sqrt{v_{ot}^2 e^{-\frac{k'}{m}t^2}}$ and v_{ot} = velocity at $F_m = 1$ and k' = new stiffness value due to the change in E.

3.3 Magnetostrictive Unidirectional Fibre Inclusions in SMA Unidirectional Reinforced Aluminium

Once again, perfect bonding between the matrix and fibres is assumed, resulting in equal strains across the composite. Further, the total volume fraction of the fibres is kept constant to that

determined in section 3.2 to enable valid comparison of energy absorption and energy absorption rates between the materials, i.e.

$$\upsilon_{fSMA} + \upsilon_{fMag} = \upsilon_f$$

where υ_{fSMA} and υ_{fMag} are the SMA fibre volume fraction and magnetostrictive fibre volume fraction respectively.

The initial orientation of the magnetic field is in the direction orthogonal to the fibre axis as shown in Figure 3-8.

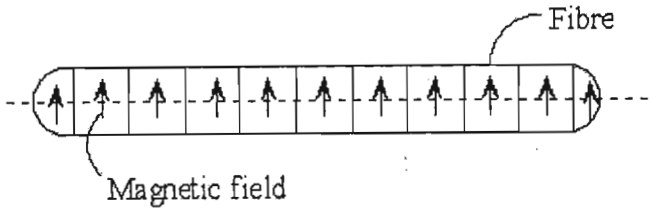

Figure 3-8 : Initial magnetic field orientation in magnetostrictive fibres

If the magnetostrictive material is activated as soon as impact occurs, then the strain in the composite is given by,

$$\varepsilon_{TOT} = \varepsilon_L + \varepsilon_{Mag}$$

where ε_{TOT} is the total strain in the composite, ε_L is the strain due to the external load and ε_{Mag} is the strain due to the magnetostrictive inclusions.

Consider first the range of strain from zero to the point of transformation. The magnetic strain component is constant and is given by,

$$\varepsilon_{Mag} = \frac{3\lambda_s}{2}\left(\frac{H^2}{H_A^2} - \frac{1}{3}\right) = const$$

where H, H_A and λ_s have been previously defined in Chapter 2.

For simplification of analysis, it is assumed that the beam is simply supported with quasistatic magnetic loading. Thus, the magnetically induced strain has no resulting deflection, but causes a prestress condition in the beam. From the previous analysis and combining stresses,

$$\sigma_c = E_c \varepsilon_{TOT} = E_c \varepsilon_L + E_c \varepsilon_{Mag}$$

The Young's modulus of the composite is determined by,

$$E_c = \upsilon_{fSMA} E_{fSMA} + \upsilon_{fMag} E_{fMag} + \left(1 - \upsilon_f\right) E_m$$

where E_{fSMA} and E_{fMag} are the modulus of the SMA fibre and magnetostrictive fibre respectively.

Solving for load results in,

$$P = \frac{8I\sigma}{Ld}\delta$$
$$= \frac{8I\delta}{Ld}\left(\sigma_L + \sigma_{Mag}\right)$$

Thus, the resulting energy absorption is given in Figure 3-9,

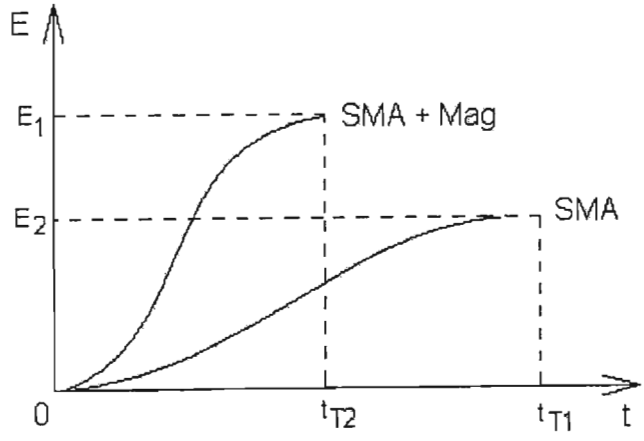

Figure 3-9 : Energy absorption as a result of magnetostrictive inclusion before SMA transition

mechanism to activate a preset magnetic field strength, facilitating immediate maximum strain within the magnetostrictive fibres.

While this method is theoretically feasible, care must be exercised in the selection of the piezoelectric layer material and geometry. The sensor forms the surface that receives the impact, and the resulting initial load and indentation must be tolerable by the piezoelectric surface in terms of fracture toughness. A material and geometry of too low fracture toughness will crack and severely impair, if not completely sever, the output of the electromagnet. Further, the piezoelectric layer needs to be flexible enough to accommodate a strain that will ensure completion of the SMA transformation process. This is vital to achieve the maximum benefit of the SMA inclusions. As already stated in section 2.4, linear piezoelectric theory deals with small displacement and structural vibrations, and assumes quasi-static motion indicating that the mechanical and electric forces are balanced at any given constant. The non-linear theory deals with the dynamics of anisotropic piezoelectrics undergoing large displacements. Thus, to be able to model the current experimental configuration, non-linear theory needs to be adopted. This on its own forms a complex and detailed analysis that is beyond the scope and objectives of this investigation.

CHAPTER 4

4 DISCUSSION OF RESULTS

The objective of this chapter is not just a discussion of the results obtained through numerical modelling, but rather, a discussion of all work undertaken and results achieved throughout the course of this investigation. Thus, an important outcome of this chapter is a clear differentiation between the author's own work and that which is borrowed from other sources to help in the achievement of the final objective.

4.1 General

The primary objective of this study is to develop a useable model for predicting the response of smart materials to impact loading. The response that is considered the focus of the investigation is energy absorption, with the load response being used as the preferred methodology. The specific material chosen is a unidirectional, fibrous metal matrix composite with aluminium as the host substrate and nitinol as the reinforcement. Table 4-1 highlights the critical properties of the materials used in the current investigation.

Table 4-1: Properties of materials used in this investigation

Material	Property					
	Young's Modulus [GPa]		Ultimate Tensile Strength [MPa]	Shape Memory Transition Strains [%]		Failure Strain [%]
Aluminium AC8A	73		265	-	-	1.14
Aluminium Oxide	310		2000	-	-	0.64
Nitinol	30 (A)	13 (M)	1600	2.21*	7.97**	14.5

* This is the strain at the start of the martensite phase transformation.

** This is the strain at the end of the martensite phase transformation.

The literature review of Chapter 2 is used as the foundation of this thesis and represents the author's interpretation of the various articles. As is evident from Chapter 2, there is very little published information that can be used directly, especially in terms of analytical models. The literature review thus serves as a means of developing a broad understanding, physically, of various individual components of the study, viz. microstructural behaviour of SMA, general impact

loading phenomenon, general behaviour of composite materials (interactive behaviour between elements), as well as magnetostrictive and piezoelectric phenomenon.

The literature review also highlights the need for a robust analytical model that can simplify the predictions of material response of metal matrix SMA specifically, and complex materials in general. Thus, the theoretical characterisation of the system presented in Chapter 3 forms the heart of the study, and the simple, yet profound concepts proposed are completely the individual work of the author. An extension of the author's individual work, and coupled to this unique theoretical characterisation, is the software code to numerically simplify the analytical model. The code is developed in conjunction with the literature review, i.e. the fundamental interactive behaviour of the various components is used to promote a logical and realistic interpretation of the proposed theory.

The reader's attention is now drawn to the results of the numerical analyses. All the results presented from this point onward are the sole effort of the author, with the exception of the comparative results of section 4.4. While the model predicted results are that of the author, the experimental results are those of Aggag et. al. and have been so accredited.

4.2 Damage Modulus

At this point the reader is asked to reflect upon the concept of the elastic modulus, or Young's modulus, E. Young's modulus is so called after the English scientist Thomas Young, who introduced the idea of a 'modulus of elasticity' after investigations of tension and compression of prismatic bars. The modulus itself has since been refined and is in effect the slope of the stress-strain diagram in the linearly elastic region of a material. From its humble beginnings, the elastic modulus has become a corner stone of modern mechanical design engineering, the most important consequence being the formulation of Hooke's law.

Hooke's law characterises the linear relationship between applied load and the resulting elongations. The most common equation, $\sigma = E\varepsilon$, is a limited version as it relates only to the normal stresses and strains developed in simple tension and compression. The generalised Hooke's law is the equations for three-dimensional stress-strain relationships. Unfortunately, all the resultant simplifications of Hooke's law and the modulus of elasticity are limited to a definite range of a materials stress-strain cycle. Consequently, the majority of engineering designs have also become limited to this finite 'operating range' of a material and thus, the full capability of a

material is not utilised. Imagine the impact of such a concept in the plastic range of a material's behaviour, or of a single factor that incorporates both elastic and plastic material responses!

This 'modulus of plasticity' is referred to in this text as the damage modulus, E_D. It may even be considered as a 'modulus of elasto-plasticity' as it incorporates elastic material behaviour as well. Advantages of E_D are that it extends Hooke's law to beyond the elastic limit of a material right up to the point of ultimate failure and it is applicable to most, if not all, materials, including ductile materials, brittle materials and exotic materials such as SMA as indicated in the figures below. Further, no new testing of materials is required as E_D is derived directly from existing material stress-strain relationships.

The concept of stiffness (modulus) degradation is not new. Kachanov initially proposed it in 1958 in terms of scalar damage concept that is based on the ratio of damage area and nominal area. Since then a number of damage formulations have appeared in the literature. While the manner in which these formulations implement the damage parameter is different (Bazant and Jirasek: 2002), the underlying concept is the same, i.e. the damage parameter is a complex derivation that is used to modify the nominal stress-strain diagram. The damage modulus, E_D, proposed in this investigation is unique firstly in its simplicity and secondly in that it does not change the material's nominal stress-strain diagram, but is in fact derived from it. Figures 4-1 and 4-2 show the derived damage modulus for an aluminium alloy, AC8A, and resulting stress-strain diagram, respectively, based on an extension of Hooke's law.

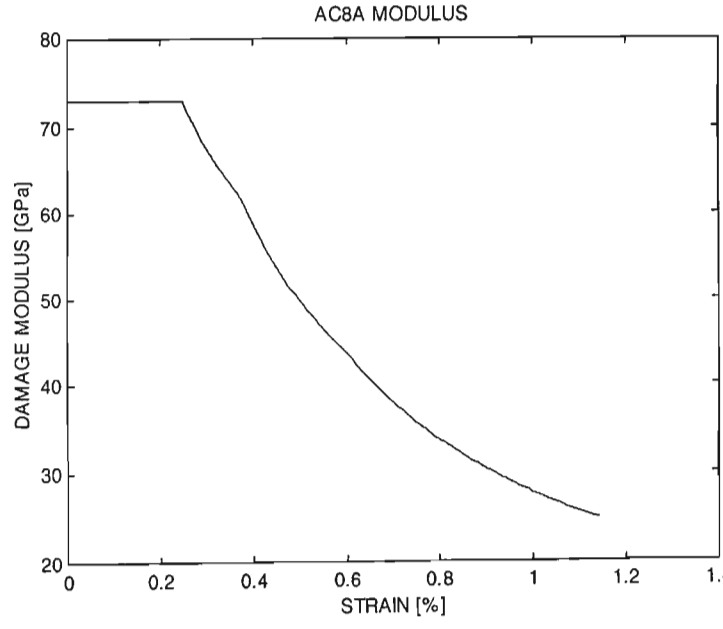

Figure 4-1: Damage modulus for AC8A aluminium alloy

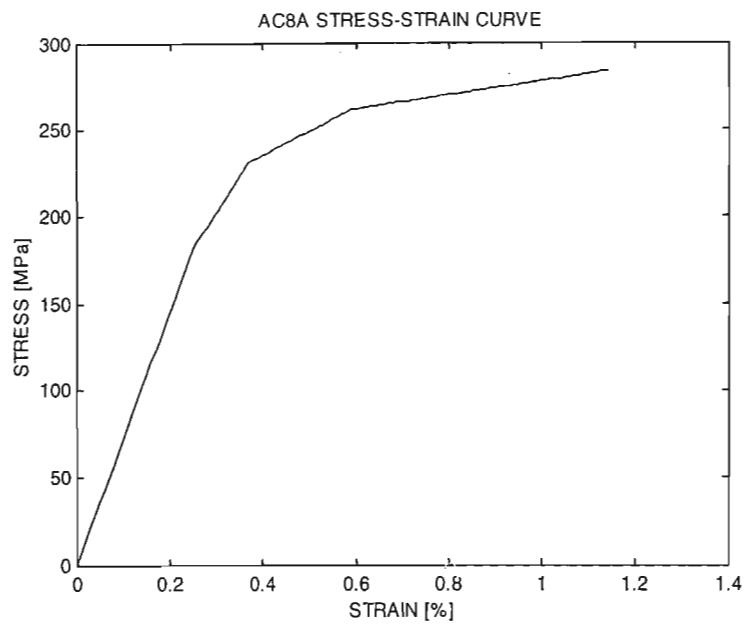

Figure 4-2: Stress-strain curve for AC8A aluminium alloy

The characteristic that is immediately apparent in Figure 4-1 is that there is a clear distinction between the elastic and plastic behavioural regions of the material. The initial constant region of E_D characterises the elastic material behaviour and is equivalent to Young's modulus, while the subsequent region characterises the material beyond the elastic limit. The reader's attention is directed to the deceasing value of E_D in the latter region of Figure 4-1 that corresponds to, very critically, a decreasing capacity of the material to sustain further load. This is a very important feature of the damage modulus as it takes into account degradation of the material through the plastic region, up to the point just before ultimate failure. Thus, E_D lends itself to the simplification of many damage models in terms of a reducing sustainable load and energy absorption capacity. Only the energy consumed through material rupture remains to be characterised.

Figure 4-3 shows the derived damage modulus for aluminium oxide (Al_2O_3). Aluminium oxide is a brittle material and does not undergo plastic deformation on a macro, bulk material level. Thus Figure 4-3 reflects a constant E_D that corresponds to the materials Young's modulus.

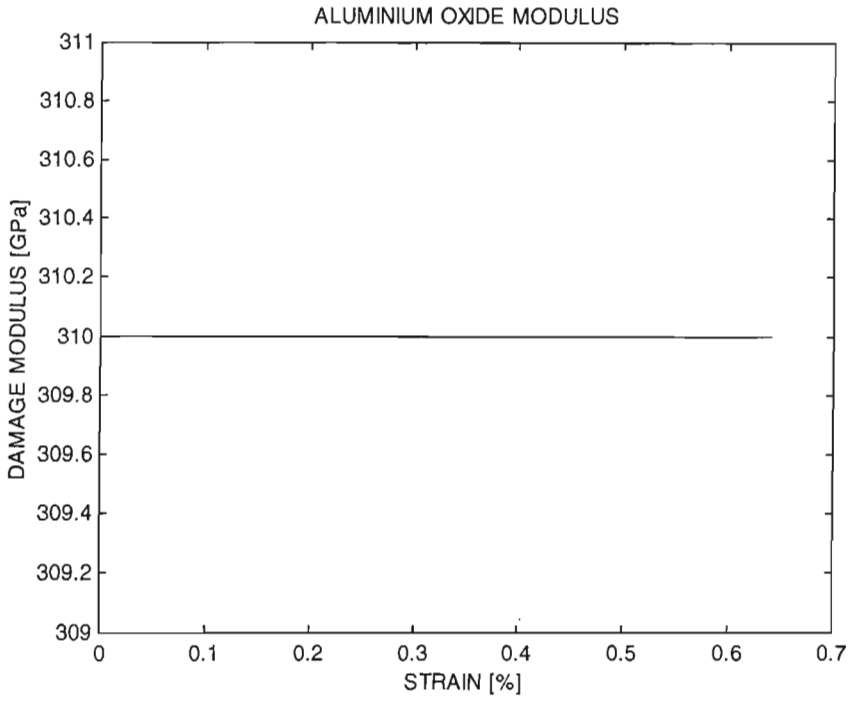

Figure 4-3: Damage modulus for aluminium oxide

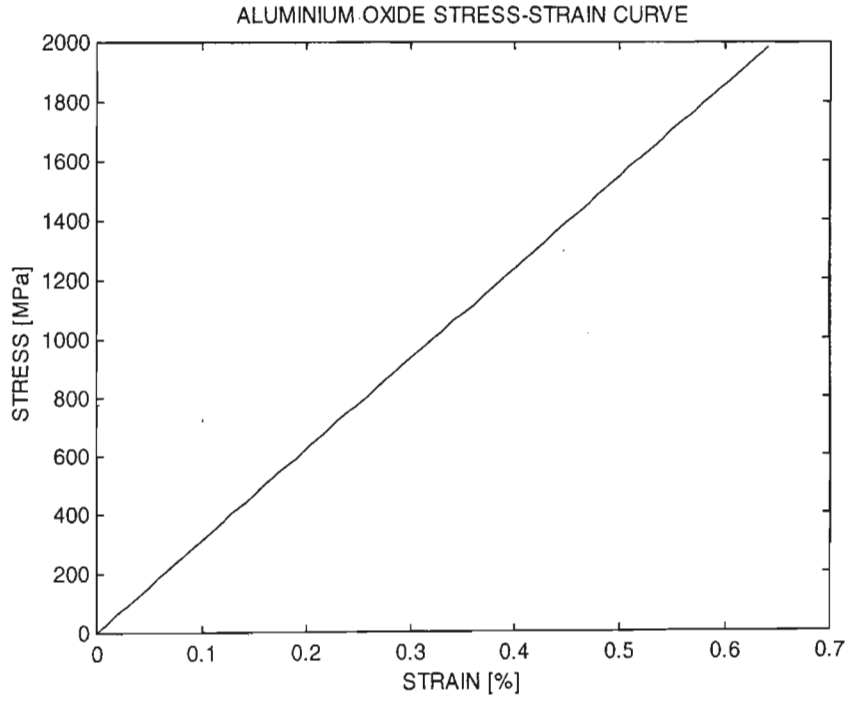

Figure 4-4: Stress-strain curve for aluminium oxide

The stress-strain curve of Figure 4-4 reinforces this purely elastic behaviour of Al_2O_3. The constant nature of the E_D-ε graph also shows that no material degradation is present during loading and that the rate of energy absorption is constant up to the point just before material rupture. This type of material behaviour helps to intuitively understand this new concept of E_D taking into account material degradation (damage) and apply this understanding to the damage modulus curve of AC8A (Figure 4-1).

The damage modulus curve and corresponding stress-strain diagram for the SMA, nitinol, are shown in Figures 4-5 and 4-6 respectively.

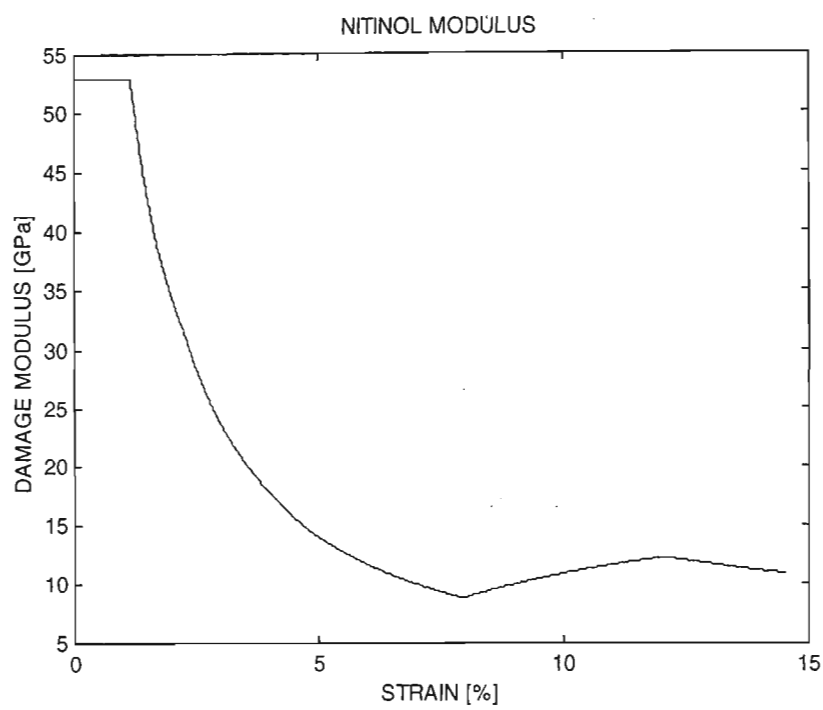

Figure 4-5: Damage modulus for nitinol

In this case, the first half of the E_D curve is very similar to Figure 4-1 (the E_D curve for AC8A), and is typical of similarly behaving materials. The initial constant E_D reflects Young's modulus and the subsequent decreasing E_D behaviour shows material degradation and damage. However, at approximately 8% strain, the shape memory response of nitinol takes effect resulting in a unique corresponding change in the materials E_D. During the shape memory transition phase, the stress-strain curve indicates a constant rate of change, similar to the initial Young's modulus rate. The corresponding phase in the E_D diagram interestingly does not reflect a constant specific value (as during the Young's modulus phase), but rather a constant differential. What is the significance of this trend? This trend emphasizes the close relationship between E_D and material energy absorption

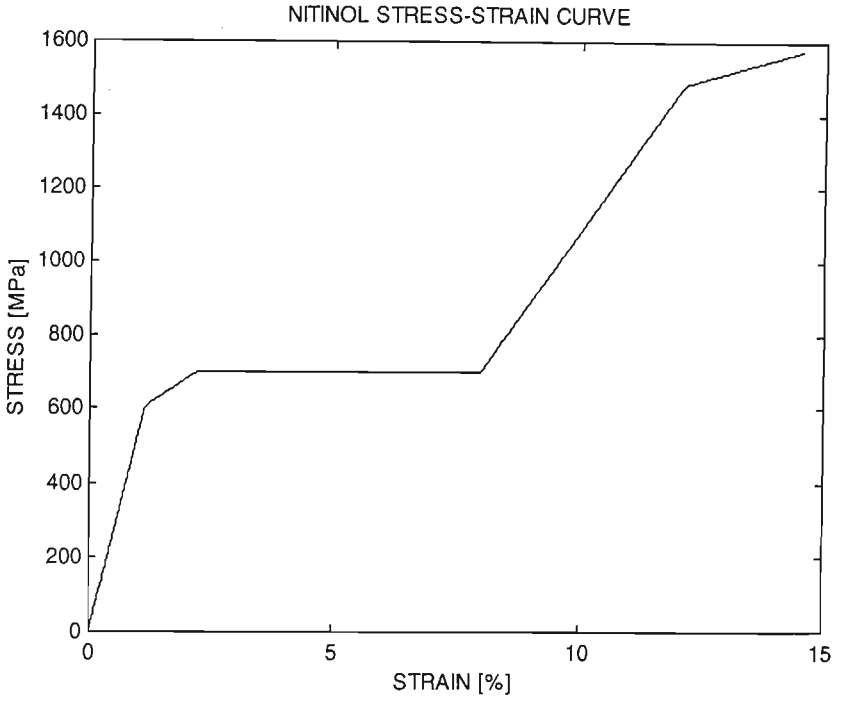

Figure 4-6: Stress-strain curve for nitinol

/ material degradation or damage discussed earlier, i.e. the increase in E_D during the shape memory transition phase indicates 'repair' of the materials properties or an increase in its energy absorption capacity. Once the shape memory transition is complete, the 'new' material properties begin to degrade and lose energy absorption capacity indicated by the corresponding decrease in E_D. Again, the only damage / energy that still needs to be considered is ultimate rupture of the material.

The author firmly believes that this new concept of a damage modulus will have enormous impact in many branches and fields of mechanical and material studies. The full consequences of E_D on other fields of study, however, is not the ultimate objective of this thesis and the author is of the opinion that adequate substantiation of this concept has been given to establish credibility to the reader. The damage modulus is an exciting new development that can one day lead to the full characterisation of a material, through its entire functional strain range, by simple equations currently only applicable up to the elastic limit.

4.3 Model Setup

Figure 3-1 describes the example used to demonstrate E_D as well as to investigate the energy absorption characteristics of SMA reinforced metal matrix composites. It is a simply supported

beam subjected to a falling mass impact load, and Chapter 3 describes the appropriate theory necessary to fully characterise the system kinematically. The reader will notice that this chapter is divided into four sub-sections, beginning with the most basic set-up and then proceeding in stages of increasing material complexity, i.e. the response of a pure aluminium beam is first characterised, followed by the response of a SMA reinforced aluminium matrix composite beam, then the composite beam with magnetostrictive inclusions and finally, an excerpt on piezoelectric control.

Along with the basic elastic stress / strength theory of the falling mass impact analysis, and the author emphasises the point that low velocity impact is only considered, the basic analysis of the pure aluminium beam also highlights three important considerations. The first is the geometric relationship between the two-dimensional beam displacement during the impact process to the one-dimensional longitudinal strain of the beam. This is very important as it facilitates the crossover from the load-displacement domain to the stress-strain domain, thus enabling the point of plasticity to be correctly determined from the material stress-strain curve. This transition also gives the author the opportunity to demonstrate the simplicity and capability of E_D. The second important consideration is the effect of the beam strain energy on the velocity of the falling mass. The velocity-displacement profile that is derived is based on the conservation of energy principle and demonstrates the integrity of the model in describing a real system. The effect of air resistance on the energy balance of the system is ignored and the effect of potential energy variation due to beam displacement is considered negligible. The velocity-displacement derivation yields an exponential relationship dependent on the stiffness of the beam, the mass of the projectile and the displacement / strain in the material (described in terms of time for simplification). Finally, this sub-section also explores, qualitatively, the amount of energy absorbed elastically compared to plastic energy absorption.

In the SMA reinforced composite analysis, the first part is devoted to basic and longitudinally reinforced fibrous composite theory, as well as application of the derived relationships discussed in the preceding paragraph. The crucial aspect of this part of the analysis is the consideration of the shape memory transition phase. In the current model, the author makes use of the previously considered (by other investigations and authors) concept of martensitic fraction. To compensate for a lack of publications in this area, and to simplify the analysis, the assumption is made that the properties of the SMA fibres vary linearly according to the martensitic fraction. However, it must be noted that by use of the damage modulus, the change in fibre properties is inherently incorporated, as E_D is based on the materials experimental stress-strain curve. Finally, this analysis sub-section ends with a derivation of the velocity-displacement relationship for a metal matrix SMA reinforced composite beam and includes characterisation through the transformation phase, another unique contribution by the author.

The analyses of the magnetostrictive and piezoelectric smart materials is very much limited in comparison to the previous two characterisations. For this discussion purposes, it is enough to say that only basic magnetostrictive theory is presented, but it is sufficient to draw the conclusion that the effect of magnetostrictive inclusions in the SMA reinforced composite can be taken into account by applying varying degrees of prestrain to the composite beam, to simulate varying degrees of magnetic field. Again, a velocity-displacement relationship is presented. No theoretical description is put forward for piezoelectric materials as the author has decided to exclude it as part of the fundamental investigation; however, a brief description of a possible control method for the magnetostrictive inclusions in the beam is presented.

4.4 Model Verification by Numerical Analysis

Numerical simulation has been employed as a means of solving the proposed analytical model for a given set of conditions. Matlab is the simulation software of choice, primarily because the author is familiar with the coding structure and capabilities. The author further believes that a line-by-line discussion of the code (presented in Appendix B) is not required and only key points are highlighted.

The first part of the code is used to define the various material properties, most important being the damage modulus for the aluminium alloy matrix, aluminium oxide fibre, SMA fibre and the resultant composite. At this point the reader is asked to recognise that all reference to 'modulus' in the code is reference to the damage modulus of the indicated material. Further on the point of E_D, it should be noted that the moduli are approximated by a series of consecutive straight lines to help with discretization and simplify the solution of the model.

After defining the damage modulus, the code proceeds to solve the analytical model in discreet time intervals. The methodology is as follows: The velocity at the beginning of the time interval is determined by subtracting the energy absorbed by the beam in the previous time interval from the total kinetic energy of the mass. This calculated velocity is then used to produce a discreet displacement through the current time interval, which in turn is transferred into the strain domain through the displacement-strain transformation equation discussed earlier. The resulting stress is determined by use of the equivalent damage modulus of the composite at that particular value of strain. The composite stress is converted, by geometric relations, into loads supported by the various components, i.e. the matrix, Al_2O_3 fibres and SMA fibres, which are finally used to determine the corresponding energy absorptions.

The final part of the code deals with determining failure of the system. The system is considered to have failed when either the stress in the composite reaches its maximum calculated strength or when the fibre strain exceeds its ultimate strain (depending on fibre volume fractions, either the Al_2O_3 fibre or nitinol fibre ultimate strain is used). Once the system has failed, the stress and strain is kept constant and the depth of the beam is allowed to decrease in a predetermined manner up to a specific value (both determined during the model verification phase) at which point complete rupture of the remaining section of the beam is assumed to take place.

With the model code now in place, the next step in the methodology is to refine the model to make it representative of the physical environment. Specifically, the strength factor, strain factor, geometric factor and depth factor (described in the methodology section of Chapter 1) is defined using real data. Experimental results obtained by Aggag et. al. on the falling mass impact of 15% Al_2O_3 fibre reinforced AC8A aluminium alloy is the closest work that could be sourced from available literature and is used to set the relevant factors for that stage of the model. These factors remain unchanged when carried through to the SMA investigation.

The results of the model verification are shown in Figures 4-7 and 4-8. Consider first the load-displacement diagram of Figure 4-7.

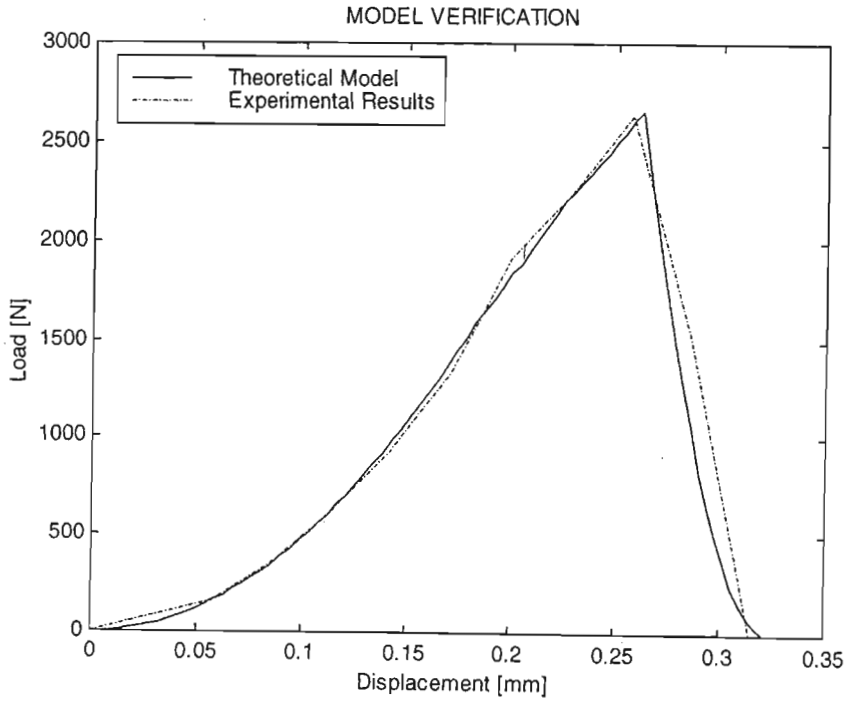

Figure 4-7 : Model verification – Experimental and predicted load-displacement results for an impact velocity of 1 m/s (modified after Aggag et. al.)

It is clearly evident that the theoretical model accurately describes the experimental trend in terms of shape of the curve, maximum load reached, strain at maximum load and maximum strain. Examining the shape of the curve yields an initial exponential increase in load followed by a phase of constant load increase up to a definite point and then a sudden decrease in load to zero. The initial exponential growth is as a result of both the matrix and fibre experiencing strain in the constant modulus regions of their respective stress-strain diagrams. Once the constant modulus strain of the matrix is exceeded, the matrix modulus (rate of change of stress) decreases and halts the exponential growth in load capacity to one that appears more linear, up to a point of maximum load capability. Interestingly, this specific point of sudden decrease in sustainable load does not only correspond to the ultimate failure strain of the composite, but also the plasticity strain (0.2 % proof stress) of the matrix.

The strain energy-displacement graph of Figure 4-8 also shows a close following of the model to the experimental data curves, with the theoretical model predicting a lower total energy absorbed by the beam. This difference in energy is attributed to the material rupture energy, which the model does not take into consideration. So far as shape of the curve is concerned, it is similar to the load-displacement curve, as expected.

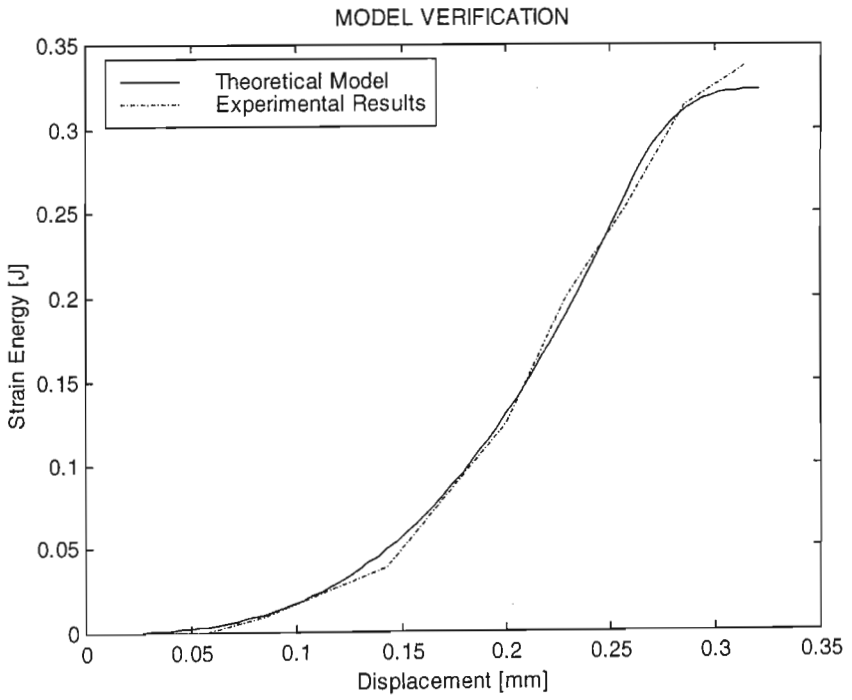

Figure 4-8 : Model verification – Experimental and predicted energy-displacement results for an impact velocity of 1 m/s (modified after Aggag et. al.)

The notable difference is that at the point of composite failure (and matrix plasticity), unlike the load curve that experiences a sudden decrease, the strain energy curve continues increasing, because of the additional work required in plastically deforming the beam, before levelling off to a final value.

4.5 SMA Response and Characterisation

With the integrity, accuracy and robustness of the model being verified in section 4.4, the thesis proceeds to the investigation of its primary objectives, i.e. to determine the effect of SMA in energy absorption during low velocity impact loading. At this level of the investigation relevant external publications are scarce; the author could not source even a single article that can be used as a comparison and discussion tool, despite an extensive literature review. Thus, the discussion of results is based purely on sound knowledge of individual component behaviour, logical reasoning and extrapolation of established trends and understanding.

Figures 4-9 and 4-10 show an example of the load and strain energy response, respectively, of a metal matrix composite beam with SMA inclusions. A 4% SMA volume fraction, out of a total fibre volume fraction of 15%, is chosen for illustration.

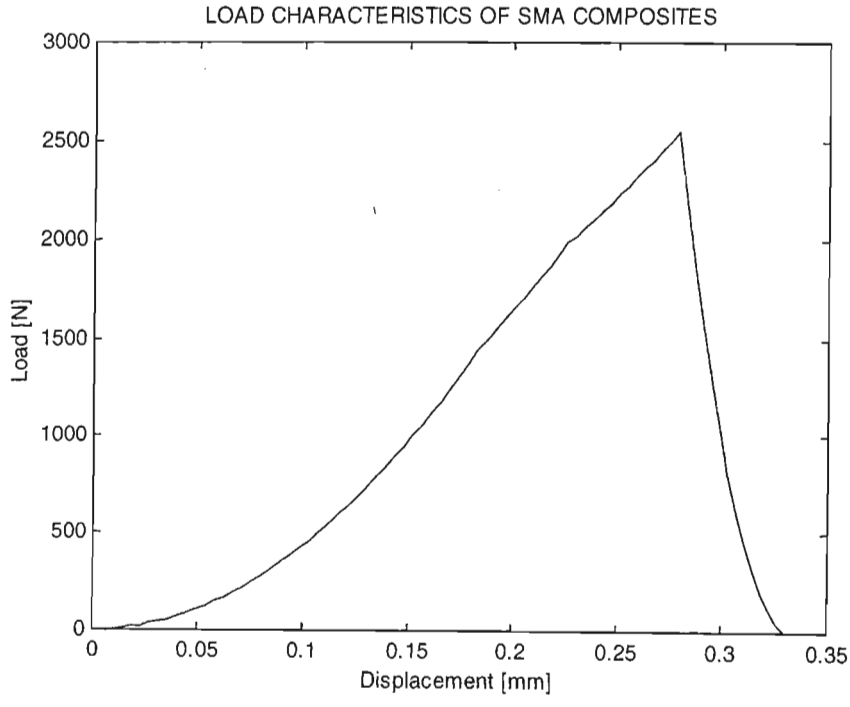

Figure 4-9 : SMA load-displacement response for 4% (chosen for purely illustrative purposes) SMA fraction

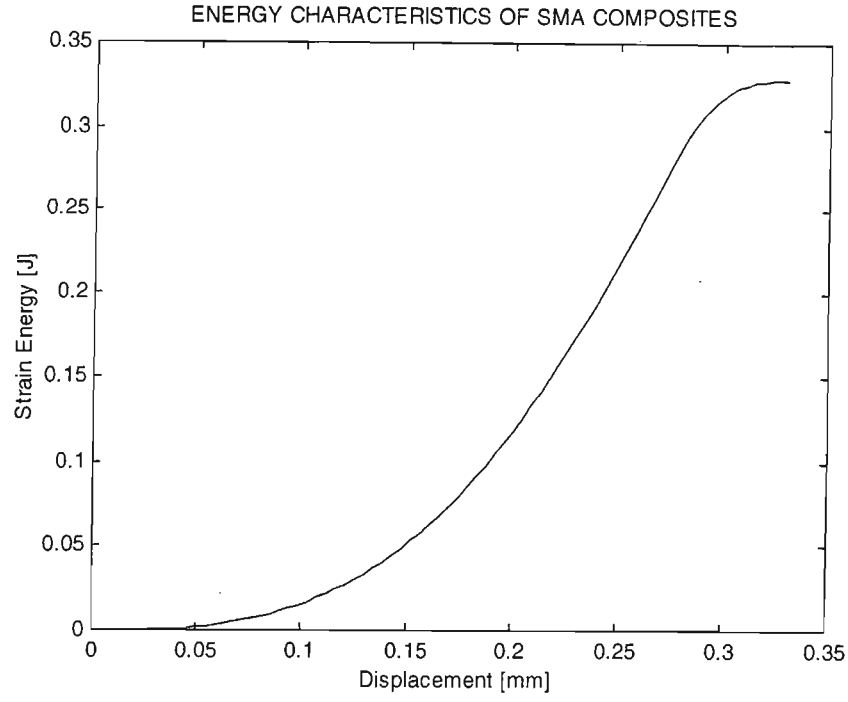

Figure 4-10 : SMA energy-displacement response for 4% (chosen for purely illustrative purposes) SMA fraction

Consider first the load-displacement diagram compared to the corresponding model verification graph of Figure 4-7. While the basic shapes of the graphs are very similar, two important details need to be highlighted. One is that the maximum load capacity of the beam with the SMA inclusions is reduced by approximately 4% as compared to the beam without the inclusions. Thus, the smart fibres diminish the capacity of the beam to sustain a load, at least for a 4% SMA volume fraction. Secondly, the displacement to maximum load is higher for the beam with the smart fibres than for the beam without. The importance of this difference is shown in Figure 4-10.

Again, the most important difference between the energy-displacement graph of Figure 4-10 and the corresponding model verification graph (no SMA inclusions) is not in the shape, but in the maximum energy absorption levels. The 4% smart fibre volume fraction gives the beam an approximate 1.6% increase in strain energy capacity. This, however, is not a direct result of the shape memory effect, but rather because of the higher toughness of the SMA fibres. One of the failure criteria is the ultimate strain of the Al_2O_3 fibres, which is approximately 0.6%, well below the initiation strain for the shape memory effect. A part of the energy that is absorbed though, must go to produce the extra displacement, off course. Thus, for this particular case, 0.002 J (0.6 %) of energy is used toward the additional displacement and the balance of 0.005 J (1.0 %) is consumed by the additional toughness of the SMA fibres. At this point the results look encouraging, but the question that needs to be asked is whether these results can be substantiated by analyses of other

SMA volume fractions, the results of which must form a definite trend and not be of an arbitrary (random) nature. Further, the effect of SMA transformation on energy absorption still needs to be determined.

The analysis of the effect of varying SMA volume fractions has been conducted and the results for the load and energy trends are depicted in Figure 4-11 and 4-12 respectively. As is evident from Figure 4-11, there is a definite trend of decreasing load capacity with increasing SMA volume fraction, which the author attributes to the lower strength of the nitinol fibres as compared to the aluminium oxide fibres. The nitinol fibre maximum strength is 20% lower than the aluminium oxide fibre maximum strength. Also evident from the Figure is that there are two clearly identifiable rates of load decrease; while there is only a 5% decrease in load capacity from 0% SMA volume fraction to 6% SMA volume fraction, there is a significantly higher decrease in load capacity (16%) between 6% and 10% SMA volume fractions.

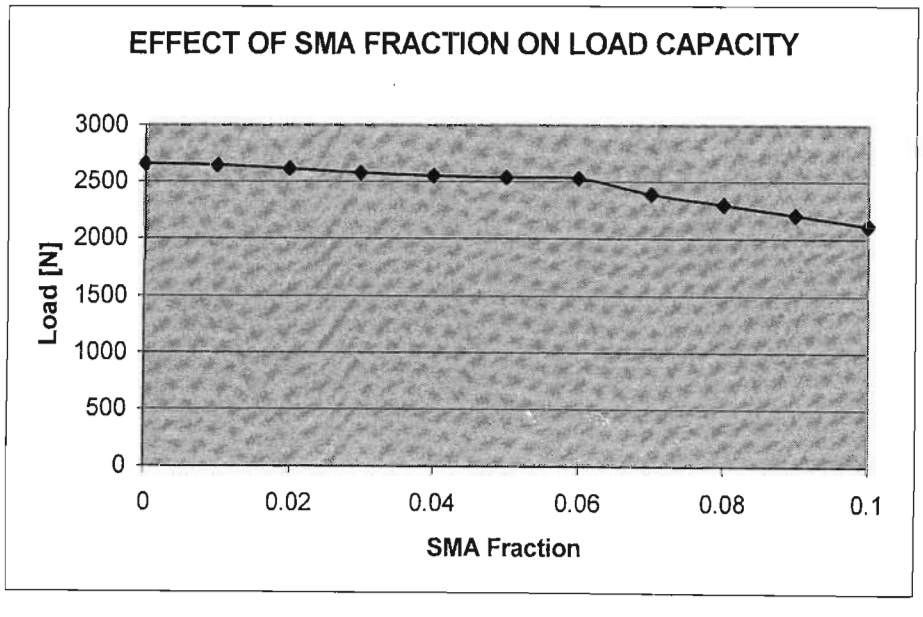

Figure 4-11 : Load capacity characteristics of varying SMA volume fractions for an impact velocity of 1 m/s

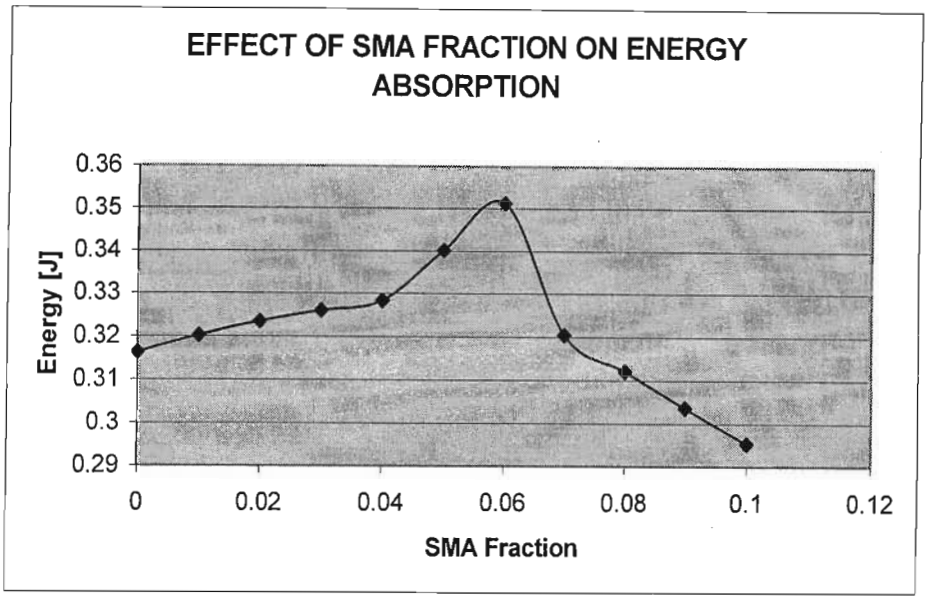

Figure 4-12 : Energy absorption characteristics of varying SMA volume fractions for an impact velocity of 1 m/s

Figure 4-12 is similar in trend in that there is an increase in energy absorption levels up to a turning point of 6% SMA volume fraction, followed by a definite decreasing energy absorption trend. The reason behind this 6% SMA volume fraction turning point is a change in failure mechanism. Up to 6% SMA volume fraction the beam fails because its ultimate strength is exceeded while SMA volume fractions in excess of 6% results in failure because the ultimate strain of the Al_2O_3 fibre is exceeded. Thus, as the SMA volume fraction is increased, the load capacity of the beam decreases, but at the same time the displacement of the beam for a particular load increases (because of the difference in Young's modulus of the fibres).

The effects of prestrain on load capacity and energy absorption are shown in Figures 4-13 and 4-14 respectively. While the load capacity graph seems to fluctuate quite dramatically, it must be noted that the range of fluctuation is just over 1% and can be considered negligible. The energy absorption curve, on the other hand, peaks at a maximum increase of approximately 30% at 0.3% prestrain, before decreasing to 35% of its original capacity. Again, this increase in energy absorption trend is not because of the shape memory effect but due to the higher toughness of the nitinol fibres and the following decrease in energy absorption capacity is as a result of the prestrain approaching the ultimate strain of the Al_2O_3 fibres.

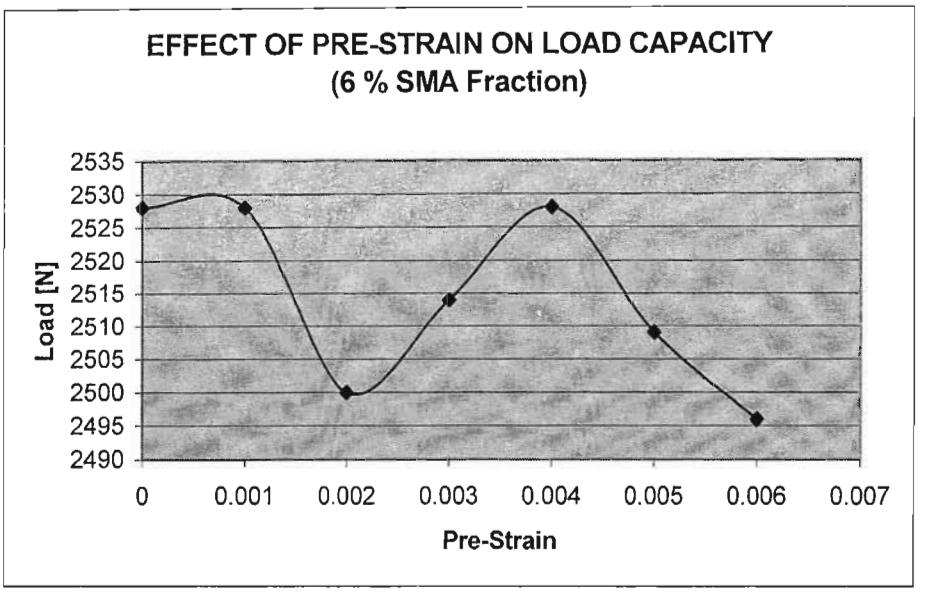

Figure 4-13 : Load capacity characteristics of varying degrees of pre-strain for an impact velocity of 1 m/s

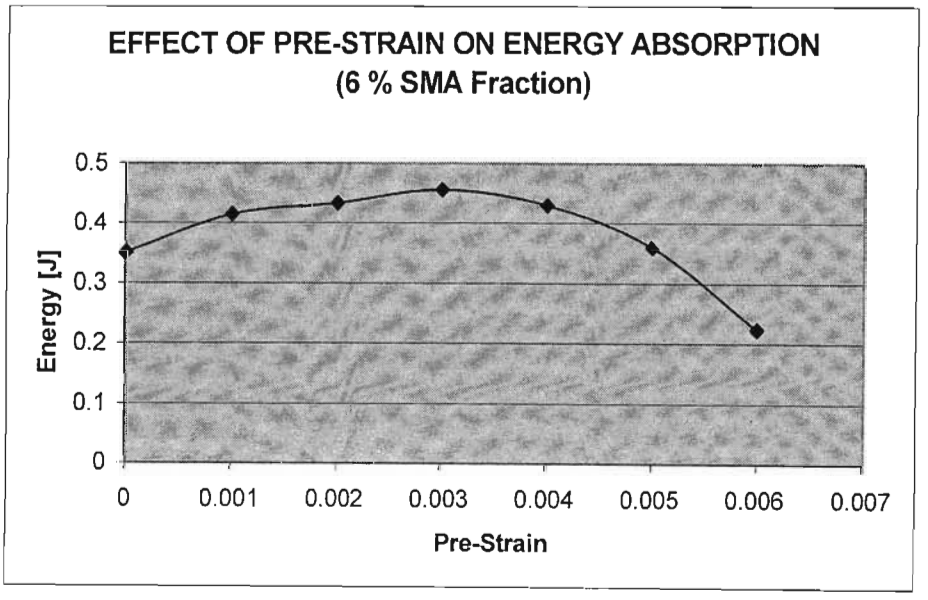

Figure 4-14 : Energy absorption characteristics of varying degrees of pre-strain for an impact velocity of 1 m/s

To evaluate the impact of the shape memory effect on load capacity and energy absorption, consider the results of Figures 4-15 and 4-16. Figure 4-15 shows the load characteristics of an AC8A aluminium alloy beam with only nitinol reinforcement (i.e. 15% SMA and 0% aluminium oxide fibres) and Figure 4-16 shows the respective energy absorption trend.

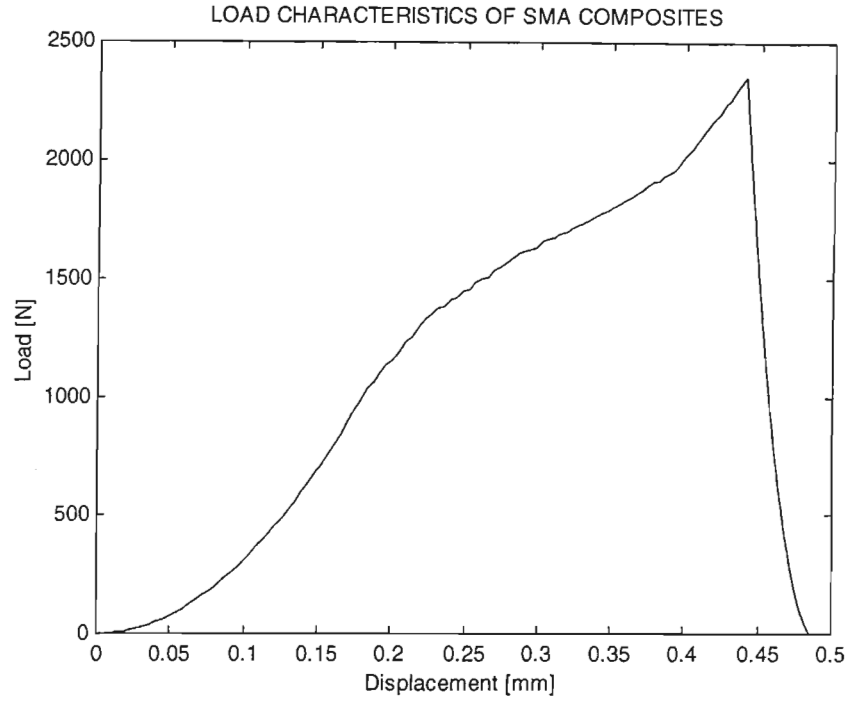

Figure 4-15 : Load capacity characteristics for 15% SMA fibre reinforcement (0% Al_2O_3 fibres)

The important characteristics of Figure 4-15 are the significantly increased displacement to failure as well as the sudden increase in load at approximately 0.4 mm (1.17 % strain). This increased displacement is carried over to the energy-displacement curve of Figure 4-16 and results in a significant increase in energy absorption (~68.5 % increase compared to 0% SMA fibre reinforcement of Figure 4-10). However, the failure mode experienced by the beam is as a result of the ultimate composite strength being exceeded and not as a result of maximum strain. Thus, the failure strain of 1.45 % is below the 2.2 % SMA transition strain and the increase in energy absorption is again the result of the increased displacement to failure.

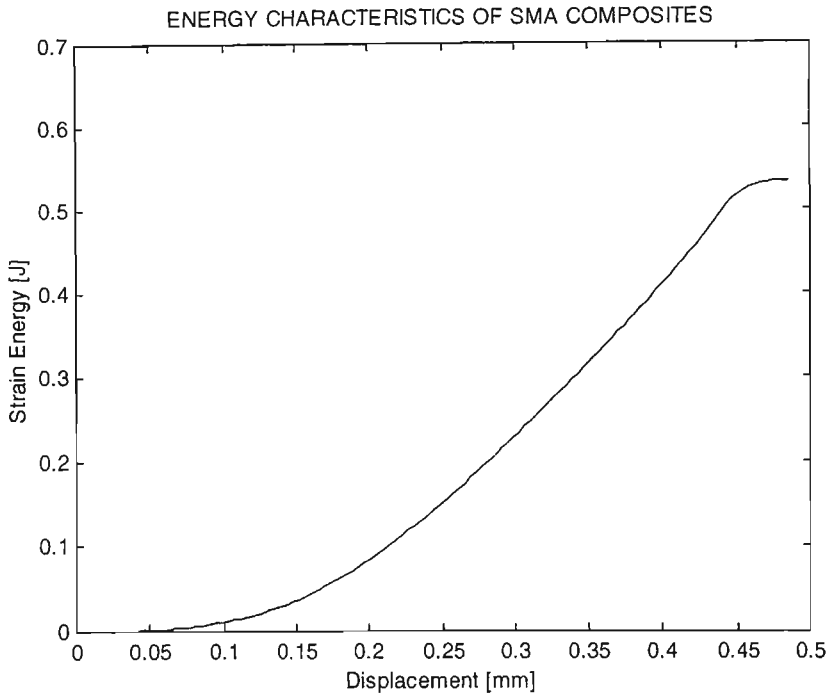

Figure 4-16 : Energy absorption characteristics for 15% SMA fibre reinforcement (0% Al_2O_3 fibres)

Figures 4-17 and 4-18 show the effect of prestrain on load capacity and energy absorption respectively. The load capacity graph shows a decreasing load trend with increasing prestrain, primarily because the prestrain imparts a preload to the beam, which causes the composite strength to be reached at a lower applied load. The energy absorption capacity of Figure 4-18 shows an initial increase of approximately 24 % before decreasing to 68 % of the initial value. The initial increase in energy absorption is because the prestrain causes the 'plasticity-like' phase, just before phase transition, to be reached sooner and the consequent decrease in energy absorption is as a result of the prestrain load approaching the ultimate strength of the composite.

Thus, the phenomenon of increased energy absorption of Figure 4-16 highlights a critical point; any energy capacity increase that is observed as a consequence of using smart SMA reinforcement is not always attributable to the shape memory effect. This implies that careful design consideration must be given to extract the maximum benefit of the smart reinforcement.

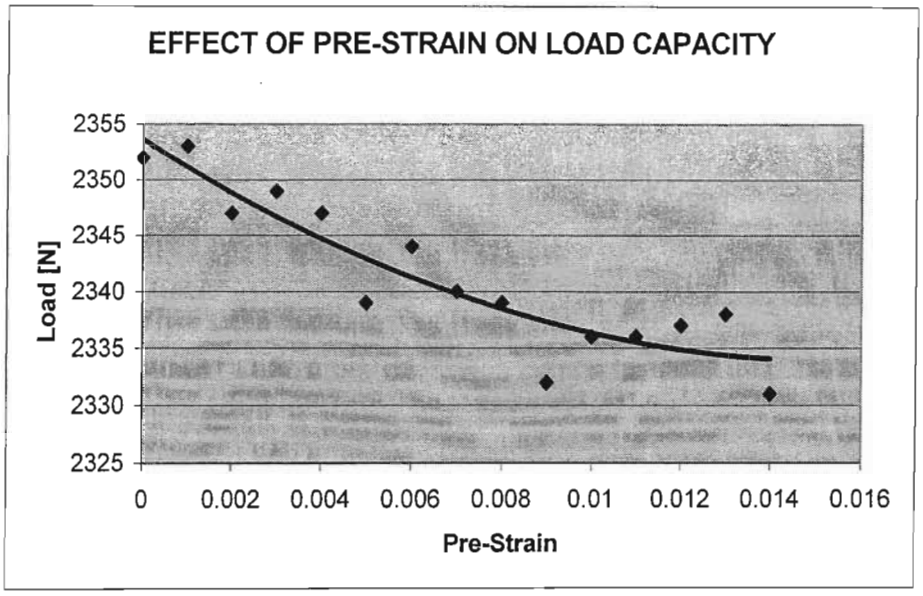

Figure 4-17 : Effect of pre-strain on load capacity for 15% SMA fibre reinforcement (0% Al_2O_3 fibres)

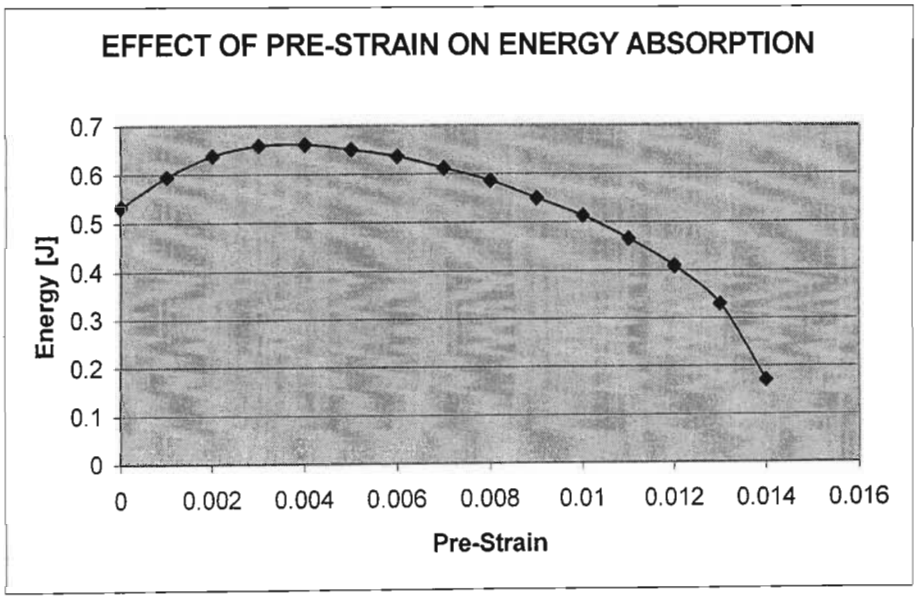

Figure 4-18 : Effect of pre-strain on energy absorption capacity for 15% SMA fibre reinforcement (0% Al_2O_3 fibres)

In a final attempt to understand the contribution of phase transition to the energy absorption capacity of a material, the failure criteria of ultimate composite strength is removed and the beam is allowed to fail only by ultimate strain of the nitinol fibre. Figure 4-19 shows the resulting energy absorption capacities for various degrees of prestrain.

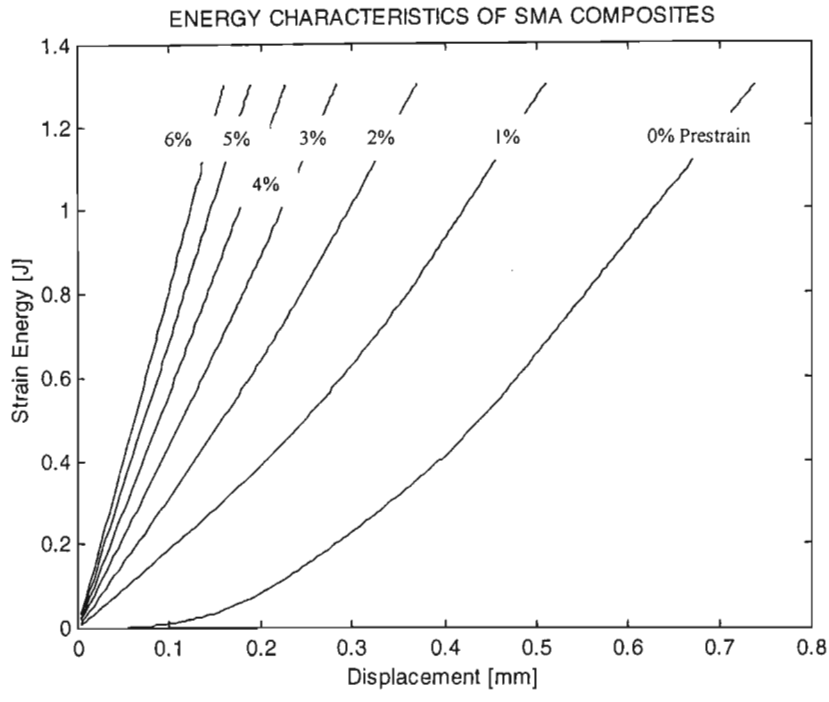

Figure 4-19 : Effect of pre-strain on non-failure energy absorption capacity through the shape memory effect of SMA

The phase transition effect of the SMA on energy absorption is clearly evident from the above figure. Importantly, the maximum energy absorption capacity of the beam is not reached for the applied impact conditions, i.e. the beam does not fail. Thus, for a non-failure condition, the effect of prestrain is not to increase the energy absorbed by the material, but to increase the rate of energy absorption, i.e. the energy is absorbed through a smaller displacement. An increase of approximately 96.5 % is observed when the energy absorption of Figure 4-19 is compared to the maximum energy absorption of Figure 4-18. The maximum energy absorption capacity of the beam is simulated to be 3.52 J, i.e. over 5 times the maximum energy absorption indicated in Figure 4-18.

The effect of prestrain on the failure (maximum) energy absorption capacity of a SMA reinforced metal matrix composite beam is to further increase the energy capacity up to a maximum of 11.61 J at 9 % prestrain as indicated in Figure 4-20.

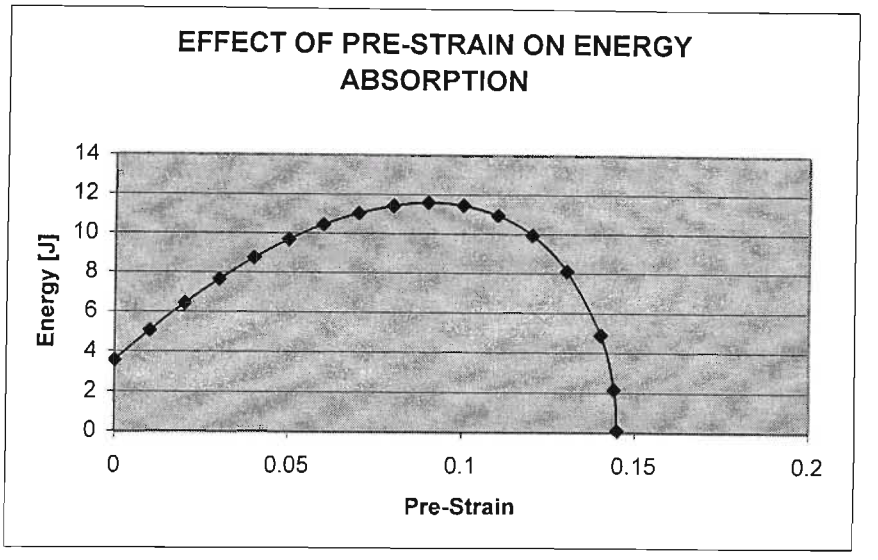

Figure 4-20 : Effect of pre-strain on failure energy absorption capacity through the shape memory effect of SMA

This is a 16.5 times increase over the maximum energy absorption of Figure 4-18 (SMA reinforced beam with no phase transition effect) and a 36 times increase over the energy absorption of Figure 4-8 (Aluminium oxide reinforced beam). While the effect of SMA phase transition on energy absorption is dramatic, the maximum stress in the beam at the maximum energy absorption (11.61 J) is 2510 MPa. Thus, in the design of a smart composite using SMA reinforcement for energy absorption, the matrix material needs to be thoroughly assessed to facilitate maximum use of the SMA phase transition effect.

In summary, the use of SMA fibres in a metal matrix composite can double the material's energy absorption capacity when loaded to below the SMA martensitic phase transition strain and can increase energy absorption levels by up to 36 times when full utilisation of the phase transition effect is made. The material, however, needs to be designed such that the failure mode is by ultimate fibre strain and not ultimate composite strength, for maximum benefit of the smart reinforcement to be achieved.

CHAPTER 5

5 CONCLUSIONS

Smart materials have enormous potential in a wide variety of industries, however, due to a lack of understanding, these materials are still considered too sophisticated to be used in ordinary day-to-day design applications. Thus, in a broader context, the aim of this thesis is to increase the understanding of the behaviour of smart materials, and in so doing help to erase the perception that these materials are beyond the reach of the vast majority of designers and engineers.

More specifically, the primary objective of this investigation is the determination of the ability of smart materials (SMA, magnetostrictive materials and piezoelectric materials) to enhance the performance of an ordinary metal-matrix composite beam in terms of load carrying capability and energy absorption capacity. The second important objective is the increase in understanding and competence for the author in peripheral activities such as numerical modelling and simulation techniques, data interpretation and evaluation, as well as a broader understanding of material behaviour in general.

Thus, the outputs of the study can be summarised as follows:

- The investigation of a magnetostrictive SMA hybrid composite with piezoelectric actuator, smart material that is capable of enhancing load attenuation and energy absorption characteristics.
- Fundamental understanding of the microstructural behaviour of SMA, magnetostrictive materials, piezoelectric materials and smart composites in general.
- Fundamental understanding and competence development in numerical modelling and simulation techniques, data interpretation and evaluation.

The methodology employed in this investigation is driven by two primary factors. The first is the unique approach that the author puts forward to attempt to simplify the characterisation of damage in not just metal matrix composites but in materials in general. The second factor is the lack of available literature on smart material energy absorption as well as a lack of precise theory for short fibre composites.

The characterisation of the energy absorption of a structural system is relatively simple in the elastic region of the materials involved. This is as a result of well-defined, predictable material

behaviour and mature analytical models. However, once the realm of plasticity is entered, the characterisation gets difficult due to complex theories surrounding various damage models. Having a practical engineering background, the author finds these complex analytical descriptions extremely frustrating and limiting to practical engineering predictions. Thus, in an attempt to facilitate simple engineering models, the concept of a damage modulus is introduced. The importance of the damage modulus is two fold. Firstly, it is a single factor that describes a material through its entire strain range and secondly it takes into account 'damage' in material modelling and thus simplifies analyses by a considerable amount.

E_D is derived from the stress-strain curve for the specific materials and thus, warrants no additional experimental investigation. The simplification in using this theory is that elastic analysis can now be used through the plastic strain range as well. Further, damage is taken into account by incorporating an effectively reducing Young's Modulus in the plastic zone.

The second factor driving the methodology of this investigation is the lack of available literature on energy absorption of smart metal matrix composites. Thus, an extensive literature review is conducted to facilitate familiarisation of relevant work as well as to develop a thorough understanding of the behaviour of the various individual material types. The literature review thus serves as a means of developing a broad understanding, physically, of various individual components of the study, viz. microstructural behaviour of SMA, general impact loading phenomenon, general behaviour of composite materials (interactive behaviour between elements), as well as magnetostrictive and piezoelectric phenomenon.

As the core of the investigation, the author develops an analytical model, based on the damage modulus concept, to predict the behaviour of a short fibre metal matrix composite during a Charpy impact test. The model is verified using the experimental results given by Aggag et. al. A smart composite Charpy test is then simulated by replacing the damage modulus characteristics of some of the fibres with the damage modulus of SMA fibres. The results obtained are then compared to those obtained by Aggag et al to quantify the effect of the SMA on impact energy absorption. Finally, to simulate the effect of the magnetostrictive inclusions, the SMA model is subject to varying degrees of pre-strain to represent the reaction of the magnetostrictive elements to varying degrees of magnetic field.

The basic elastic stress / strength theory of the falling mass impact analysis highlights two important considerations. The first is the geometric relationship between the two-dimensional beam displacements during the impact process to the one-dimensional longitudinal strain of the beam. This is very important as it facilitates the crossover from the load-displacement domain to

the stress-strain domain, thus enabling the point of plasticity to be correctly determined from the material stress-strain curve. The second important consideration is the effect of the beam strain energy on the velocity of the falling mass. The velocity-displacement profile that is derived is based on the conservation of energy principle and demonstrates the integrity of the model in describing a real system. The effect of air resistance on the energy balance of the system is ignored and the effect of potential energy variation due to beam displacement is considered negligible.

The theoretical modelling is executed with numerical modelling using the MATLAB® software package.

The results show that a 4% smart fibre volume fraction gives the beam an approximate 1.6% increase in strain energy capacity. This, however, is not a direct result of the shape memory effect, but rather because of the higher toughness of the SMA fibres. Of the additional energy that is absorbed, 0.002 J (0.6 %) is used toward the additional displacement and the balance of 0.005 J (1.0 %) is consumed by the additional toughness of the SMA fibres.

The analysis of the effect of varying SMA volume fractions show a definite trend of decreasing load capacity with increasing SMA volume fraction, which the author attributes to the lower strength of the nitinol fibres as compared to the aluminium oxide fibres.

An analysis of the effect of prestrain shows a similar trend in that there is an increase in energy absorption levels up to a turning point of 6% SMA volume fraction, followed by a definite decreasing energy absorption trend. The reason behind this 6% SMA volume fraction turning point is a change in failure mechanism. Up to 6% SMA volume fraction the beam fails because its ultimate strength is exceeded while SMA volume fractions in excess of 6% results in failure because the ultimate strain of the Al_2O_3 fibre is exceeded. Thus, as the SMA volume fraction is increased, the load capacity of the beam decreases, but at the same time the displacement of the beam for a particular load increases (because of the difference in Young's modulus of the fibres).

The effects of prestrain on load capacity and energy absorption for 6 % smart fibre reinforcement (9 % aluminium oxide fibres) shows a relatively constant load capacity characteristic. The energy absorption curve, on the other hand, peaks at a maximum increase of approximately 30% at 0.3% prestrain, before decreasing to 35% of its original capacity. Again, this increase in energy absorption trend is not because of the shape memory effect but due to the higher toughness of the nitinol fibres and the following decrease in energy absorption capacity is as a result of the prestrain approaching the ultimate strain of the Al_2O_3 fibres.

The important characteristic of the analysis of 15 % smart fibre reinforcement (no aluminium oxide fibres) is the significantly increased displacement to failure. This increased displacement is carried over to the energy-displacement curve and results in a significant increase in energy absorption (~68.5 % increase compared to 0% SMA fibre reinforcement). However, the failure mode experienced by the beam is as a result of the ultimate composite strength being exceeded and not as a result of maximum strain and the increase in energy absorption is again the result of the increased displacement to failure.

The effect of prestrain on the 15 % smart fibre reinforced beam shows a decreasing load trend with increasing prestrain, primarily because the prestrain imparts a preload to the beam, which causes the composite strength to be reached at a lower applied load. The energy absorption capacity shows an initial increase of approximately 24 % before decreasing to 68 % of the initial value. The initial increase in energy absorption is because the prestrain causes the 'plasticity-like' phase, just before phase transition, to be reached sooner and the consequent decrease in energy absorption is as a result of the prestrain load approaching the ultimate strength of the composite.

Thus, the phenomenon of increased energy absorption described above highlights a critical point; any energy capacity increase that is observed as a consequence of using smart SMA reinforcement is not always attributable to the shape memory effect. This implies that careful design consideration must be given to extract the maximum benefit of the smart reinforcement.

Finally, the effect of the phase transition phenomenon of shape memory alloys on the energy absorption characteristics of the beam is investigated. For a non-failure condition, the effect of prestrain is not to increase the energy absorbed by the material, but to increase the rate of energy absorption. An increase of approximately 96.5 % is observed when the energy absorption is compared to the maximum energy absorption of the smart beam with no phase transition. The maximum energy absorption capacity of the beam is simulated to be 11.61 J, with prestrain effects, resulting in a 36 times increase in energy absorption capacity over the aluminium oxide reinforced beam.

Thus in summary, the use of SMA fibres in a metal matrix composite can double the material's energy absorption capacity when loaded to below the SMA martensitic phase transition strain and can increase energy absorption levels by up to 36 times when full utilisation of the phase transition effect is made. The material, however, needs to be designed such that the failure mode is by ultimate fibre strain and not ultimate composite strength, for maximum benefit of the smart reinforcement to be achieved.

The thesis thus achieves its objective in investigating the ability of smart materials to enhance the energy absorption characteristics of regular fibre reinforced metal-matrix composite materials subject to low velocity impact loading. Of equal importance to the achievement of this objective is the introduction in the thesis of the unique damage modulus that goes to the foundation of material characterisation for mechanical engineering design and has profound implications in damage theory and future design methodologies. Significant learning has taken place in the execution of this PhD endeavour and this thesis will no doubt contribute to other investigations in the field of smart materials.

In terms of future work in this field of study, this investigation opens up two critical avenues of research. The first is a direct follow-on to the results presented in the current thesis and includes experimental investigation of various SMA reinforcement materials as well as an investigation into appropriate matrix substrates to complement the phase transition effect of SMA in energy absorption. Further, a practical attempt needs to be made in using magnetostrictive inclusions and piezoelectric sensors to control the onset of martensitic transformation in SMA. The second avenue of research is the qualification of the damage modulus concept by experimental methods. The author foresees numerous loading conditions being analytically modelled, for homogenous and composite materials, using the damage modulus concept and then experimentally verified to determine the extent to which this concept can be applied.

REFERENCES

Agbossou, A., Mahut, T. and Pastor, J., (1998), " Dynamic Analysis of Piezoelectric Fibre Composite in an Active Beam Using Homogenisation and Finite Element Methods", *journal of Intelligent Material Systems and Structures, Vol.9, No.12, p.1009-1016*, Technomic Publishing, United States of America.

Aggag, G. A., Han, K. S., Nam, H. W. and Takahashi, K., (1999), " The dynamic behaviour of metal-matrix composites under low-velocity impact", *Composites Science and Technology, Vol. 60, p.817-823*, Elsevier.

Alderson, K. L., Alderson, A. and Evans, K. E., (1997), " The Interpretation of the Strain-dependent Poisson's Ratio in Auxetic Polyethylene", *Journal of Strain Analysis, Vol.32, p.201-212.*

Anderson, T. A., Calvert, P. D., Denham, H. B. and Madenci, E., (1997), "Embedded PVF2 Sensors for Smart Composites", *Proceedings of SPIE – The International Society for Optical Engineering, Vol.3040, p.138-147*, Society of Photo-Optical Instrumentation Engineers, United States of America.

Atherton, D. L. and Jiles, D. C., (1986), " Theory of Ferromagnetic Hysteresis ", *Journal of Magnetisation and Magnetic Materials, Vol.61, p.48-60.*

Bazant, Z. P. and Jirasek, M., (2002), "Nonlocal Integral Formulations of Plasticity and Damage: Survey of Progress", *Journal of Engineering Mechanics, p.1119-1149.*

Belingardi, G., Gugliotta, A. and Vadori, R., (1998), " Fragmentation of Composite Material Plates Submitted to Impact Loading: Comparison Between Numerical and Experimental Results", *Journal of Key Engineering Materials, Vol.144, p.75-88*, Politecnico di Torino, Italy.

Birman, V., (1997), " Review of Mechanics of Shape Memory Alloy Structures ", *Journal of Applied Mechanics Review, Vol.50, No.11, Pt.1, p.629-645*, ASME, United States of America.

Birman, V., Chandrashekhara, K. and Sain, S., (1996a), " Approach to Optimisation of Shape Memory Alloy Hybrid Composite Plates Subjected to Low Velocity Impact", *Journal of Composites, Part B : Engineering, Vol.27B, p.439-446*, Elsevier, United Kingdom.

Birman, V., Chandrashekhara, K. and Sain, S., (1996b), " Global Strength of Hybrid Shape Memory Composite Plates Subjected to Low Velocity Impact", *Journal of Reinforced Plastics Composites, Vol.16, p.791-809.*

Brinson, L. C., (1993), " One-dimensional Constitutive Behaviour of Shape Memory Alloys : Thermomechanical Derivation with Non-constant Material Functions and Redefined Martensite Internal Variable", *Journal of Intelligent Material System Structures, Vol.4, p.229-242.*

Brinson, L. C. and Lammering, R., (1993), " Finite Element Analysis of the Behaviour of Shape Memory Alloys and their Application", *International Journal of Solids and Structures, Vol.30, p.3261-3280.*

Casciati, F., Faravelli, L. and Petrini, L., (1998), "Energy Dissipation in Shape Memory Alloy Devices", *Journal of Computer-Aided Civil and Infrastructure Engineering, Vol.13, No.6, p.433-442*, University of Pavia, Italy.

Chandra, N. and Rajendran, A. M., (1998), " Micromechanics Based Modelling of Damage in Composites Under High Velocity Impact – A Review", *Proceedings of the 1998 5th International Conference on Structures Under Shock and Impact, p.421-432*, Computational Mechanics Inc., United States of America.

Charles, J. L., Collombet, F., Jeronimidis, G., Lalbin, X. and Lataillade, J. L., (1997), "Methodology and Tools for the Study of Composite Structures Under Impact Loading: Application to Long Fibre Laminated Structures", *Journal De Physique. IV, Vol.7, No.3, p.163-168*, Ecole Nationale Superieure d'Arts et Metiers, France.

Chattopadhyay, A. and Seeley, C. E., (1997), "A Higher Order Theory for Modelling Composite Laminates with Induced Strain Actuators", *Journal of Composites Part B: Engineering, Vol.28, No.3, p.243-252*, Elsevier, England.

Chaudhry, Z., Kiesling, T. C., Paine, J. S. N. and Rogers, C. A., (1996), *Proceedings of the 37th AIAA / ASME / ASCE / AHS / ASC Structures, Structural Dynamics and Materials Conference p. 1448,* ASME, United States of America.

Collombet, F., Lalbin, X. and Lataillade, J. L., (1997), " Impact Behaviour of Laminated Composites: Physical Basis for Finite Element Analysis", *Journal of Composites Science and Technology, Vol.58, No.3-4, p.463-478*, Lab Materiaux Endommagement Fiabilite – ENSAM, France.

Dapino, M. J., Flatau, A. B. and Smith R. C., (1998), "An Active and Structural Strain Model for Magnetostrictive Transducers", *Journal of Proceedings of the SPIE – The International Society for Optical Engineering, Vol.3329, Pt.1-2, p.198-209*, SPIE - Int. Soc. Opt. Eng., United States of America.

Dang, X. and Liu, D., (1998), " Testing and Simulation of Laminated Composites Subjected to Impact Loading", *ASTM Special Technical Publication, No.1330, p.273-284*, ASTM, United States of America.

Dharani, L. R. and Flocker, F. W., (1998), " Modelling Interply Debonding in Laminated Architectural Glass Subject to Low Velocity Impact", *Journal of Structural Engineering Mechanics, Vol.6, No.5, p.485-496*, Stress Engineering Services, United States of America.

Ellis, R. L., Jia, H., Lalande, F. and Rogers, C. A., (1997), *Proceedings of the 38th AIAA / ASME /ASCE / AHS / ASC Structures, Structural Dynamics and Materials Conference*, ASME, United States of America.

Evans, K. E., Smith, C. W. and Wootton, R. J., (1999), "Interpretation of Experimental Data for Poisson's Ratio of Highly Nonlinear Materials", *Journal of Experimental Mechanics, Vol.39, No.4, p.356-362*, Sage Publications Inc., United States of America.

Funakubo, H., (1987), " Shape Memory Alloys ", *Gordon & Bleach*, New York.

Furuya, Y., (1996), " Design and Material Evaluation of Shape Memory Composites", *Journal of Intelligent Material Systems and Structures, Vol.7, p.321-330*, Technomic Publishing, United States of America.

Giannakopoulos, A. E., Ramamurty, U, Sridhar, S. and Suresh, S., (1999), " An Experimental Study of Spherical Indentation on Piezoelectric Materials", *Journal ACTA Materialia, Vol.47, No.8, p.2417-2430*, Elsevier, England.

Hamouda, A. M. S. and Hashmi, M. S. J., (1998), "Testing of Composite Materials at High Rates of Strain: Advances and Challenges", *Journal of Materials Processing Technology, Vol.77, No.1-3, p.327-336*, Dublin City University, United Kingdom.

Harding, J. and Ruiz, C., (1998), " Mechanical Behaviour of Composite Materials Under Impact Loading", *Journal of Key Engineering Materials, Vol.141-143, Pt.2, p.403-426*, University of Oxford, United Kingdom.

Jiles, D. C., (1991), " Introduction to Magnetism and Magnetic Materials ", Chapman & Hall, New York.

Joshi, S. P. and Mannas, J. R., (1993), " Study of Smart-Sensing Elements in a Dynamic Stress Field", *SPIE – The International Society for Optical Engineering, Vol.1918, p.264-275*, SPIE – Int. Soc. for Opt. Engineering, United States of America.

Lewis, M. W., (1998), " On Predicting and Modelling Material Failure Under Impact Loading", *Proceedings of the 1998 5th International Conference on Structures Under Shock and Impact, p.569-578*, Computational Mechanics Inc., United States of America.

Li, S., Liang, C. and Rogers, C. A., (1991), "Active Damage Control of Hybrid Material Systems using Induced Strain Actuators", *Proceedings of the 32nd AIAA/ASME/ASCE/AHS/ASC Structures, Structural Dynamics and Materials Conference, p.1190-1203*, AIAA, United States of America.

Liang, C. and Rogers, C. A., (1990), "One-dimensional Thermomechanical Constitutive Relations for Shape Memory Materials", *Journal of Intelligent Material System Structures, Vol.1, p.207-234.*

Liang, C. and Rogers, C. A., (1991), "Multi-dimensional Constitutive Relations of Shape Memory Alloys", *Proceedings of the 32nd AIAA/ASME/ASCE/AHS/ASC Structures, Structural Dynamics and Materials Conference, Part 1, p.178-185*, AIAA, United States of America.

Livingston, J. D., (1982), "Magnetomechanical Properties of Amorphous Metals", *Phys. Stat. Sol. (a), Vol.70, p.591.*

Mines, R. A. W., (1998), " mpact Energy Absorption of Polymer Composite Sandwich Beams", *Journal of Key Engineering Materials, Vol.141-143, Pt.2, p.553-572*, University of Liverpool, United Kingdom.

Miyazaki, S., Sandstrom, R. and Wei, Z. G., (1998), " Shape-Memory Materials and Hybrid Composites for Smart Systems. II. Shape-Memory Hybrid Composites", *Journal of Materials Science, Vol.33, No.15, p.3763-3783*, Royal Institute of Technology, United Kingdom.

Nagaki, S. and Tanaka, K., (1982), " Thermomechanical Description of Materials with Internal Variables in the Process of Phase Transformation", *Ingenieur-Archiv, Vol.51, p.287-299.*

Needleman, A., (1997), " Numerical Modelling of Crack Growth Under Dynamic Loading Conditions", *Journal of Computational Mechanics, Vol.19, No.6, p.463-469*, Brown University, United States of America.

Paine, J. S. N. and Rogers, C. A., (1994a), " Active Materials and Smart Structures", *SPIE – The International Society for Optical Engineering, Vol.2427, p.358*, SPIE – Int. Soc. for Opt. Engineering, United States of America.

Paine, J. S. N. and Rogers, C. A., (1994b), "Smart Structures and Materials 1994: Smart Structures and Intelligent Syatems", *SPIE – The International Society for Optical Engineering, Vol.2190, p.402*, SPIE – Int. Soc. for Opt. Engineering, United States of America.

Rao, S. S. and Sunar, M., (1999), "Recent Advances in Sensing and Control of Flexible Structures via Piezoelectric Materials Technology", *Journal of Applied Mechanics Review, Vol.52, No.1, p.1-16*, ASME, United States of America.

Schulgasser, K., (1992), "Relationships between the Effective Properties of Transversely Isotropic Piezoelectric Composites", *Journal of Mechanics, Physics and Solids, Vol.40, p.473-479.*

Sittner, P., Takakura, M., Tokuda, M. and Ye, M., (1998), "Calculation of Mechanical Behaviours of Shape Memory Alloy Under Multi-Axial Loading Conditions", *International Journal of Mechanical Sciences, Vol.40, No.2-3, p.227-235*, Pergamon-Elsevier, England.

Tanaka, K., (1986), " A Thermomechanical Sketch of Shape Memory Effect : One Dimensional Tensile Behaviour", *Res Mechanica, Vol.18, p.251-263.*

Tanaka, K., (1990), " Phenomenological Description on Thermomechanical Behaviour of Shape Memory Alloys", *Journal of Pressure Vessel Technology, Vol.112, p.158-163.*

Tanaka, K., (1991), " Analysis of Recovery Stress and Cyclic Deformation in Shape Memory Alloys", *Advances in Continuum Mechanics, p.441-451*, Springer-Verlag, Berlin.

Taya, M., (1999), " Micromechanics Modelling of Smart Composites ", *Journal of Composites Part A: Applied Science and Manufacturing, Vol.30, No.4, p.531-536*, Elsevier, United Kingdom.

Ullakko, K., (1996), " Magnetically Controlled Shape Memory Alloys: A New Class of Actuator Materials", *Journal of Materials Engineering and Performance, Vol.5, No.3, p.405-409*, ASM Int., United States of America.

Wang, B., (1992), " Three-dimensional Analysis of an Ellipsoid Inclusion in a Piezoelectric Material", *International Journal of Solids Structures, Vol.29, p.293-308.*

Yu, N., (1995), " Micromechanical Modelling of Effective Electro-thermo-elastic Properties of Two-phase Piezoelectric Composites", *IUTAM Symposium on Microstructure - Property Interactions in Composite Materials, p.397-405.*

APPENDIX A

PRELIMINARY LITERATURE REVIEW AND SELECTED BIBLIOGRAPHY

The objective of this appendix is to present the reader with the initial preliminary literature review that was conducted to assist the author with choosing the topic for this PhD thesis. As a consequence of this review, an extensive list of available literature on the subjects of impact loading and smart materials was drawn up. This list is also presented in this appendix as a selected bibliography. Note that all references quoted in the preliminary literature review can be found in the selected bibliography.

A1. Preliminary Literature Review

In recent years, SMA has been given an increasing amount of attention and consideration to engineering applications. This increasing popularity stems from their characteristic high damping capacity, large recoverable strain and recovery stress and remarkable property changes due to stress or thermal induced martensitic transformations. Further, Shape memory materials can be easily fabricated into various forms such as fibres, wires, ribbons, particles and thin films and thus, facilitate commercial viability.

While most early efforts in understanding the behaviour of embedded shape memory materials concentrated on thermoplastics and thermosets, partly due to their technical simplicity in manufacturing, recent engineering approaches have been extended to metal or silicon matrices (Miyazaki, Sandstrom & Wei : 1998). The advantages of metal matrix shape memory alloys has been cited by Miyazaki et. al. (1998) as their ability to achieve unique properties such as self-strengthening or self-relaxation and high damping capacity.

The unique properties of shape memory materials can essentially be ascribed to their ability to transform between the austenite and martensite phase under specific shear stress or thermal conditions. The transformation of austenite to martensite by the application of cooling results in no significant deformation and the material microstructure reverts to the austenite phase upon reheating. The critical temperatures in this process are the martensite start temperature (the temperature at which the martensite transformation begins), martensite finish temperature (the temperature to which the material needs to be cooled for the entire microstructure to complete the transformation to martensite), austenite start temperature (the temperature to which the martensitic

microstructure needs to be heated to initiate the transformation to the austenitic phase) and austenite finish temperature (the temperature that needs to be reached to ensure complete transformation to the austenite phase). The transformation of austenite to martensite by the application of shear stress results in significant deformation (compared to thermally induced martensite) and will only revert to the austenitic phase upon unloading if the temperature is above the austenite finish temperature (Sittner, Takakura & Tokuda : 1998). If the temperature is less than the austenite start temperature, then the deformation will be kept as residual strain until heated to the austenite finish temperature. This is referred to as the pseudoelastic behaviour of SMA (Figure A-1).

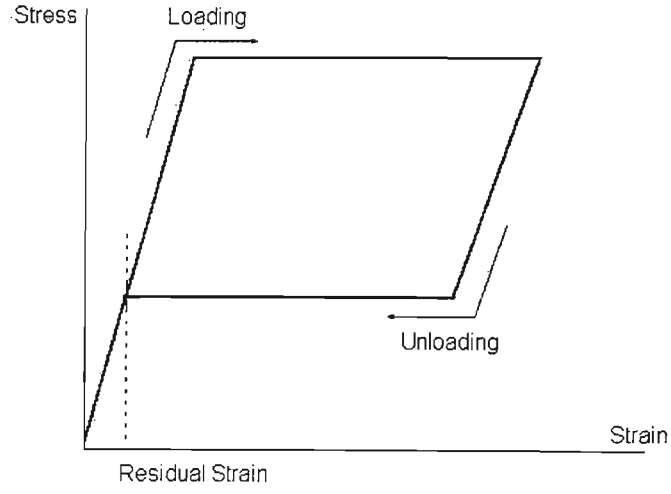

Figure A-1: The pseudoelastic behaviour of shape memory alloys (modified after Sittner et.al. : 1998)

Thus, the shape memory effect can be similarly depicted as (Figure A-2),

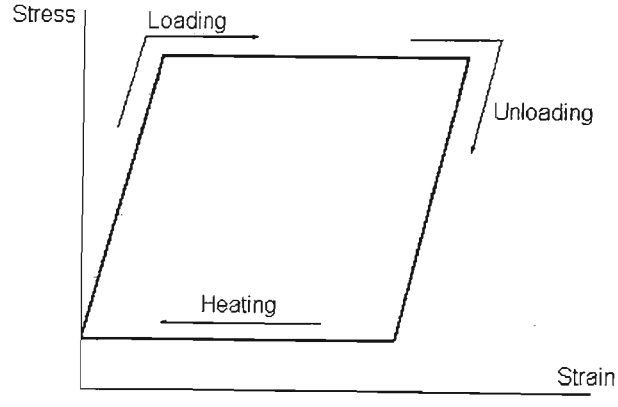

Figure A-2: The shape memory effect of shape memory alloys (after Sittner et. al. : 1998)

The stress induced martensite transformation will only take place if the applied stress reaches the critical transformation stress. However, martensite can still be obtained if the applied stress is lower than the critical stress through the assistance of cooling (Figure A-3), i.e. cooling decreases the critical stress threshold.

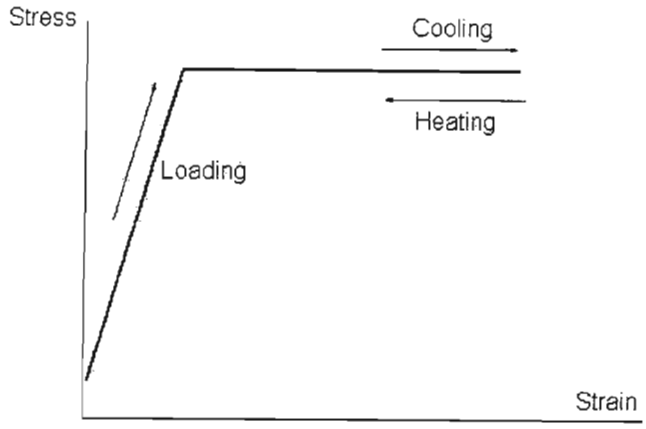

Figure A-3: The two-way shape memory effect of shape memory alloys (after Sittner et. al. : 1998)

The primary objectives of Sittner et. al. (1998) was the calculation of mechanical behaviours of SMA under multi-axial loading conditions and the results of the investigation can be summarized as follows,

- The shape memory alloy has a path dependent deformation behaviour.
- The zero stress state always corresponds to the zero strain state as in the elastic deformation.
- Under non-proportional multi-axial loading, the original strain cannot be recovered, i.e. no shape memory (possibly because some martensite variants produced in the previous loading history disappears in the temperature cycle).

The most fundamental application of SMA is in material design to increase tensile strength. Compressive residual stresses due to manufacturing processes is beneficial to mechanical properties such as yield stress and fracture toughness and in composites arises from the generally higher coefficient of thermal expansion of the filler to the matrix. The introduction of SMA to the matrix can allow the filler (SMA) to shrink in the matrix at the operating temperature or with increasing applied stress, thus producing compressive stress to contribute to the tensile properties of the composite under load bearing conditions.

Miyazaki et. al. (1998) describes the design approach for the SMA fibre metal matrix composite as follows (Figure A-4),

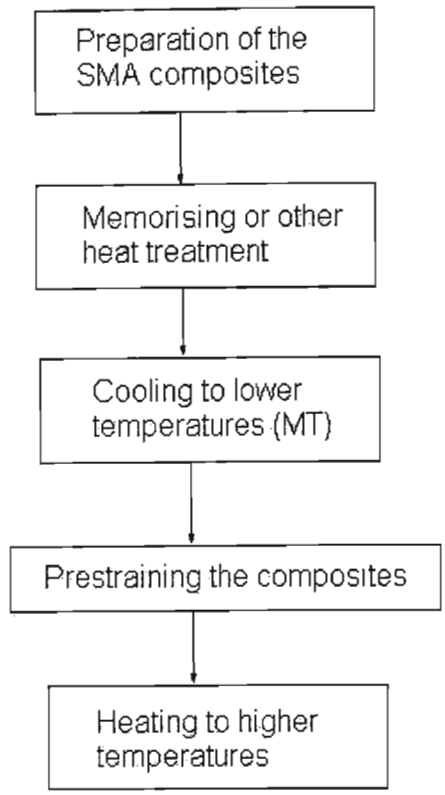

Figure A-4: Design approach for SMA fibre metal matrix composites (after Miyazaki et. al. : 1998)

This concept can be applied to a polymer matrix with SMA fibres and a metal matrix with SMA particles composites as well. In general, the matrix compressive residual stress increases with increasing fibre volume fraction and prestrain within a limited range and optimal prestrain and fibre volume fractions can be found. Yield stress also increases with increasing temperature within a limited temperature range. The enhancement of the resistance to fatigue crack propagation is suggested to be ascribed to the combination of compressive residual stress, higher stiffness of the composite, the stress induced martensitic transformation and the dispersion of mechanical strain energy at the crack tip. Prestrain, on the other hand, generally contributes to the damage accumulation for failure and decreases the elongation and ductility of the composite.

In determining the prestrain, elongation and ductility of a SMA composite it has to be realised that Poisson's ratio is strictly defined only for small strain linear elastic behaviour. For highly nonlinear elastic materials, such as smart materials, it becomes necessary to define a strain varying Poisson's

ratio. Consequently, Evans, Smith and Wootton (1999) have attempted interpretation of experimental data for Poisson's ratio of highly nonlinear materials by defining various Poisson's ratios based on various forms of strain. The usual strain quoted is the engineering strain (sometimes called the nominal or Cauchy strain) and is a measure of extension relative to initial length. When dealing with larger extensions it is common to refer to the true strain or Hencky strain. Most textbooks define true strain as a summation of the ratio of extension to the instantaneous length. The resulting integral returns the answer in logarithmic format and hence, this true strain is sometimes referred to as the log true strain. Since the integral returns a secant value of the extension and not a localised tangent value, it follows that if the deformation is nonlinear, this true strain may not accurately reflect instantaneous conditions, but more those relative to starting conditions. Thus, an instantaneous true strain is defined as the ratio between extension and instantaneous length. This instantaneous strain is used to define the instantaneous Poisson's ratio for greater accuracy in modeling the behaviour of highly nonlinear materials. The instantaneous Poisson's ratio can be determined experimentally, graphically or numerically.

Evans et. al. (1999) goes on to describe various smoothing techniques that can be applied to a set of experimental data to reduce the amount of noise. A summary of these techniques is presented here,

- Polynomial regression can be performed automatically on many spreadsheet packages. however, it is sometimes best to consider fitting several regressions to separate portions of the data set rather than as a whole to avoid smothering localised effects.

- Moving average or weighted average techniques use a fixed number of data within a frame that is moved along the entire data set. An arithmetic mean or weighted mean is calculated for each step along the data set. The number of data included in the moving frame is important, since this number controls the smoothing effect; the greater the number of points, the greater the smoothing effect. However, the larger the number of data in the moving frame, the more localised effects are blurred out and the more data are lost at the start and finish of the data set. This method is not good with very noisy data.

- The Fourier transform method is more complicated to use than the other methods, but is much more powerful. It overcomes the limitations of the frame size or statistical reliability of a polynomial fit to a small data set, no data are lost at the start and end of the set, it is possible to see clearly what information is being discarded (as noise) and what is kept and it is easy to change the amount of information being discarded. The method works by

transforming the original data set into its frequency spectrum where it is possible to discern the higher frequency noise component. The frequencies to be retained and discarded are chosen. The data retained can then be transformed back from the frequency domain to its original domain.

While the design approach presented in Figure A-4 appears straight forward, the first step tends to prove difficult to implement. Miyazaki et. al. (1998) was initially unsuccessful in embedding Ti-Ni directly into a polymer matrix due to manufacturing difficulties and problems associated with interfacial bonding. The interfacial bonding issue was eventually overcome by alternatively incorporating SMA wires into the polymer matrix using coupling sleeves. In general, fibre reinforced thermoplastics offer substantial advantages over fibre reinforced thermosets because of their excellent specific stiffness, high fracture toughness, low moisture absorption and possible fast and cost effective manufacturing processes. Thermoplastics, however, require high processing temperatures that affect the microstructure of the SMA; the transformation temperature of the SMA shifts upwards while the peak recovery stress drops. The lower processing temperatures of thermosets only mildly affect the transformation characteristics of SMA, though some dynamic properties of the SMA fibres may be significantly affected (Miyazaki et. al. : 1998).

Furuya and colleagues (Furuya, Sasaki & Taya : 1993; Furuya, Mori, Shibata, Taya, Watanabe & Yamada : 1993) have developed three kinds of fabrication procedures.

- The Ti-Ni fibres were arranged in a fixed holder in a mould, then molten aluminium (970K) was poured into the mould followed by pressurisation at sixty-five megapascals. Because the melting temperature of aluminium is not very high, even though a thin layer with a thickness of less than three micrometers of the fibre surface was affected by diffusion interaction, most of the Ti-Ni fibres remained unaffected during the processing. The composite was then subjected to heat treatment (773 K, thirty minutes) to shape memorise the Ti-Ni fibres, followed by ice water quenching to induce martensitic transformation. A specific tensile prestrain was applied and then the composite was heated to a temperature above the austenite finish point.

- Aluminium powders and Ti-Ni fibres were placed into a mould and pressed at two-hundred megapascals in air at room temperature to form a green sheet and then it was sintered in a vacuum furnace (10^{-4} torr) at 843 K for one hour. A shape memory treatment was simultaneously made during the sintering process. The porosity of the as-sintered composite was eight percent. The high elongation of the aluminium matrix at room temperature (up to twelve percent) was used to provide prestrains of up to four to five

percent to the Ti-Ni fibres. Pure aluminium, Al-1100, has a very low yield stress and hence, 6061-T6 and 6082-T6 aged aluminium alloys have been more recently used for structural applications.

- Ti-Ni fibres were wound around or longitudinally laced onto thin aluminium alloy sheets with rectangular end notches. The fibre laced prepreg sheets were stacked on a pair of hot press dies or loaded into a vacuum canister and were then hot pressed at proper temperatures and pressures. A thin layer (within three micrometers) of interfacial phases such as Al_3Ti and Al_3Ni was produced because of the interfacial reactions between the Ti-Ni fibre and the matrix. The optimum hot pressing conditions for Al-6061 were found to be 773 K for thirty minutes at fifty-four megapascals. The material could be either directly water quenched and then aged, or cooled down in the furnace while keeping the pressure constant, followed by a solution treatment and T6 ageing. A loading and unloading process was applied to the composite at room temperature to produce various prestrains. The processing procedure resulted in good macro scale homogeneity and little internal porosity, and various volume fractions of Ti-Ni fibres could be embedded into the aluminium matrix.

More recently, within the last three to four years, smart composites have been manufactured by sheath rolling; the fibres were laminated between plates of the matrix material and then inserted into a stainless steel pipe and vacuum encapsulated. The sealed laminates were then sheath rolled at various temperatures and then reheated at the temperatures for different times. A thirty micrometer reaction interfacial layer was formed between the fibres and the matrix and was found to be effective for stress conductivity.

Upon completion of the composite manufacture, the embedded SMA fibres can be actively controlled by electric current heating and hence undergo the reverse martensitic transformation, giving rise to a change of stiffness, vibration frequency and amplitude, acoustic transmission or shape of the composite. Active property control can be accomplished through a) the change in stiffness (inherent modulus) of the embedded SMA elements or b) activating the pre-strained SMA elements to generate a stress. These two techniques are termed active property tuning (APT) and active strain energy tuning (ASET) respectively. Generally, APT requires a large volume fraction of SMA fibres that are embedded without prior plastic elongation and do not create any large internal forces. ASET, however, may be equally effective with an order of magnitude smaller volume fraction of SMA fibres that are 'active' and impart large internal stresses throughout the structure (Miyazaki et. al. : 1998). When fibres are activated by passing a current through them, they will try to contract to their normal length, and therefore generate a large, uniformly distributed

shear load along the length of the fibres. High strain SMA fibres have a relatively high ultimate strength and can absorb and dissipate a large amount of strain energy, first through the stress induced martensitic transformation and then through plastic yielding. These SMA composites are thus, ideally suited for impact damage control as compared to advanced composites such as graphite/epoxy and glass/epoxy that have poor resistance to impact damage because of the lack of an effective mechanism for dissipating impact strain energy.

SMA dissipates strain energy of the order of four times of high alloy steel and sixteen times that of many graphite/epoxy composites through the stress induced martensitic transformations (Miyazaki et. al. : 1998). This strain energy absorbing capacity can be used to actively control the propagation of cracks. Paine and colleagues (Paine & Rogers : 1994a; Paine & Rogers : 1994b; Chaudhry, Kiesling, Paine & Rogers : 1996) made recent studies to improve the impact damage resistance of brittle thermoset matrix composite materials by hybridising the composites with SMA. The low velocity impact test was performed using an instrumented drop weight impact tester; the dissipated impact energy and deflection, during impact were determined from force-time data. The results showed that the composite with SMA fibres resisted the cutting action through distributing the impact load over a greater surface area, because the SMA remained intact during the perforation event. The monolithic graphite/epoxy and glass/epoxy and the aluminium and Kevlar hybrids all failed locally from a punched or cut hole from the local transverse shear stresses at the edge of the impact site. Further testing of composites (graphite/bismaleimide) embedded with SMA fibres revealed greatly improved impact resistance due to an increase in peak impact force and a reduction of the impacted induced delamination area. Testing with a reduced volume fraction of SMA fibres, however, resulted in an increased delamination area as compared to plain graphite/epoxy composites, though absorption of impact energy was increased. A quasi-static model demonstrates that contact deformation, global bending deformation and transverse shear deformation are the energy absorption mechanisms for SMA graphite/epoxy composites under a low velocity impact (Pain et. al. : 1994a; Paine et. al. : 1994b; Chaudhry et. al. : 1996). At very low velocities, the contact energy absorption is the most effective mechanism, while the shear deformation absorbs most of the impact energy at higher impact velocities. The total energy absorption of the SMA hybrid composites increases when the stress induced martensitic transformation occurs.

The ballistic impact resistance of graphite composites was investigated by Ellis, Jia, Lalande and Rogers (1997) using a nine-millimeter Beretta handgun with the projectile velocity greater than nine hundred feet per second (274.32 m/s). The results suggest that the high strain absorption capabilities of the SMA were not fully utilised at ballistic velocities because of the high strain rate effects coupled with a strain mismatch between the relatively tough SMA fibres and the brittle

cured epoxy resin. The SMA fibres were found to be more effectively used when embedded between layers of the thermoplastic extended chain polyethylene (ECPE or Spectra) prepregs. Though the energy absorption was increased when compared to the plain graphite composite, the SMA fibres were still not fully utilised as evidenced by the lack of fibres strained to failure.

An ideal actuation material would display a large stroke, high recovery force and superior dynamic response (Miyazaki et. al. : 1998). SMA exhibit large strokes and forces, but suffer from a slow response. Ferroelectric ceramics are very sensitive to applied stresses through the direct piezoelectric effect and generate powerful forces by means of the converse piezoelectric effect. The ceramics are characterised by excellent dynamic response (of the order of microseconds) but their displacements are quite small (of the order of a few micrometers) due to their small strain magnitude. Piezoelectric thin films can be fabricated with various techniques such as sputtering, chemical vapour deposition (CVD) and sol-gel processing. Blaszkiewicz, Chen, Meyer, Newnham and Xu (1992) first successfully deposited thin films of PZT and PLZT, 0.6 and 1.4 nm in thickness respectively on Ti-Ni SMA foils by the sol-gel process and multi-step spin-on coating techniques. The PZT films were found to adhere well to the Ti-Ni alloy for strains as large as 0.4% and their ferroelectric properties remained unchanged during repeated cycling through the shape memory transformation. It is very important that the fabrication steps be minimised and if deposited on amorphous SMA films, both types of the amorphous thin films be crystallized simultaneously, so as not to promote degradation of performance due to second phases and chemical interactions via diffusion. Although the hetrostructures have good piezoelectric properties, the cracking of the piezoceramic thin film layer remains a crucial problem.

By coupling Ti-Ni SMA to PZT via a TiO_2 buffer layer, the final composite material can sense and actuate to dampen structural vibration without the use of external control as depicted in Figure A-5 (Miyazaki et. al. : 1998).

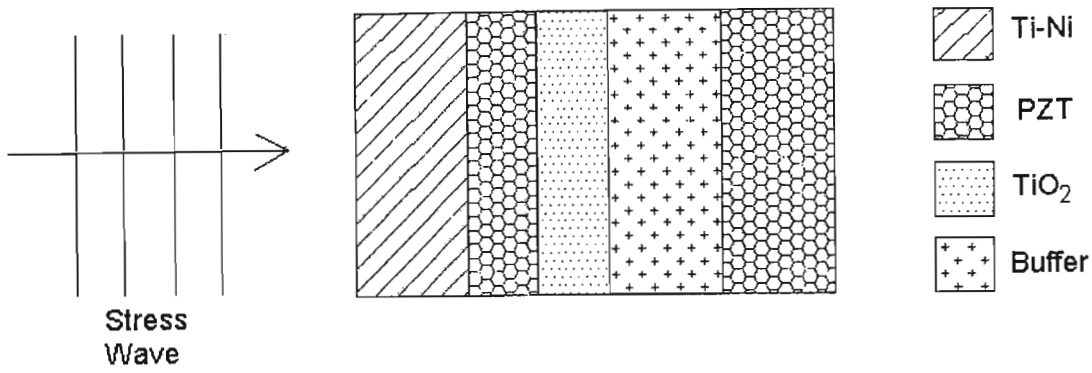

Figure A-5: Self-sensing and actuation of a SMA PZT smart material (after Miyazaki et. al. : 1998)

The stress wave propagates through the Ti-Ni SMA producing a stress induced martensitic transformation where some of the mechanical energy is converted into heat. The wave further produces a voltage across the first ferroelectric layer that can be used to produce an out-of-phase stress wave by the second ferroelectric layer, and in turn attenuate the stress wave. A mechanical metallic impedance buffer (such as aluminium, titanium or Ti-Ni) is used to provide time for the counter-stress attenuation to occur.

As compared to ferroelectrics, magnetostrictive materials provide large displacements, higher counter forces and output energy density and superior manufacturing capabilities. Terfenol-D, for example, can be fabricated with the conventional magnetron sputtering techniques. Amorphous films show a sharp increase in the magnetostriction at low magnetic fields and no hysteresis during cycling of the field, whereas the crystalline films exhibit magnetostrictive hysteresis loops and large remanence and coercivity which limit their application (Miyazaki et. al. : 1998). Because amorphous Terfenol-D films do not involve annealing at elevated temperatures, which may address undesirable chemical interactions or diffusion, the fabrication of hybrid composite films seem easier and simpler. Magnetostrictive materials application, however, has been limited by poor fracture toughness, eddy current losses at higher frequencies and bias and prestress requirements.

A2. Selected Bibliography of Impact Loading and Smart Materials

Impact Loading

Alien, D. H. and Searcy, C. R., (1998), "Prediction of Damage Evolution in Laminated Composites Subjected to Impact Loading", *Journal of Mechanical Behaviour of Advanced Materials American Society of Mechanical Engineers, Vol.84, p.229-230*, ASME, United States of America.

Altay, B. and Doyum, A. B., (1997), "Low - Velocity Impact Damage in Glass Fibre/Epoxy Cylindrical Tubes", *Journal of Materials and Design, Vol. 18, No.3, p. 131-135*, Middle East Technical University, Turkey.

Anderson, T. A., Calvert, P. D., Denham, H. B. and Madenci, E., (1997), " Embedded PVF2 Sensors for Smart Composites", *Proceedings of SPIE- The International Society for Optical Engineering, Vol.3040, p. 138-1'47*, Society of Photo-Optical Instrumentation Engineers, United States of America.

Andrades, L. and Benitez, F. G., (1997), " In-Plane Impact Loading of Composites: Optical Evaluation and Crack Severity Assessment for Graphite-Epoxy", *Journal De Physique. IV, Vol.7, No.3, p. 169-174*, University of Seville, Spain.

Aschenbrenner, R. J., Grace, C., Kelkar, A. D., Sankar, J. and Schoeppner, G., (1997), " Behaviour of Tensile Preloaded Composites Subjected to Low-Velocity Impact Loads", *Recent advances in Solids/Structures and Applications of Metallic Materials American Society of Mechanical Engineers, Pressure Vessels and Piping Division, Vol. 369, p. 39-46*, ASME, United States of America.

Bank, L. C. and Gentry, T. R., (1998), " Finite-Element Modeling and Model Verification of Steel W-Beam Guardrails Subject to Pendulum Impact Loading", *Journal of Transportation Research Record, No. 1647, p. 147-157*, Georgia Institute of Technology, United States of America.

Banthia, N., Gupta, P. and Yan, C., (1999), " Impact Resistance of Fibre Reinforced Wet-Mix Shotcrete - Part I: Beam Tests", *Journal of Materials and Structures, Vol.32, No.222, p.563-570*. University of British Columbia, Canada.

Belingardi, G., Gugliotta, A. and Vadori, R., (1998), "Fragmentation of Composite Material Plates Submitted to Impact Loading: Comparison Between Numerical and Experimental Results", *Journal of Key Engineering Materials, Vol. 144, p.75-88*, Politecnico di Torino, Italy.

Benzeggagh, M. L. and Chotard, T. J., (1998), " On the Mechanical Behaviour of Pultruded Sections Submitted to Low-Velocity Impact", *Journal of Composites Science and Technology, Vol.58, No.6, p.839-854*, Universite de Technologie de Compiegne, France.

Beppu, M. and Miyamoto, A., (1998), " 3-D Dynamic Analysis and Computer Graphics Application to Impact Failure Simulation for Reinforced Concrete Slabs", *Proceedings of the 1998 5th International Conference on Structures Under Shock and Impact, p. 727-741*, Computational Mechanics Inc., United States of America.

Berstad, T., Hopperstad, O. S. and Langseth, M., (1999), " Impact Loading of Plates: Validation of Numerical Simulations by Testing", *International Journal of Offshore and Polar Engineering, Vol.9, No. 1, p. 10-15*, Norwegian University of Science and Technology, Norway.

Boniface, L., Foreman, A. and Hitchen, S., (1998), "Comparative Evaluation of Solid and Hollow S2 Glass Fibre-Epoxy Laminates", *Journal of Plastics, Rubber and Composites Processing and Applications, Vol.27, No.5, p.234-239*. University of Surrey, United Kingdom.

Bonini, J., Collombet, F., Lalbin, X., Lataillade, J. L. and Martin, V., (1998), " Damage Criteria for the Study of Impacted Composite Laminates", *Journal of Composites Science and Technology, Vol.58, No.5, p.679-686*. Esplanade des Arts el Metiers, France.

Caulfield, D. F., Clemons, C. M. and Giacomin, A. J., (1999), " Dynamic Fracture Toughness of Cellulose-Fibre-Reinforced Polypropylene: Preliminary Investigation of Microstructural Effects", *Journal of Elastomers and Plastics, Vol.3l, No.4, p.367-378*, USDA Forest Service, United States of America.

Chandra, N. and Rajendran, A. M., (1998), " Micromechanics Based Modeling of Damage in Composites Under High Velocity Impact - A Review", *Proceedings of the 1998 5th International Conference on Structures Under Shock and Impact, p.421 -432*, Computational Mechanics Inc., United States of America.

Charles, J. L., Collombet, F., Jeronimidis, G., Lalbin, X. and Lataillade, J. L., (1997), "Methodology and Tools for the Study of Composite Structures Under Impact Loading: Application to Long Fibre Laminated Structures", *Journal De Physique. IV, Vol. 7, No. 3, p. 163-168*, Ecole Nationale Superieure d'Arts et Metiers, France.

Christoforou, A. P. and Yigit, A. S., (1998), " Effect of Flexibility on Low Velocity Impact Response", *Journal of Sound and Vibration, Vol.217, No.3, p.563-578*, Kuwait University, Kuwait.

Collombet, F., Lalbin, X. and Lataillade, J. L., (1997), " Impact Behaviour of Laminated Composites: Physical Basis for Finite Element Analysis", *Journal of Composites Science and Technology, Vol.58, No.3-4, p.463-478*. Lab Materiaux Endommagement Fiabilite - ENSAM, France.

Czigany, T., Karger-Kocsis, J. and Moskala, E. J., (1999), " Stress Oscillation in Amorphous Copolyesters Due to Tensile Impact", *Journal of Polymer Engineering and Science, Vol.39, No.8, p. 1404-1411*, Universitaet Kaiserslautern, Germany.

Dang, X. and Liu, D., (1998), "Testing and Simulation of Laminated Composites Subjected to Impact Loading", *ASTM Special Technical Publication, No. 1330, p.273 -284*, ASTM, United States of America.

Dang, X., Liu, D. and Raju, B., (1998), " Size Effects on Impact Response of Composite Laminates", *International Journal of Impact Engineering, Vol.21, No. 10, p.837-854*, Michigan State University, United States of America.

Daves, T., Neogi, D. and Tessier, N. J., (1997), " Energy Absorbing Characteristics of Novel Composite Materials", *Structures Under Extreme Loading Conditions American Society of Mechanical Engineers, Pressure Vessels and Piping Division, Vol.351, p.325-340*, ASME, United States of America.

De Freitas, M. and Reis, L., (1997), " Damage Growth Analysis of Low Velocity Impacted Composite Panels", *Journal of Composite Structures, Vol.38, No. 1-4, p-509-515*. Institute of Superior Technico, Portugal.

Dharani, L. R. and Flocker, F. W., (1998), " Modeling Interply Debonding in Laminated Architectural Glass Subject to Low Velocity Impact", *Journal of Structural Engineering Mechanics, Vol.6, No.5, p.485-496*. Stress Engineering Services, United States of America.

Dodds, R. H. and Koppenhoefer, K. C., (1997), "Loading Rate Effects on Cleavage Fracture of Pre-Cracked CVN Specimens: 3-D Stadies" *Journal of Engineering Fracture Mechanics, Vol.58, No.3, p.249-270*. University of Illinois, United States of America.

Dodds, R. H. and Koppenhoefer, K. C., (1999), "Numerical Investigation of Loading Rate Effects in Pre-Cracked CVN Specimens", *ASTM Special Technical Publication, No. 13 32, p. 135-153*, ASTM, United States of America.

Donze, F. V. and Magnier, S. A., (1998), " Numerical Simulations of Impacts Using a Discrete Element Method", *Journal of Mechanics of Cohesive-Frictional Materials, Vol.3, No.3, p.257-276*, Universite du Quebec a Montreal, Canada.

Erki, M. A. and Meier, U., (1999), " Impact Loading of Concrete Beams Externally Strengthened with CFRP Laminates", *Journal of Composites for Construction, Vol.3, No.3, p.l 17-124*, Royal Military Coil. of Canada, Canada.

Evans, K. E., Jones, N. and Roach, A. M., (1998), " Penetration Energy of Sandwich Panel Elements Under Static and Dynamic Loading. Part I", *Journal of Composite Structures, Vol.42, No.2, p.l 19-134*, Elsevier, United Kingdom.

Friedrich, K., Karger-Kocsis, J., Keith, S. and Yuan, Q., (1997), " Crash and Energy Absorption Behaviour of Interleaved Carbon-Fibre-Reinforced Epoxy Tubes", *Journal of Material Science Letters, Vol.l6, No.22, p.l793-1796*. Royal Institute of Technology, United Kingdom.

Gary, G. and Zhao, H., (1997), " Experimental Investigation of Compressive Failure Strength of Fibre-Reinforced Polymer-Matrix Composite Plates Under Impact Loading", *Journal of Composites Science and Technology, Vol.57, No.3, p.287-292*, Ecole Polytechnique, France.

Hamouda, A. M. S. and Hashmi, M. S. J., (1998), "Testing of Composite Materials at High Rates of Strain: Advances and Challenges", *Journal of Materials Processing Technology, Vol.77, No.1-3, p.327-336*, Dublin City University, United Kingdom.

Harding, J. and Ruiz, C., (1998), "Mechanical Behaviour of Composite Materials Under Impact Loading", *Journal of Key Engineering Materials, Vol. 141-143, Pt.2, p.403-426.* University of Oxford, United Kingdom.

Hiramatsu, M., Takeda, N., Wan, L. and Yuan, J., (1997), "Characterisation of Effects of Strain Rate and Temperature on Impact Compressive Damage Progress of Glass Fibre Reinforced Composites", *Journal of Transactions of the Japan Society of Mechanical Engineers, Part A, Vol.63, No.616, p.2598-2603*, Japan Society of Mechanical Engineers, Japan.

Hojo, M., Kurokawa, T., Kusaka, T. and Ochiai, S., (1997), "Finite Element Simulation of Impact End Notched Flexure Test Using Ramped Incident Waves (Verification of the Proposed Method for Estimating Energy Release Rate)", *Transactions of the Japan Society of Mechanical Engineers, Part A, Vol.63, No.605, p. 158-164*, Japan Society of Mechanical Engineers, Japan.

Hojo, M., Kurokawa, T., Kusaka, T. and Ochiai, S., (1998), "Evaluation of Mode H Interlaminar Fracture Toughness of Composite Laminates Under Impact Loading", *Journal of Key Engineering Materials, Vol. 141-143, Pt.2, p-477-498*, Hyogo Prefectural Institute of Industrial Research, Japan.

Inou, N., Kuroda, H., Ujihashi, S. and Yamanaka, T., (1997), " Energy-Absorption Abilities of CFRP Cylinders During Impact Crushing", *Journal of Thin-Walled Structures, Vol.28, No.3-4, p.297-307*, Tokyo Institute of Technology, Japan.

Jang, J., Kim, H., Park, J., Park, R. and Yun, Y., (1997), "Failure of Ceramic/Fibre-Reinforced Plastic Composites Under Hypervelocity Impact Loading", *Journal of Materials Science Vol.32, No.1, p.23-33.* Royal Institute of Technology, United Kingdom.

Kelkar, A. D., Rajeev, K. and Sankar, J., (1998), " Analysis of Tensile Preloaded Composites Subjected to Low-Velocity Impact Loads", *Proceedings of the 1998 39th AIAA /ASME/ ASCE/AHS/ASC Structures, Structural Dynamics and Materials Conference and Exhibit and AIAA /ASME/AHS Adaptive Structures Forum. Part 3, Vol.3, p. 1978-1987*, AIAA, United States of America.

Kishore and Venkatraman, S., (1997), " Role of the Interface in Foam-Bearing Glass-Epoxy Composites Subjected to Impact Loading", *Journal of Composite Interfaces, Vol.5, No. I, p.55-67*, Indian Institute of Science, India.

Kobayashi, Y., Morita, R., Nagasaka, I., Ohnishi, N. and Yamaguchi, T., (1999), "Toughness Evaluation Method Using Strength and Impulse of a Material Under Tensile Impact Loading", *Journal of the Japan Institute of Metals, Vol.63, No.4, p.502-507*, Chubu University, Japan.

Krasowsky, A. J. and Orynyak, I. V., (1998), "Modeling of Elastic Response of a Three-Point Bend Specimen Under Impact Loading", *Journal of Engineering Fracture Mechanics, Vol.60, No.5, p.563-575*. National Academy of Sciences of Ukraine, Ukraine.

Kwon, Y. W. and Wojcik, G. W., (1998), "Impact Study of Sandwich Composite Structures with Delamination", *Journal of Composite Materials, Vol.32, No.5, p.406-430.* Naval Postgraduate School, United States of America.

Lewis, M. W., (1998), " On Predicting and Modeling Material Failure Under Impact Loading", *Proceedings of the 1998 5th International Conference on Structures Under Shock and Impact, p.569-578.* Computational Mechanics Inc., United States of America.

Mines, R. A. W., (1998), "Impact Energy Absorption of Polymer Composite Sandwich Beams", *Journal of Key Engineering Materials, Vol-141-143, Pt.2, p.553-572.* University of Liverpool, United Kingdom.

Miyazaki, N., Satoh, M. and Sutoh, M., (1999), "Experimental Evaluation of Impact Damage in FRP Laminates", *Journal of the Society of Material Science, Vol.48, No.5, p.507-511*, Kyushu University, Japan.

Morozov, Y. A., Popov, G. Y. and Usov, A. V., (1999), "On the Tangential Stress Intensity Factor for Semi-Infinite Cylindrical Crack Edge Under Impact Loading of the Crack Borders", *Journal of Problemy Prochnosti, No.3, p.63-72*, Odesskij Gosudarstvennyj University, Ukraine.

Needleman, A., (1997), " Numerical Modeling of Crack Growth Under Dynamic Loading Conditions", *Journal of Computational Mechanics, Vol. 19, No.6, p.463-469.* Brown University, United States of America.

Shapochkin, E. V. and Shapochkina, V. A., (1997), " Total Plastic Strain Under Local Impact Loading", *Journal of Fizika I Khimiya Obrabotki Materialov, No. 1, p. 104-108*, Moskovskaya Gosudarstvennaya Akademiya Priborostroeniya I Informatiki, Russia.

Shioya, T., Takeda, N. and Yuan, J., (1999), " High Temperature Impact Response of Silicon Nitride Ceramics", *Journal of Key Engineering Materials, Vol. 166, p. 19-24*, University of Tokyo, Japan.

Tai, N-H., Tseng, C-M. and Yip, M-C., (1999), "Influences of Thermal Cycling and Low-Energy Impact on the Fatigue Behaviour of Carbon/PEEK Laminates", *Journal of Composites Part B: Engineering, Vol.30, No.8, p.849-865*, Elsevier, United Kingdom.

Takeda, N. and Wan, L., (1995), "Impact Compression Damage Evolution in Unidirectional Glass Fibre Reinforced Polymer Composites", *High Strain Rate Effects on Polymer, Metal and Ceramic Matrix Composites and Other Advanced Materials American Society of Mechanical Engineers, Aerospace Division, Vol.48, p. 109-113*, ASME, United States of America.

Wierzbicki, T., (1999), " Petalling of Plates Under Explosive and Impact Loading", *International Journal of Impact Engineering, Vol.22, No.9, p.935-954*, Massachusetts Institute of Technology, United States of America.

Woldesenbet, E., (1999), " High Strain Rates Properties of Composite Materials", *Proceedings of the 1999 ASME Energy Sources Technology Conference*, ASME, United States of America.

Zukas, J. A., (1995), "Numerical Modeling of High Velocity Impact in Non-Metallic Materials", *High Strain Rate Effects on Polymer, Metal and Ceramic Matrix Composites and Other Advanced Materials American Society of Mechanical Engineers, Aerospace Division, Vol.48, p.49-62*, ASME, United States of America.

Smart Materials – General

Adeli, H. and Saleh, A., (1998), "Integrated Structural / Control Optimisation of Large Adaptive / Smart Structures", *International Journal of Solids and Structures, Vol.35, No.28-29, p.3815-3830*, Elsevier, England.

Agnes, G. S. and Mall, S., (1999), " Structural Integrity Issues During Piezoelectric Vibration Suppression of Composite Structures", *Journal of Composites Part B: Engineering, Vol.30, No.7,p.727-738*, Elsevier, England.

Aizawa, S., Higasino, M. and Kakizawa, T., (1998), "Case Studies of Smart Materials for Civil Structures", *Journal of Smart Materials and Structures, Vol.7, No.5, p.617-626*, IOP Publishing, United Kingdom.

Austin, F., Clifford, R. and Van Nostrand, W., (1997), "Some Applications of Smart Materials in Industry", *Proceedings of US-Japan Workshop on Smart Materials and Structures*, Minerals, Metals and Materials Society / AIME, United States of America.

Banks, H. T. and Kurdila, A. J., (1996), "Hysteretic Control Influence Operators Representing Smart Material Actuators: Identification and Approximation", *Proceedings of the IEEE Conference on Decision and Control, Vol.4, p.3711-3716*, IEEE, United States of America.

Baz, A., Oh, J. and Ruzzene, M., (1999), " Control of the Dynamic Characteristics of Passive Magnetic Composites", *Journal of Composites Part B: Engineering, Vol.30B, p.739-751*, Elsevier, United Kingdom.

Berman, J. and White, S., (1996), " Theoretical Modeling of Residual and Transformational Stresses in SMA Composites", *Journal of Smart Materials and Structures, Vol.5, No.6, p.731-743*, IOP Publishing, United Kingdom.

Birman, V., (1996), " Thermal Effects of Measurements of Dynamic Processes in Composite Structures Using Piezoelectric Sensors", *Journal of Smart Materials and Structures, Vol.5, No.4, p.379-385*, IOP Publishing, United Kingdom.

Birman, V., (1997), " Review of Mechanics of Shape Memory Alloy Structures ", *Journal of Applied Mechanics Review, Vol.50, No.11, Pt 1, p.629-645*, ASME, United States of America.

Blaszkiewicz, M., Chen, J., Meyer, R., Newnham, R. E. and Xu, Q. C., (1992), *Journal of American Ceramic Society, Vol.75, p.2891*. United States of America.

Canon, E. and Lenczner, M., (1998), " Models of Thin Plates with Piezoelectric Inclusions and Electronic Circuits", *Journal of Comptes Rendus Del Academic Des Sciences Serie II Fascicule B - Mechanique Physique Astronomic, Vol-326, No. 12, p.793-798*, Elsevier, France.

Casciati, F., Faravelli, L. and Petrini, L., (1998), "Energy Dissipation in Shape Memory Alloy Devices", *Journal of Computer-Aided Civil and Infrastructure Engineering, Vol.13, No.6, p.433-442*. University of Pavia, Italy.

Chattopadhyay, A. and Seeley, C. E., (1997), " A Higher Order Theory for Modeling Composite Laminates with Induced Strain Actuators", *Journal of Composites Part B: Engineering, Vol.28, No.3, p.243-252*, Elsevier, England.

Chaudhry, Z., Kiesling, T. C., Paine, J. S. N. and Rogers, C. A., (1996), *Proceedings of the 37th AIAA /ASME/ASCE/AHS/ASC Structures, Structural Dynamics and Materials Conference p. 1448*, ASME, United States of America.

Cross, L. E., (1995), " Boundary Conditions for Shape Memory in Ceramic Material Systems", *Journal of Intelligent Material Systems and Structures, Vol.6, No. 1, p.55-61*, Technomic Publishing, United States of America.

DeGiorgi, V. G., Lindner, D. K. and McDermott, S. H., (1998), " Combining Modeling Methodologies for Improved Understanding of Smart Material Characteristics", *Journal of intelligent Material Systems and Structures, Vol.9, No.7, p.509-521*, Technomic Publishing, United States of America.

DeGiorgi, V. G. and McDermott, S. H., (1997), "Structural and Performance Predictions for an Active Composite Panel", *Proceedings of SPIE- The International Society for Optical Engineering, Vol.3044, p.422-432*, SPIE - Int. Soc. for Opt. Engineering, United States of America.

Delaey, L., Stalmans, R. and Van Humbeeck, J., (1996), "Modeling of the Thermomechanical Behaviour of Shape Memory Wires embedded in Matrix Materials", *SPIE – The International Society for Optical Engineering, Vol.2779, p.511-516*, SPIE - Int. Soc. For Opt. Engineering, United States of America.

Delaey, L., Stalmans, R. and Van Humbeeck, J., (1997), " Modeling of Adaptive Composite Materials with Embedded Shape Memory Alloy Wires", *Proceedings of Materials for Smart Systems Symposium II, Vol.459, p.119-130*, Materials Research Society, United States of America.

Dukkipati, R. V., Molyet, K. E. and Naganathan, N. G., (1999), "Study of Induced Strain Transfer in Piezoceramic Smart Material Systems", *Journal of Smart Materials and Structures, Vol.8, No.5, p.672-690*, TOP Publishing, United Kingdom.

Dukkipati, R. V., Naganathan, N. G., Peelamedu, S. M. and Yu, Y., (1999), "Active Strain-Transfer Analysis in a Piezoceramic System using a Finite-Element Method and Experimental Investigation", *Journal of Smart Materials and Structures, Vol.8, No.5, p.654-662*, IOP Publishing, United Kingdom.

Ellis, R. L., Jia, H., Lalande, F. and Rogers, C. A., (1997), *Proceedings of the 38th AIAA /ASME/ ASCE/AHS/ASC Structures, Structural Dynamics and Materials Conference*, ASME, United States of America.

Evans, K. E., Smith, C. W. and Wootton, R. J., (1999), "Interpretation of Experimental Data for Poisson's Ratio of Highly Nonlinear Materials", *Journal of Experimental Mechanics, Vol.39, No.4, p.356-362*. Sage Publications Inc., United States of America.

Fang, D. N., Hwang, K. C. and Jiang, B., (1997), "The Effective Properties of Piezocomposites, Part H: The Effective Electroelastic Moduli", *Journal of ACTA Mechanica Sinica, Vol. 13, No.4, p.347-354*. Science China Press, Peoples Republic of China.

Furuya, Y., (1996), " Design and Material Evaluation of Shape Memory Composites", *Journal of Intelligent Material Systems and Structures, Vol.7, p.321-330*, Technomic Publishing, United States of America.

Furuya, Y., Mori, T., Shibata, S., Taya, M., Watanabe, R. and Yamada, Y., (1993), "Smart Structures and Materials 1993: Smart Materials", *SPIE- The International Society for Optical Engineering, Vol. 1916, p.373*, SPIE - Int. Soc. for Opt. Engineering, United States of America.

Furuya, Y., Sasaki, A. and Taya, M., (1993), "Material Transformations", *Journal of Intelligent Material Systems and Structures, Vol.34, p.224*, Technomic Publishing, United States of America.

Furuya, Y, Shimamoto, A. and Taya, M., (1997), "Enhancement of Mechanical Properties of TiNi Fibre Composites by Shape Memory Effect", *Proceedings of US-Japan Workshop on Smart Materials and Structures*, Minerals, Metals and Materials / AIME, United States of America.

Gardiner, P. T., Sirkis, J. S. and Spillman, W. B., (1996), "Smart Materials and Structures: What are they?". *Journal of Smart Materials and Structures, Vol.5, No.3, p.247-254*, IOP Publishing, United Kingdom.

Gao, D. Y. and Russell, D. L., (1996), " An Extended Beam Theory for Smart Materials Applications .1. Extended Beam Models, Duality-Theory, and Finite Element Simulations", *Journal of Applied Mathematics and Optimisation, Vol.34, No.3, p.279-298*, Virginia Polytech Institute and State University, United States of America.

Gao, D. Y. and Russell, D. L., (1998), "Extended Beam Theory for Smart Materials Applications. Part II: Static Formation Problems", *Journal of Applied Mathematics and Optimisation, Vol.38, No.1, p.69-94*, Virginia Polytechnic Institute and State University, United States of America.

Ge, S. S., Gong, J. Q. and Lee, T. H., (1998), "Dynamic Modeling of a Smart Materials Robot", *AIAA Journal, Vol.36, No.8, p.1 466-1478*, American Institute of Aeronautics and Astronautics, United States of America.

Gobin, P. F., Guenin, G., Morin, M., Salvia, M. and Tatibouet, J., (1996), "Composites-Based Smart Materials", *Proceedings of Conference on Progress in Advanced Materials and Mechanics, Vol. I*, Peking University Press, China.

Gobin, P. F. and Tatibouet, J., (1996), " Proceedings of the 3rd International Conference on Intelligent Materials and 3rd European Conference on Smart Structures and Materials", *SPIE- The International Society for Optical Engineering, Vol.2779, p. 1017*, SPIE - Int. Soc. for Opt. Engineering, United States of America.

Gopinathan, S. V., Lim, Y-H., Varadan, V. K. and Varadan, V. V., (1999), " Finite Element Simulation of Smart Structures Using an Optimal Output Feedback Controller for Vibration and Noise Control", *Journal of Smart Materials and Structures, Vol.8, No. 3, p.324-337*, IOP Publishing, United Kingdom.

Gorbet, R. B. and Morris, K. A., (1998), " Generalised Dissipation in Hysteretic Systems ", *Proceedings of the IEEE Conference on Decision and Control, Vol.4, p.4133-4138*, IEEE, United States of America.

Goswami, S. and Kant, T., (1998), "Active Vibration Control of Intelligent Stiffened Laminates Using Smart Piezoelectric Materials by the Finite Element Method", *Journal of Reinforced Plastics and Composites, Vol.17, No.16, p.1472-1493*, Indian Institute of Technology Bombay, India.

Hilton, H. H., Ling, S. F., Vinson, J. R., Yi, S. and Ying, M., (1999), "Finite Element Formulation for Anisotropic Coupled Piezoelectro-Hygro-Thermo-Viscoelasto-Dynamic Problems", *International Journal for Numerical Methods in Engineering, Vol.45, No. 11, p. 1531-1546*, John Wiley & Sons Ltd., England.

Hou, Z., Noori, M. N. and Shakeri, C., (1996), " Smart Materials and Structures - A Review", *Proceedings of the Materials Engineering Conference, Vol.2, p.863-876*, ASCE, United States of America.

Hughes, D. C., Lagoudas, D. C., Shu, S. G. and Wen, J. T., (1997), "Modeling of a Flexible Beam by Shape Memory Alloy Wires", *Journal of Smart Materials and Structures, Vol.6, No.3, p.265-277*, IOP Publishing, United Kingdom.

Hughes, D. C. and Wen, J. T., (1995), " Preisach Modeling of Piezoceramic Hysteresis: Independent Stress Effect", *SPIE- The International Society for Optical Engineering, Vol.2442, p-328-336*, SPIE - Int. Soc. for Opt. Engineering, United States of America.

Inman, D. J. and Van Nostrand, W. C., (1995), "Finite Element Model for Active Constrained Layer Damping", *SPIE - The International Society for Optical Engineering, Vol.2427, p. 124-139*, SPIE - Int. Soc. for Opt. Engineering, United States of America.

James, R. D. and Kinderlehrer, D. S., (1993), " Mathematical Approaches to the Study of Smart Materials", *SPIE- The International Society for Optical Engineering, Vol. 1919, p.2-18*, SPIE - Int. Soc. for Opt. Engineering, United States of America.

Jia, J. and Rogers, C. A., (1990), " Formulation of a Laminated Shell Theory Incorporating Embedded Distributed Actuators", *Journal of Mechanical Design, Vol. 112, No.4, p.596-604*, Virginia Polytech Institute and State University, United States of America.

Joshi, S. P. and Mannas, J. R., (1993), "Study of Smart-Sensing Elements in a Dynamic Stress Field", *SPIE- The International Society for Optical Engineering, Vol. 1918, p.264-275*, SPIE - Int. Soc. for Opt. Engineering, United States of America.

Kamita, T. and Matsuzaki, Y., (1997), " Pseudoelastic Hysteresis of Shape Memory Alloys", *Proceedings of US-Japan Workshop on Smart materials and Structures*, Minerals, Metals and Materials Society / AIME, United States of America.

Kang, Z. C. and Wang, Z. L., (1998), " Functional and Smart Materials: Structural Evolution and Structure Analysis", *Georgia Institute of Technology*, Plenum Publishing Corp., United States of America.

Krawczuk, M., Ostachowicz, W. and Zak, A., (1998), " Natural Frequencies of Multi-Layer Composite Plate with Embedded Shape Memory Alloy Wires", *Journal of Intelligent Material Systems and Structures, Vol.9, No.3, p.232-237*, Technomic Publishing, United States of America.

Kurdila, A. J., Lagoudas, D. C. and Webb, G. V., (1998), "Hysteresis Modeling of SMA Actuators for Control Applications", *Journal of Intelligent Material Systems and Structures, Vol.9, No.6, p.432-448*, Technomic Publishing, United States of America.

Leclercq, S., Lin, P. H., Lexcellent, C. and Tobushi, H,, (1994), "Thermodynamical Modeling of Recovery Stress Associated with R-Phase Transformation in TiNi Shape Memory Alloys", *Journal of Materials Transactions, Vol.35, No.5, p.325-331.* Cent Nati de la Recherche Scientifique, France.

Librescu, L., Oh, S. Y. and Song, O., (1999), "Vibration Control of Advanced Rotating Blades via Incorporation of Smart Materials Technology", *Collection of Technical Papers-AIAA /ASME/ASCE/AHS/ASC Structures, Structural Dynamics and Materials Conference,Vol.4, p.2753-2762*. United States of America.

Lim, Y-H., Varadan, V. K. and Varadan, V. V., (1999), "Closed Loop Finite Element Modeling of Active Structural Damping in the Time Domain", *Journal of Smart Materials and Structures, Vol.8, No.3, p.390-400*, IOP Publishing, United Kingdom.

Lin, F. and Zhang, W., (1994), " Smart Structure Damping Modeling", *Proceedings of the IEEE Conference on Decision and Control, Vol.4, p.3975-3980*, IEEE, United States of America.

Mackerle, J., (1998), " Smart Materials and Structure - A Finite – Element Approach : A Bibliography (1986-1997)", *Journal of Modeling and Simulation in Materials Science and Engineering, Vol.6, No.5, p.293-334*, IOP Publishing, United Kingdom.

Manson, G., Tomlinson, G. R. and Worden, K., (1993), "Pseudo-Fault Induction in Engineering Structures", *Proceedings of Adaptive Structures and Material Systems American Society of Mechanical Engineers Aerospace Division, Vol.35, p.449-455*, ASME, United States of America.

Maruszewski, B. M., Restuccia, L. and Starosta, R., (1995), "Thermodynamic Model of an Elasto-Viscoelasto-Porous Smart Material Architecture", *SPIE- The International Society for Optical Engineering, Vol.2442, p.524-531*, SPIE - Int. Soc. for Opt. Engineering, United States of America.

Matsuzaki, Y., (1997), " Smart Structures Research in Japan ", *Journal of Smart Materials and Structures, Vol.6, No.4, p.R1-R10*, IOP Publishing, United Kingdom.

Miyazaki, S., Sandstrom, R. and Wei, Z. G., (1998), " Shape-Memory Materials and Hybrid Composites for Smart Systems. II. Shape-Memory Hybrid Composites", *Journal of Materials Science, Vol.33, No. 15, p.3763-3783*. Royal Institute of Technology, United Kingdom.

Naganathan, N. G., Seshu, P. and Thirupathi, S. R., (1997), "A Finite-Element Static Analysis of Smart Turbine Blades", *Journal of Smart Materials and Structures, Voi.6, No.5, p.607-615*, IOP Publishing, United Kingdom.

Otsuka, K. and Ren, X. B., (1999), " Recent Developments in the Research of Shape Memory Alloys", *Journal of intermetallics. Vol.7, No.5, p.511-528*, Elsevier, England.

Paine, J. S. N. and Rogers, C. A., (1994a), " Active Materials and Smart Structures", *SPIE- The International Society for Optical Engineering, Vol.2427, p.358*, SPIE - Int. Soc. for Opt. Engineering, United States of America.

Paine, J. S. N. and Rogers, C. A., (1994b), "Smart Structures and Materials 1994: Smart Structures and Intelligent Systems", *SPIE - The International Society for Optical Engineering, Vol.2190, p.402*, SPIE - Int. Soc. for Opt. Engineering, United States of America.

Roytbued, A. and Yu, Y., (1995), " Modeling of Polydomain Smart Materials", *Proceedings of Materials for Smart Systems Symposium, Vol-360, p. 151-156*, Materials Research Society, United States of America.

Schetky, L. M., (1998), " Engineering Applications for Shape Memory Alloys: Present Status, Future Potential", *Proceedings of the International Conference on Displacive Phase Transformations and their Applications in Materials Engineering, Minerals*, Metals and Materials Society / AIME, United States of America.

Sirkis, J. S., (1996), " What Does it Take to be Smart?", *Proceedings of SPIE- The International Society for Optical Engineering, Vol.2718, p.4-18*, SPIE - Int. Soc. for Opt. Engineering, United States of America.

Sittner, P., Takakura, M., Tokuda, M. and Ye, M., (1998), "Calculation of Mechanical Behaviours of Shape Memory Alloy Under Multi-Axial Loading Conditions", *International Journal of Mechanical Sciences, Vol.40, No.2-3, p.227-235*, Pergamon-Elsevier, England.

Suhir, E., (1996), " Dynamic-Response of a One-Degree-of-Freedom Linear-System to a Shock Load During Drop Tests - Effect of Viscous Damping", *IEEE Transactions on Components Packaging and Manufacturing Technology Part A, Vol. 19, No.3, p.435-440*, IEEE, United States of America.

Tao, X. and Thompson, B. S., (1994), "Note on the Experimentally-Determined Elastodynamic Response of a Slider-Crank Mechanism Featuring a Macroscopically-Smart Connecting Rod with Ceramic Piezoelectric Actuators and Strain Gauge Sensors", *Proceedings of the 23rd Biennial Mechanisms Conference American Society of Mechanical Engineers, Design Engineering Division, Vol.71, Pt.2, p.63-69*, ASME, United States of America.

Taya, M., (1999), "Micromechanics Modeling of Smart Composites", *Journal of Composites Part A: Applied Science and Manufacturing, Vol.30, No.4, p.531-536*, Elsevier, United Kingdom.

Wang, Z., Wu, J. S. and Wu, X. D., (1999), " Variation of Electrical Resistance of Near Stoichiometric NiTi During Thermo-Mechanic Procedures", *Journal of Smart Materials and Structures, Vol.8, No.5, p.574-578*, IOP Publishing, United Kingdom.

Piezoelectric Materials

Aboudi J., (1999), " Micromechanical Prediction of the Response of Electrostrictive Multiphase Composites", *Journal of Smart Materials and Structures, Vol.8, No.5, p.663-671*, IOP Publishing, United Kingdom.

Adali, S., Ashida, F., Noda, N., Tauchert, T. R. and Verijenko, V., (2000), " Developments in Thermopiezoelasticity with Relevance to Smart Composite Structures", *Journal of Composite Structures, Vol.48, No.1-3, p.31-38*, Elsevier, United Kingdom.

Agbossou, A., Mahut, T. and Pastor, J., (1998), " Dynamic Analysis of Piezoelectric Fibre Composite in an Active Beam Using Homogenisation and Finite Element Methods", *Journal of Intelligent Material Systems and Structures, Vol.9, No.12, p.1009-1016*, Technomic Publishing, United States of America.

Agbossou, A., Pastor, J. and Viet, H. N,, (1999), "Homogenisation Techniques and Application to Piezoelectric Composite Materials", *International Journal of Applied Electromagnetics and Mechanics, Vol. 10, No.5, p.391-403*, IOS Press, Netherlands.

Akimoto, N., Igarashi, H., Ishii, K. and Tashirio, S., (1999), "Jump Phenomena of Current in Piezoelectric-Ceramic Vibrators Under High Power Conditions", *Journal of the European Ceramic Society, Vol.19, No.6-7, p.1157-1160*, Switzerland.

Akpan, U. O. and Orisamolu, I. R., (1999), "Probabilistic Characterisation of the Performance of Actively Controlled Smart Structures", *Proceedings of the SPIE-The International Society for Optical Engineering, Vol.3667, p.836-846*, SPIE - Int. Soc. Opt. Eng., United States of America.

Albareda, A., Briot, R., Gonnard, P., Guyomar, D. and Perrin, V., (1998), "Characterisation of the Piezoelectric Ceramic Mechanical Nonlinear Behaviour", *Proceedings of the Eleventh IEEE International Symposium on Applications of Ferroelectrics, p.353-356*, IEEE, United States of America.

Alford, N. McN., Calderon-Moreno, J. M., Guiu, F., Meredith, M., Penn, S. J. and Reece, M. J., (1999), "Anisotropic and Cyclic Mechanical Properties of Piezoelectrics – Compression Testing", *Journal of the European Ceramic Society, Vol.19, No.6-7, p.1321-1324*, Switzerland.

AlRaweshidy, H. S., Bhatti, A. and Murtaza, G., (2000), "Finite Element Analysis of Piezoelectric Polymer-Coated D-Fibre Intended for Electric Field Sensing", *Journal of Fibre and Integrated Optics, Vol.19, No.1, p.79-85*, Taylor & Francis Ltd., England

Antes, H. and Daros, C. H., (2000), "Dynamic Fundamental Solutions for Transversely Isotropic Piezoelectric Materials of Crystal Class 6 mm". *International Journal of Solids and Structures, Vol.37, No.11, p.1639-1658*, Elsevier, England.

Arnold, W., Gebhardt, W. and Hirsekorn, S., (1999), " Modeling of Graded 1-3 Composite Piezoelectric Transducers", *Journal of Materials Science Forum, Vol.308-311, p.521-526*, Germany.

Audigier, D., Eyraud, L. and Guyomar, D., (1998), " Characterisation of Piezoceramic Under Uniaxial Stress", *Proceedings of the Eleventh IEEE International Symposium on Applications of Ferroelectrics, p.307-310*, IEEE, United States of America.

Audrain, P., Lethiecq, M., Levassort, F. and TranHuuHue, L. P., (1999), " Influence of the Different Loss Parameters on Piezoelectric Material Performance", *Journal of Ferroelectrics, Vol.224, No. 1-4, p.605-612*, Gordon Breach Scientific Publications Ltd., England.

Batra, R. C., Dell'Isola, F. and Vidoli, S., (2000), " Saint-Venant's Problem for a Second-Order Piezoelectric Prismatic Bar", *International Journal of Engineering Science, Vol.38, No. 1, p.21-45*, Elsevier, United Kingdom.

Beige, H., Hauke, T., Lobmann, P., Mueller, V., Seifert, S., Seifert, W. and Steinhausen, R., (1998), "Clamping of Piezoelectric Thin Films on Metallic Substrates: Influence on the Effective Piezoelectric Modulus D/Sub 33/", *Proceedings of the Eleventh IEEE International Symposium on Applications on Ferroelectrics, p.93-96*, IEEE, United States of America.

Beige, H., Hauke, T., Schoenecker, A., Seifert, S., Seifert, W., Sporn, D., Starke, S., Steinhausen, R. and Watzka, W., (1999), 'Finescaled Piezoelectric 1-3 Composites: Properties and Modeling", *Journal of the European Ceramic Society, Vol.19, No.6-7, p.1289-1294*, Switzerland.

Benjeddou, A., Ohayon, R., Osmont, D. and Rahmoune, M., (1999), "New Thin Piezoelectric Plate Models", *Journal of Intelligent Material Systems and Structures, Vol.9, No. 12, p. 1017-1029*, Technomic Publishing, United States of America.

Bogdanov, S. V., (1999), " Relative Signs of Piezoelectric Constants of Pyroelectric Crystals", *Journal Avtometriya, No.1, p.3-11*, Allerton Press, Russia.

Bowen, C. R., Mahon, S. W. and Perry, A., (1999), " Finite Element Modeling of 3-3 Piezocomposites", *Journal of Scripta Materiala, Vol.41, No.9, p.1001-1007*, England.

Bowman, K. J., Shelley, W. F. II and Wan S., (1999), " Functionally Graded Piezoelectric Ceramics", *Journal of Materials Science Forum, Vol.308-311, p.515-520*, Germany.

Caballero, A. C., Duran, P., Fernandez, J. P., Moure, C. and Villegas, M., (1999), "Factors Affecting the Electrical Conductivity of Donor-Doped Bi//4Ti//3O//1//2 Piezoelectric Ceramics", *Journal of the American Ceramic Society, Vol.82, No.9, p.2411-2416*, United States of America.

Cain, M. G., Gee, M. G. and Stewart, M., (1999), " Real Time Evaluation of Piezoelectric Materials", *National Physics Laboratory Report, Report No. NPL CMMT(A)149*, United Kingdom.

Calderon-Moreno, J. M., Guiu, F., Jimenez, B., Reece, M. J. and Sohn, K. S., (1999), "Anisotropy in the Indentation Fracture Piezoelectric Titanate Ceramics", *Journal of Ferroelectrics, Vol.228,No.l,p.lll-128*, Gordon & Breach, Switzerland.

Chakravorty, H. H., Ghosh, A. K. and Munshi, T. K., (1999), "Electrical Response of Piezoelectric Materials Under Mechanical Excitation", Journal of Applied Physics, Vol.86, No. 10, p.5753-5756, Amer Institute of Physics, United States of America.

Chen, Y. and Tian, W., (1999), "On the Bueckner Work Conjugate Integral and its Relations to the J-integral and M-integral in Piezoelectric Materials", *Journal Acta Mechanica Sinica, Vol.31, No.5, p.625-632*, Chinese Journal of Mechanics Press, China.

Chou, T. W., Ruan, X. and Safari, A., (1999), " Effective Elastic, Piezoelectric and Dielectric Properties of Braided Fabric Composites", *Journal of Composites Part A (Applied Science and Manufacturing), Vol.30A, No. 12, p.1435-1444*, Elsevier, United Kingdom.

Christman, J. A., Kim, S. H., Kingon, A. I., Maiwa, H., Maria, J. P. and Streiffer, S. K., (1999), "Measurement and Calculation of PZT Thin Film Longitudinal Piezoelectric Coefficients", *Journal of Integrated Ferroelectrics, Vol.24, No.1-4, p. 139-146*, Gordon & Breach, Netherlands.

Cohen, R.E., (2000), " Theory of Ferroelectrics: A Vision for the Next Decade and Beyond", *Journal of The Physics and Chemistry of Solids, Vol.61, No.2, p. 139-146*, Elsevier, United Kingdom.

Cross, L. E., Fousek, J. and Litvin, D. B., (1999), "Possible Piezoelectric Composites Based on the Flexoelectric Effect", *Journal of Materials Science Letters, Vol.39, No.5, p.287-291*, Elsevier, Netherlands.

Danforth, S. C., Panda, R. K. and Safari, A., (1999), " Multiple Moulds Route for Fabricating Piezoelectric Ceramic/Polymer Composites" *Journal of Material Science Letters, Vol. 18, No. 17, p. 1395-1397*, Elsevier, Netherlands

Dasgupta, D., Hudd, J., Martin, A., Tunnicliffe, D. and Wells, P., (1999), "Development and Comparison of Low Profile Piezoelectric Sensors for Impact and Acoustic Emission (AE) Detection in CFRP Structures", *British Aerospace Journal, Vol.167, p.102-111*, Trans Tech Publications, England.

Desmare, R., Lethiecq, M., Levassort, F. and Tran-Huu-Hue, L. P., (1999), " Effective Electroelastic Moduli of 3-3(0-3) Piezocomposites", *Journal of IEEE Transactions on Ultrasonics, Ferroelectrics and Frequency Control, Vol.46, No.4, p. 1028-1034*, IEEE, United States of America.

Desmare, R., Lethiecq, M., Levassort, F., Tran-Huu-Hue, L. P. and Wolny, W,, (1999), "Modeling of Multilayer Piezoelectric Structures", *Journal of Ferroelectrics, Vol.224, No.1-4, p. 195-202*, Gordon & Breach, Switzerland.

Ding, H. J., Guo, F. L. and Xu, R. Q., (1999), " Exact Axisymmetric Solutions for Laminated Transversely Isotropic Piezoelectric Circular Plate (I) - Exact Solutions for Piezoelectric Circular Plate", *Journal of Science in China Series E - Technological Sciences, Vol.42, No.4, p.388-395*. Science Press, Peoples Republic of China.

Dong-Guk, K. and Ho-Gi, K., (1998), " A New Characterisation of Piezoelectric Thin Films", *Proceedings of the Eleventh IEEE International Symposium on Applications of Ferroelectrics, p.65-68*, IEEE, United States of America.

Dukkipati, R. V., Naganathan, N. G. and Peelamedu, S. M., (1999), " Active Strain-Transfer Analysis in a Piezoceramic System Using a Finite-Element Method and Experimental Investigation", *Journal of Smart Materials and Structures, Vol.8, No.5, p.654-662*. United Kingdom.

Dunn, M. L., Jiang, Y. L. and Ledbetter, H., (1999), " Thermoelectroelastic Moduli of Textured Piezoelectric Polycrystals: Exact Solutions and Bounds for Film Textures", *Journal of Applied Physics, Vol.86, No.8, p.4626-4634*, AIP, United States of America.

Fukada, E., (1998), "History and Recent Progress in Piezoelectric Polymer Research", *Proceedings of the IEEE Ultrasonics Symposium, Vol. 1, p-597-606*, IEEE, United States of America.

Garcia, J. E. and Perez, R., (1999), "A Method to Determine Second Order Nonlinear Coefficients in Piezoelectric Ceramics", *Journal Boletin De La Sociedad Espanola De Ceramica Y Vidrio, Vol.38, No.5, p.514-517*, Sociedad Espanola Ceramica Vidrio, Spain.

Giannakopoulos, A. E., Ramamurty, U, Sridhar, S. and Suresh, S., (1999), "An Experimental Study of Spherical Indentation on Piezoelectric Materials", *Journal ACTA Materialia, Vol.47, No.8, p.2417-2430*, Elsevier, England.

Han, X. L. and Wang, T. C., (1999), "Fracture Mechanics of Piezoelectric Materials", *International Journal of Fracture, Vol.98, No.1, p.15-35*, Kluwer Academic Publishers, Netherlands.

Jian-Guo, Z., Shan-Qing, L. and Zheng-Xing, L., (1999), " Three-Dimensional and Simplified Analysis on Static Electromechanical Mechanism of Piezoelectric Materials", *Journal of Shanghai Jiaotong University, Vol.33, No.6, p.737-741*, Shanghai Jiaotong University Press, China.

Jin, J., Tao, B. and Wan, J., (1999), " Analysis of an Adaptive Sandwich Beam with a 1-5 Type Piezoelectric Core", *Journal of Gong Cheng Li Xue/Engineering Mechanics, Vol. 16, No.6, p.113-118*, China.

Keitel, U., Kreher, W., Schoenecker, A., Sporn, D. and Watzka, W., (1999), "Smart Structures by Integrated Piezoelectric Thin Fibres (II): Properties of Composites and their Physical Description", *Journal of Ferroelectrics, Vol.224, No.1-4, p.7-12*, Gordon & Breach, Switzerland.

Kim, B. W., Kim, S. H. and Yoo, J. H., (1999), "Improved Calculation Model for Analysis of Left Bracket 111 Right Bracket InGaAs/GaAs Strained Piezoelectric Superlattices", *ETRI Journal, Vol.21, No.4, p.65-82.*

Kuang, Z. B., Liu, Z. X., Nishioka, T. and Shen, S. P., (2000), " Nonlinear Electromechanical Interfacial Fracture for Piezoelectric Materials", *Journal of Mechanics of Materilas, Vol.32, No.1, p.57-64*, Elsevier, Netherlands.

Li, J. Y., (2000), " The Effective Electroelastic Moduli of Textured Piezoelectric Polycrystalline Aggregates", *Journal of The Mechanics and Physics of Solids, Vol.48, No.3, p.529-552*, Elsevier, England.

Mould, J., Powell, D. J. and Wojcik, G. L., (1998), " Dielectric and Mechanical Absorption Mechanisms for Time and Frequency Domain Transducer Modeling", *Proceedings of the IEEE Ultrasonics Symposium, Vol.2, p.1019-1024*, IEEE, United States of America.

Mukherjee, B. K. and Sherrit, S., (1998), " The Use of Complex Material Constants to Model the Dynamic Response of Piezoelectric Materials", *Proceedings of the IEEE Ultrasonics Symposium, Vol. 1, p.633-640*, IEEE, United States of America.

Narita, F., Ozawa, E. and Shindo, Y., (1999), "Impact Response of a Finite Crack in an Orthotropic Piezoelectric Ceramic", *Journal of ACTA Mechanica, Vol. 137, No. 1, p.99-107*, Elsevier, England.

Nishioka, T., Shengping, S. and Zhen-Bang, K., (1999), " Impact Interfacial Fracture for Piezoelectric Ceramic", *Journal of Mechanics Research Communications, Vol.26, No.3, p.347-352*, Elsevier, United Kingdom.

Ootao, Y. and Tanigawa, Y., (2000), "Three-Dimensional Transient Piezothermoelasticity for a Rectangular Composite Plate Composed of Cross-Ply and Piezoelectric Laminae", *International Journal of Engineering Science, Vol.38, No. 1, p.47-71*, Elsevier, United Kingdom.

Pan, E. and Tonon, F., (2000), "Three-Dimensional Green's Functions in Anisotropic Piezoelectric Solids", *International Journal of Solids and Structures, Vol.37, No.6, p.943-958*, Elsevier, England.

Pannkoke, K., Schonecker, A., Sporn, D. and Watzka, W., (1999), "Smart Structures by Integrated Piezoelectric Thin Fibres (1): Preparation, Properties and Integration of Fibres in the System Pb(Zr,Ti)O/Sub 3/", *Journal of Ferroelectrics, Vol.224, No.1-4, p.1-6*, Gordon & Breach, Switzerland.

Pan, Y. S. and Sze, K. Y., (1999), " Hybrid Finite Element Models for Piezoelectric Materials", *Journal of Sound and Vibration, Vol.226, No.3, p.519-547*, Academic Press Ltd., England.

Pearce, D., (1999), "Piezoelectrics Spring into Action", *Journal of Materials World, Vol.7, No. 12, p.748-750*. United Kingdom.

Poizat, C. and Sester, M., (1999), " Effective Properties of Composites with Embedded Piezoelectric Fibres", *Journal of Computational Materials Science, Vol. 16, No. 1-4, p.89-97*, Elsevier, Netherlands.

Rao, S. S. and Sunar, M., (1999), "Recent Advances in Sensing and Control of Flexible Structures via Piezoelectric Materials Technology", *Journal of Applied Mechanics Review, Vol.52, No.1, p.1-16*, ASME, United States of America.

Shang,F. and Wang, Z., (1997), "Cylindrical Buckling of Piezoelectric Laminated Plates", *Journal Of ACTA Mechanica Solida Sinica, Vol. 18, No.2, p. 101-108*, Huazhong University of Science and Technology, China.

Shi, W. and Zhen-Bang, K., (1999), "Energy Release Rate in Piezoelectric Media", *International Journal of Fracture, Vol.96, No.3, p.L31-36*, Kluwer Academic Publishers, Netherlands.

Takenaka, T., (1999), " Piezoelectric Properties of Some Lead - Free Ferroelectric Ceramics", *Journal of Ferroelectrics, Vol.230, No.1-4, p.87-98*, Gordon & Breach, Switzerland.

Yang, J. S., (1999), " Nonlinear Theory for Thin Piezoelectric Plates in Moderately Large Extensional Deformations", *Journal of Mechanics Research Communications, Vol.26, No.4, p.421-426*, Elsevier, United Kingdom.

Yu, N., (1999), "On Overall Properties of Smart Piezoelectric Composites", *Journal of Composites Part B- Engineering, Vol.30, No.7, p. 709-712*, Elsevier, England.

Zhang, Q. M. and Zhao, J., (1999), " Electromechanical Properties of Lead Zirconate Titanate Piezoceramics Under the Influence of Mechanical Stress", *Journal of IEEE Transactions on Ultrasonics, Ferroelectrics and Frequency Control, Vol.46, No.6, p. 1518-1526*, IEEE, United States of America.

Magnetostrictive Materials

Abell, J. S. and Bi, Y. J., (1997), " Microstructural Characterisation of Terfenol-D Crystals Prepared by the Czochralski Technique", *Journal of Crystal Growth, Vol. 172, No.3-4, p,440-449*, Elsevier, Netherlands,

Adly, A. A., Bergqvist, A. and Mayergoyz, I. D., (1991), "Preisach Modeling of Magnetostrictive Hysteresis", *Journal of Applied Physics, Vol.69, No.8, Pt.2B, p.5777-5779*, AIP, United States of America.

Benbouzid, M. E. H., Body, C. and Spornic, S. A., (1997), " Computer - Aided Design of Magnetostrictive Devices Using Terfenol-D", *Journal of European Transactions on Electrical Power, Vol.7, No.5, p.351-359*, VDE-Verlag, Germany.

Benbouzid, M. E. H., Engdahl, G., Kvarnsjo, L., Meunier, G. and Reyne, G., (1995), "Dynamic Modeling of Giant Magnetostriction in Terfenol-D Rods by the Finite Element Method", *Journal of IEEE Transactions on Magnetics, Vol.31, No.3, p-1821-1824*, IEEE, United States of America.

Benbouzid, M. E. H., Meunier, G. and Reyne, G., (1994), " A 2-D Dynamic Formulation for Nonlinear Finite Element Modeling of Terfenol-D Rods", *Proceedings of the Second Internal Conference on Computation in Electromagnetics*, IEE, United Kingdom.

Bergqvist, A., Engdahl, G. and Kvarnsjo, L., (1990), " A Method for Measuring Eddy Current Impedances in Giant Magnetostrictive Materials", *Journal of IEEE Transactions on Magnetics, Vol.26, No.5, p-2574-2576*, IEEE, United States of America.

Bergqvist, A. and Engdahl, G., (1994), "A Phenomenological Magnetomechanical Hysteresis Model", *Journal of Applied Physics, Vol.75, No. 10, Pt.2A, p.5496-5498*, AIP, United States of America.

Bergqvist, A. and Engdahl, G., (1996), "A Model for Magnetomechanical Hysteresis and Losses in Magnetostrictive Materials", *Journal of Applied Physics, Vol.79, No.8, Pt.2B, p.6476-6478*, AIP, United States of America.

Bemadou, M. and Song He, (1999), " Numerical Approximation of Unstressed or Prestressed Magnetostrictive Materials", *Journal of Proceedings of the SPIE-The International Society for Optical Engineering, Vol.3667, p. 101-109*, SPIE - Int. Soc. Opt. Eng., United States of America.

Besbes, M., Razek, A. and Ren, Z., (1996), " Finite Element Analysis of Magneto-Mechanical Coupled Phenomena in Magnetostrictive Materials", *Journal of IEEE Transactions on Magnetics, Vol.32, No.3, Pt.1, p.1058-1061*, IEEE, United States of America.

Body, C., Cugat, O., Meunier, G. and Reyne, G., (1996), " Finite Element Modeling of a Magnetostrictive Micromembrane", *Proceedings of Actuator 96. 5th International Conference on New Actuators, p.308-311*, AXON Technologie Consult GmbH, Bremen, Germany.

Body, C., Meunier, G. and Reyne, G., (1997), "Nonlinear Finite Element Modeling of Magneto-Mechanical Phenomenon in Giant Magnetostrictive Thin Films", *Journal of IEEE Transactions on Magnetics, Vol.33, No.2, Pt.1, p. 1620-1623*, IEEE, United States of America.

Brandon, D. and Rogers, R. C., (1993), "Microstructural Models of Magnetostrictive Materials", *Journal of Proceedings of the SPIE- The International Society for Optical Engineering, Vol. 1919, p 114-123*, SPIE - Int. Soc. Opt. Eng., United States of America.

Busbridge, S. C., Kendall, D. and Piercy, A. R., (1994), " Application of the Ratio d/chi to the Investigation of Magnetisation Processes in Giant Magnetostrictive Materials", *Journal of Applied Physics, Vol.76, No. 10, Pt.1, p.7006-7008*, AIP, United States of America.

Carman, G. P., Kwok-Shun, C. and Wang D., (1995), "Micro-Mechanical Model of a Composite Containing a Conservative Nonlinear Electro-Magneto-Thermo-Mechanical Material", *Journal of Intelligent Material Systems and Structures, Vol.6, No.5, p.691-699*, California University, United States of America.

Carman, G. P. and Mitrovic, M., (1995), " Nonlinear Constitutive Relations for Magnetostrictive Materials with Applications to 1-D Problems", *Journal of Intelligent Material Systems and Structures, Vol.6, No.5, p.673-683*, California University, United States of America.

Carman, G. P., Mitrovic, M. and Greg, P., (1995), " Nonlinear Behaviour of Magnetostrictive Materials", *Proceedings of the 10th Conference on Engineering Mechanics, Vol.2, p.714 - 717*, ASCE, United States of America.

Carman, G. P., Mitrovic, M. and Roberts, M., (1995), " Nonlinear Behaviour of Coupled Magnetostrictive Material Systems: Analytical/Experimental", *Journal of Proceedings of the SPIE- The International Society for Optical Engineering, Vol-2441, p.341-354*, SPIE - Int. Soc. Opt. Eng., United States of America.

Carman, G. P., Weisensel, G. N. and Zrostlik, R. L., (1999), "Advanced Magnetostrictive Finite Element Method (FEM) Modeling Development", *Journal of Proceedings of the SPIE-The International Society for Optical Engineering, Vol.3667, p.110-121*, SPIE - Int. Soc. Opt. Eng., United States of America.

Cedell, T. and Weston, R. S., (1998) "Finite Elements Solutions to Magnetostriction. I. Harmonic Modeling", *Journal of Finite Elements in Analysis and Design, Vol.30, No.3, p. 187-196*, Elsevier, Netherlands.

Chang, Y. L., Li, Q., Ouyang, S. and Yuan, R. Z., (1995), " Study of Boundary Free Tb-Dy-Fe Magnetostrictive Materials", *Proceedings of the Materials for Smart Systems Materials Research Society Symposium, Vol-360, p. 183-188*, United States of America.

Chen, L. and Jones, B., (1996), " Magnetostriction: Revealing the Unknown", *Journal of IEEE Aerospace and Electronics Systems Magazine, Vol.11, No.3, p.3-6*, IEEE, United States of America.

Churikova, I. V., Lopatin, S. S., Lopatina, I. B. and Lupeiko, T. G., (1991), " Magnetoelectric Properties of Mixtures of Piezoelectric and Magnetostrictive Materials with a Polymer Binder", *Journal Neorganicheskie Materialy, Vol.27, No. 12, p.2678-2679*, Russia.

Clephas, B. and Janocha, H., (1998), " Actuators Based Upon Piezoelectric and Magnetostrictive Solid-State Transducers", *Journal of Automatisierungstechnische Praxis, Vol.40, No.4, p. 10-17*, Oldenbourg, Germany.

Dapino, M. J., Flatau, A. B. and Smith R. C., (1998), "An Active and Structural Strain Model for Magnetostrictive Transducers", *Journal of Proceedings of the SPIE- The International Society for Optical Engineering, Vol.3329, Pt.1-2, p. 198-209*, SPIE - Int. Soc. Opt. Eng., United States of America.

Dapino, M. J., Flatau, A. B. and Smith R. C., (1999), " A Coupled Structural - Magnetic Strain Model for Magnetostrictive Transducers", *Journal of Proceedings of the SPIE- The International Society for Optical Engineering, Vol.3668, Pt.1-2, p.405-416*, SPIE - Int. Soc. Opt. Eng., United States of America.

Dasgupta, A. and Kannan, K. S., (1994a), " Finite Element Scheme for Modeling the Magnetoelastic Response of Magnetostrictive Smart Structures", *Proceedings of the Second International Conference on Intelligent Materials, p719-730*, Technomic Publishing Co., United States of America.

Dasgupta, A. and Kannan, K. S., (1994b), " Nonlinear Finite Element Scheme for Modeling the Magnetoelastic Response of Magnetostrictive Smart Structures", *Journal of Proceedings of the SPIE— The International Society for Optical Engineering, Vol-2190, p.182-193*, SPIE - Int. Soc. Opt. Eng., United States of America.

Dasgupta, A. and Kannan, K. S., (1997a), " A Nonlinear Quasi-Static Finite Element Scheme for Magnetized and Deformable Bodies Including Magnetostrictives", *Journal of Proceedings of the SPIE - The International Society for Optical Engineering, Vol-3041, p.652-664*, SPIE - Int. Soc. Opt. Eng., United States of America.

Dasgupta, A. and Kannan, K. S., (1997b), " A Nonlinear Galerkin Finite Element Theory for Modeling Magnetostrictive Smart Structures", *Journal of Smart Materials and Structures, Vol.6, No.3, p.341-350*, IOP Publishing, United Kingdom.

Dasgupta, A. and Kannan, K. S., (1998), "A New Magnetic Field Based Weighted-Residual Quasi-Static Finite Element Scheme for Modeling Bulk Magnetostriction", *Journal of Proceedings of the SPIE- The International Society for Optical Engineering, Vol.3321, p.684-697*, SPIE - Int. Soc. Opt. Eng., United States of America.

Della Torre, E. and Reimers, A., (1999), "Fast Preisach Based Magnetostriction Model for Highly Magnetostrictive Materials", *Journal of IEEE Transactions on Magnetics, Vol.35, No.3, Pt.1, p.1239-1242*, IEEE, United States of America.

DeSimone, A., (1994), " Magnetisation and Magnetostriction Curves for Highly Magnetostrictive Materials", *Proceedings of the Second International Conference on Intelligent Materials, p.426-436*, Technomic Publishing Co., United States of America.

DeSimone, A., (1996), " Characterisation of the Macroscopic Response of Magnetostrictive Materials via Microstructural Analysis", *Journal of Zeitschrift fur Angewandte Mathematik Und Mechanik, Vol.76, Suppl., No.2, p.397-400.*, Akademie Verlag, Germany.

Dougherty, J. P., Harshe, G. and Newnham, R. E., (1993a), "Magnetoelectric Effect in Composite Materials", *Journal of Proceedings of the SPIE-The International Society for Optical Engineering, Vol. 1919, p.224-235*, SPIE - Int. Soc. Opt. Eng., United States of America.

Dougherty, J. P., Harshe, G. and Newnham, R. E., (1993b), " Theoretical Modeling of Magnetoelectric Composites", *International Journal of Applied Electromagnetics in Materials, Vol.4, No.2, p. 161-171*, Netherlands.

Du, T., Zhang, H. and Zhu, H., (1997), "Effect of V on Microstructure and Magnetic Properties of Polycrystal Tb-Dy-Fe Alloy", *Journal of Alloys and Compounds, Vol.258, No. 1-2, p.20-23*, Elsevier, Switzerland.

Engdahl, G. and Kvarnsjo, L., (1989), " A Set-Up for Dynamic Measurements of Magnetic and Mechanical Behaviour of Magnetostrictive Materials", *Journal of IEEE Transactions on Magnetics, Vol.25, No.5, p-4195-4197*, IEEE, United States of America.

Engdahl, G. and Kvarnsjo, L., (1991), "Examination of the Interaction Between Eddy Currents and Magnetoelasticity in Terfenol-D", *Journal of Applied Physics, Vol.69, No.8, Pt.2B, p.5783-5785*, AIP, United States of America.

Engdahl, G. and Svensson, L., (1988), " Simulation of the Magnetostrictive Performance of Terfenol-D in Mechanical Devices", *Journal of Applied Physics, Vol.63, No.8, Pt.2B, p.3924-3926*, AIP, United States of America.

Faunce, C. A., Lord, D. G., Ludwig, A. and Quandt, E., (1998), " Magnetic Properties and Microstructure of Giant Magnetostrictive TbFe/FeCo Multilayers", *Journal of Applied Physics, Vol.83, No.11, p.7267-7269*, AIP, United States of America.

Flynn, C. P. and Huth, M., (1999), "Strain-Induced Perpendicular Magnetisation in TbFe//2(l 11) Thin Films on LiNbO//3", *Journal of Magnetism and Magnetic Materials, Vol.204, No.3, p.204-208*, Netherlands.

Forsythe, S. E. and Piquette, J. C., (1999), " One Dimensional Phenomenological Model of Hysteresis. I. Development of the Model", *Journal of the Acoustical Society of America, Vol.106, No.6, p.3317-3327*, Acoust. Soc. America through AIP, United States of America.

Fu-Shin, L., (1999), " Multi-energetic modeling for magnetostrictive actuators". *Proceedings of the Eighteenth IASTED International Conference on Modeling, Identification and Control*, ACTA Press, California, United States of America.

Greenough, R. D., Reed, I. M. and Schulze, M. P., (1993), "Characterisation of Magnetostrictive Materials with Computer Modeling", *Journal of IEEE transactions on Magnetics, Vol.29, No.6, Pt.1, p.2386-2388*, IEEE, United States of America.

Greenough, R. D., O'Connor, K. and Reed, J. M., (1995), "Characterisation of Magnetostrictive or Piezoelectric Materials and Transducers", *Proceedings of the IEE Colloquium on Innovative Actuators for Mechatronic Systems, Digest No.1995/170, p.8/1-3*, IEE, London, United Kingdom.

Hornreich, R. M., Rubinstein, H. and Spain, R. J., (1971), " Magnetostrictive Phenomena in Metallic Materials and Some of their Device Applications", *Journal of IEEE Transactions on Magnetics, Vol.MAG-7, No. I, p-29-48*, IEEE, United States of America.

Hughes, D. and Wen, J. T., (1997), " Preisach Modeling of Piezoceramic and Shape Memory Alloy Hysteresis", *Journal of Smart Materials and Structures, Vol.6, No.3, p.287-300*, IOP Publishing, United Kingdom.

James, R. D. and Tickle, R., (1999), "Magnetic and Magnetomechanical Properties of Ni2MnGa", *Journal of Magnetism and Magnetic Materials, Vol. 195, No.3, p.627-638*, Elsevier, Netherlands.

Janocha, H., Jendritza, D. J. and Schafer, J., (1994), "Piezoelectric and Magnetostrictive Materials for Use in Smart Actuators", *Proceedings of Joint Hungarian-British Conference on Mechatronics, p397-404*,Comput. Mech. Publications, Southampton, United Kingdom.

Kaczkowski, Z., (1970), " Effect of Magnetic Field on the Piezomagnetic Parameters of Some Magnetostrictive Materials", *Journal of Ultrasonics, Vol.8, No.4, p.239-242*, Netherlands.

Kaczkowski, Z. and Malkinski, L., (1984), " Delta E - Effect and Internal Friction in the Amorphous Fe-Si-B Alloy", *Journal of Magnetism and Magnetic Materials, Vol.41, No.1-3, p.343-345*, Netherlands.

Kim, C. and Li, Y., (1998), "Review of the Researches on Magnetostrictive Materials", *Journal of Mocaxue Xuebao/Tribology, Vol.18, No.3, p.313-319*, Chungnam National University, Korea.

Kondo, K., (1997), " Dynamic Behaviour of Terfenol-D ", *Journal of Alloys and Compounds, Vol.258, No.1-2, p.56-60*, Elsevier, Switzerland.

Kronmuller, H., (1995), " Recent Developments in High-Tec Magnetic Materials", *Journal of Magnetism and Magnetic Materials, Vol. 140-144, Pt.1, p.25-28*, Netherlands.

Lammering, R., (1998), "Design, Optimisation and Realization of Smart Structures", *Proceedings of the 4th European Conference on Smart Structures and Materials in conjunction with the 2nd International Conference on Micromechanics, Intelligent Materials and Robotics*, IOP Publishing, Bristol, United Kingdom.

Ma, L., (1993), "Computation of Magnetostrictive Materials", *Journal of Proceedings of the SPIE - The International Society for Optical Engineering, Vol. 1919, p.47-54*, SPIE - Int. Soc. Opt. Eng., United States of America.

McMasters, D., (1991), " Magnetostrictive Materials", *Proceedings of the International Workshop on Power Transducers for Sonics and Ultrsonics, p.125-131*, Springer-Verlag, Germany

McMasters, D. and Snodgrass, J. D., (1997), " Optimised Terfenol-D Manufacturing Processes", *Journal of Alloys and Compounds, Vol.258, p.24-29*, Elsevier, Switzerland.

Rinaldi, S. and Turilli, G., (1985), "Theory of Linear Magnetoelastic Effects", *Journal of Physical Review B (Condensed Matter), Vol.31, No.5, p.3051-3058*, United States of America.

Smith, R. C., (1997), " Modeling Techniques for Magnetostrictive Actuators ", *Journal of Proceedings of the SPIE - The International Society for Optical Engineering, Vol.3041, p.243-253*, SPIE - Int. Soc. Opt. Eng., United States of America.

Squire, P., (1999), "Magnetostrictive Materials for Sensors and Actuators", *Ferroelectrics Journal Vol.228, No.1-4, p.305-319*, Gordon & Breach, Switzerland.

Ullakko, K., (1996), " Magnetically Controlled Shape Memory Alloys: A New Class of Actuator Materials", *Journal of Materials Engineering and Performance, Vol.5, No.3, p.405-409*, ASM Int.. United States of America.

APPENDIX B

MATLAB® NUMERICAL SIMULATION

The objectives of this appendix are to provide a brief, but adequate description of the numerical software used in the current thesis and to present the numerical code developed by the author for results predictions (It must be noted that the information presented for the former objective is not the authors own work, but has been summarized from MATLAB documentation sourced from the MathWorks website at www.mathworks.com). Only functionality used in the current investigation is highlighted.

B1. General Description of MATLAB

The name MATLAB stands for 'matrix laboratory' and the program was originally written to provide easy access to matrix software developed by the LINPACK and EISPACK projects. Today, it is a high-performance language for technical computing. It integrates computation, visualization, and programming in an environment where problems and solutions are expressed in familiar mathematical notation. Typical uses include,

- Math and computation
- Algorithm development
- Data acquisition
- Modeling, simulation, and prototyping
- Data analysis, exploration, and visualization
- Scientific and engineering graphics
- Application development, including graphical user interface building

The MATLAB system consists of five main parts:

- **Development Environment**
  This is the set of tools and facilities that facilitate the use of MATLAB functions and files. Many of these tools are graphical user interfaces. It includes the MATLAB desktop and command window, a command history, an editor and debugger, and browsers for viewing help, the workspace, files, and the search path.

- **The MATLAB Mathematical Function Library**

  This is a collection of computational algorithms ranging from elementary functions like sum, sine, cosine, and complex arithmetic, to more sophisticated functions like matrix inverse, matrix eigenvalues, Bessel functions, and fast Fourier transforms.

- **The MATLAB Language**

  This is a high-level matrix/array language with control flow statements, functions, data structures, input/output, and object-oriented programming features.

- **Graphics**

  MATLAB has extensive facilities for displaying vectors and matrices as graphs, as well as annotating and printing these graphs. It includes high-level functions for two-dimensional and three-dimensional data visualization, image processing, animation, and presentation graphics. It also includes low-level functions that allow full customization of the appearance of graphics as well as building of complete graphical user interfaces.

- **The MATLAB Application Program Interface (API)**

  This is a library that allows the writing of C and Fortran programs that interact with MATLAB. It includes facilities for calling routines from MATLAB (dynamic linking), calling MATLAB as a computational engine, and for reading and writing MAT-files.

B2. The MATLAB Language

One of the major benefits of the MATLAB language is that it does not work with single numbers, but rather with entire matrices. In MATLAB, a matrix is a rectangular array of numbers. Special meaning is sometimes attached to 1-by-1 matrices, which are scalars, and to matrices with only one row or column, which are vectors.

Matrices are entered into MATLAB in several different ways:

- Enter an explicit list of elements.
- Load matrices from external data files.
- Generate matrices using built-in functions.

The basic conventions for entering an explicit list of elements is to separate the elements of a row with blanks or commas, use a semicolon to indicate the end of each row and surround the entire list

of elements with square brackets. Thus, to enter matrix $A = \begin{bmatrix} 16 & 3 & 2 & 13 \\ 5 & 10 & 11 & 8 \\ 9 & 6 & 7 & 12 \\ 4 & 15 & 14 & 1 \end{bmatrix}$ into MATLAB, for example, the following command line is used:

A = [16 3 2 13; 5 10 11 8; 9 6 7 12; 4 15 14 1]

MATLAB displays the matrix just entered as,

A =

16 3 2 13
5 10 11 8
9 6 7 12
4 15 14 1

Once the matrix is entered, it is automatically remembered in the MATLAB workspace and can simply be referred to as A.

The element in row i and column j of A is denoted by $A(i,j)$. For example, $A(4,2)$ is the number in the fourth row and second column and is 15. It is also possible to refer to the elements of a matrix with a single subscript, $A(k)$. This is the usual way of referencing row and column vectors, but it can also apply to a fully two-dimensional matrix, in which case the array is regarded as one long column vector formed from the columns of the original matrix. So, $A(8)$, for example, is another way of referring to the value 15 stored in $A(4,2)$. If an element outside the dimensions of a matrix is referenced, MATLAB returns an error prompt, however, if a value in an element outside of the matrix is stored, the size increases to accommodate the newcomer, for example,

$X = A$;
$X(4,5) = 17$
X =

16 3 2 13 0
5 10 11 8 0
9 6 7 12 0
4 15 14 1 17

The colon is one of the most important MATLAB operators and occurs in several different forms. The expression

```
1:10
```

is a row vector containing the integers from 1 to 10, i.e.,

```
1 2 3 4 5 6 7 8 9 10
```

To obtain non-unit spacing, an increment is specified, for example,

```
100:-7:50
```

is

```
100 93 86 79 72 65 58 51
```

and

```
0:pi/4:pi
```

is

```
0 0.7854 1.5708 2.3562 3.1416
```

Subscript expressions involving colons refer to portions of a matrix. $A(1{:}k,j)$ is the first k elements of the jth column of A. So,

```
sum(A(1:4,4))
```

computes the sum of the first four elements in the fourth column. The colon by itself refers to all the elements in a row or column of a matrix and the keyword 'end' refers to the last row or column. So,

```
sum(A(:,end))
```

computes the sum of all the elements in the last column of A.

Like most other programming languages, MATLAB provides mathematical expressions that are made up from variables, numbers, operators and functions.

In defining variables, MATLAB does not require any type declarations or dimension statements, i.e. when MATLAB encounters a new variable name, it automatically creates the variable and

allocates the appropriate amount of storage. If the variable already exists, MATLAB changes its contents and, if necessary, allocates new storage. For example,

num_students = 25

creates a 1-by-1 matrix named *num_students* and stores the value 25 in its single element.
Variable names consist of a letter, followed by any number of letters, digits, or underscores. MATLAB uses only the first 31 characters of a variable name. Further, MATLAB is case sensitive; it distinguishes between uppercase and lowercase letters.

For numbers, MATLAB uses conventional decimal notation, with an optional decimal point and leading plus or minus sign. Scientific notation uses the letter e to specify a power-of-ten scale factor and imaginary numbers use either *i* or *j* as a suffix. Some examples of legal numbers are

3 -99 0.0001
9.6397238 1.60210e-20 6.02252e23
1*i* -3.14159*j* 3e5*i*

All numbers are stored internally using the long format specified by the IEEE (Institute of Electrical and Electronics Engineers) floating-point standard. Floating-point numbers have a finite precision of approximately 16 significant decimal digits and a finite range of approximately 10^{-308} to 10^{+308}.

Expressions use familiar arithmetic operators and precedence rules, i.e,

+	Addition
-	Subtraction
*	Multiplication
/	Division
\	Left division
^	Power
'	Complex conjugate transpose
( )	Specify evaluation order

MATLAB uses a dot, or decimal point, as part of the notation for multiplicative array operations. Thus, the list of array operators includes

+	Addition
-	Subtraction
.*	Element-by-element multiplication
./	Element-by-element division
.\	Element-by-element left division
.^	Element-by-element power
.'	Unconjugated array transpose

MATLAB also provides a large number of standard elementary mathematical functions, including abs, sqrt, exp, and sin. Taking the square root or logarithm of a negative number is not an error; the appropriate complex result is produced automatically. MATLAB also provides many more advanced mathematical functions, including Bessel and gamma functions. Most of these functions accept complex arguments.

Some of the functions, like sqrt and sin, are built-in, i.e. they are part of the MATLAB core so they are very efficient, but their computational details are not readily accessible. Other functions, like gamma and sinh, are implemented in M-files. The codes of these functions can be viewed and even modified if necessary.

Several special functions provide values of useful constants, such as,

pi	3.14159265...
i	Imaginary unit, $\sqrt{-1}$
j	Same as *i*
eps	Floating-point relative precision, 2^{-52}
realmin	Smallest floating-point number, 2^{-1022}
realmax	Largest floating-point number, $(2-\varepsilon)2^{1023}$
Inf	Infinity
NaN	Not-a-number

Infinity is generated by dividing a nonzero value by zero, or by evaluating well-defined mathematical expressions that overflow, i.e., exceed *realmax*. Not-a-number is generated by trying to evaluate expressions like 0/0 or *Inf-Inf* that do not have well defined mathematical values. The function names are not reserved and it is possible to overwrite any of them with a new variable. The original function is restored with the 'clear' command.

B3. Graphics

MATLAB has extensive facilities for displaying vectors and matrices as graphs, as well as annotating and printing these graphs.

The plot function has different forms, depending on the input arguments. If y is a vector, 'plot(y)' produces a piecewise linear graph of the elements of y versus the index of the elements of y. If two vectors are specified as arguments, plot(x,y) produces a graph of y versus x. For example, these statements use the colon operator to create a vector of x values ranging from zero to 2π, compute the sine of these values, and plot the result (see Figure B-1).

```
x = 0:pi/100:2*pi;
y = sin(x);
plot(x,y)
```

The axes are labeled and the graph titled by,

```
xlabel('x = 0:2\pi')
ylabel('Sine of x')
title('Plot of the Sine Function','FontSize',12)
```

The characters \pi create the symbol π.

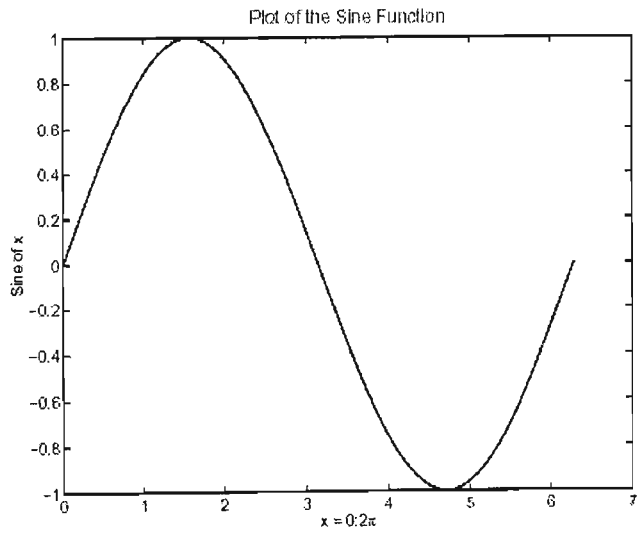

Figure B-1: Example of a simple x-y plot in MATLAB

Multiple *x-y* pair arguments create multiple graphs with a single call to plot. MATLAB automatically cycles through a predefined (but user settable) list of colors to allow discrimination among sets of data.

It is also possible to specify color, line styles, and markers (such as plus signs or circles) when you plot your data using the plot command.

plot(*x*,*y*,'*color_style_marker*')

where *color_style_marker* is a string containing from one to four characters (enclosed in single quotation marks) constructed from a color, a line style, and a marker type. Color strings are '*c*', '*m*', '*y*', '*r*', '*g*', '*b*', '*w*', and '*k*'. These correspond to cyan, magenta, yellow, red, green, blue, white, and black. Linestyle strings are '-' for solid, '--' for dashed, ':' for dotted and '-.' for dash-dot. The marker types are '+', 'o', '*', and 'x' and the filled marker types are 's' for square, 'd' for diamond, '^' for up triangle, 'v' for down triangle, '>' for right triangle, '<' for left triangle, 'p' for pentagram, 'h' for hexagram, and none for no marker.

When the arguments to plot are complex, the imaginary part is ignored except when plot is given a single complex argument. For this special case, the command is a shortcut for a plot of the real part versus the imaginary part. Therefore,

plot(*Z*)

where *Z* is a complex vector or matrix, is equivalent to

plot(real(*Z*),imag(*Z*))

The hold command enables the addition of plots to an existing graph. When the command

hold on

is typed, MATLAB does not replace the existing graph when another plotting command is issued; it adds the new data to the current graph, rescaling the axes if necessary.

For example, these statements first create a contour plot of the peaks function, then superimpose a pseudocolor plot of the same function. The result is evident in Figure B-2.

```
[x,y,z] = peaks;
contour(x,y,z,20,'k')
hold on
pcolor(x,y,z)
shading interp
hold off
```

The hold on command causes the pcolor plot to be combined with the contour plot in one figure.

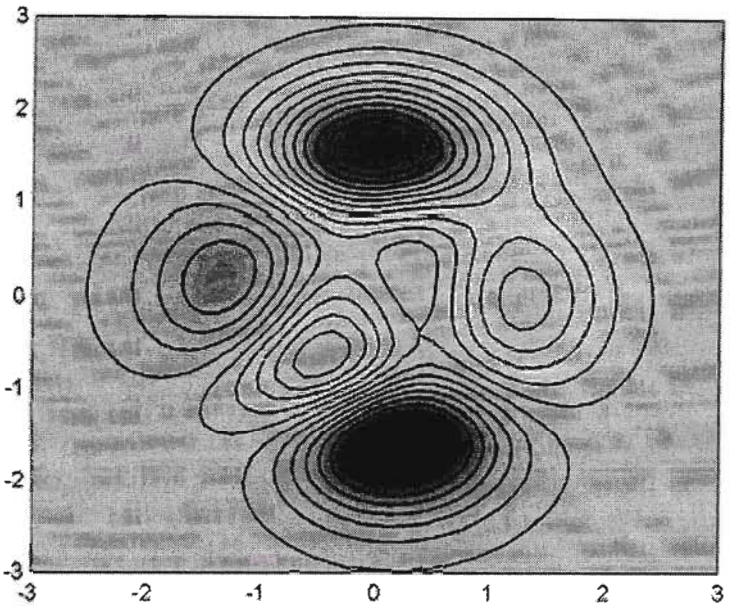

Figure B-2: Example of a plot using the 'hold on' command

Graphing functions automatically open a new figure window if there are no figure windows already on the screen. If a figure window exists, MATLAB uses that window for graphics output. If there are multiple figure windows open, MATLAB targets the one that is designated the "current figure" (the last figure used or clicked in).

The subplot command enables you to display multiple plots in the same window or print them on the same piece of paper. Typing

```
subplot(m,n,p)
```

partitions the figure window into an *m*-by-*n* matrix of small subplots and selects the *p*th subplot for the current plot. The plots are numbered along first the top row of the figure window, then the second row, and so on. For example, these statements plot data in four different subregions of the figure window (Figure B-3)

.

```
t = 0:pi/10:2*pi;
[X,Y,Z] = cylinder(4*cos(t));
subplot(2,2,1); mesh(X)
subplot(2,2,2); mesh(Y)
subplot(2,2,3); mesh(Z)
subplot(2,2,4); mesh(X,Y,Z)
```

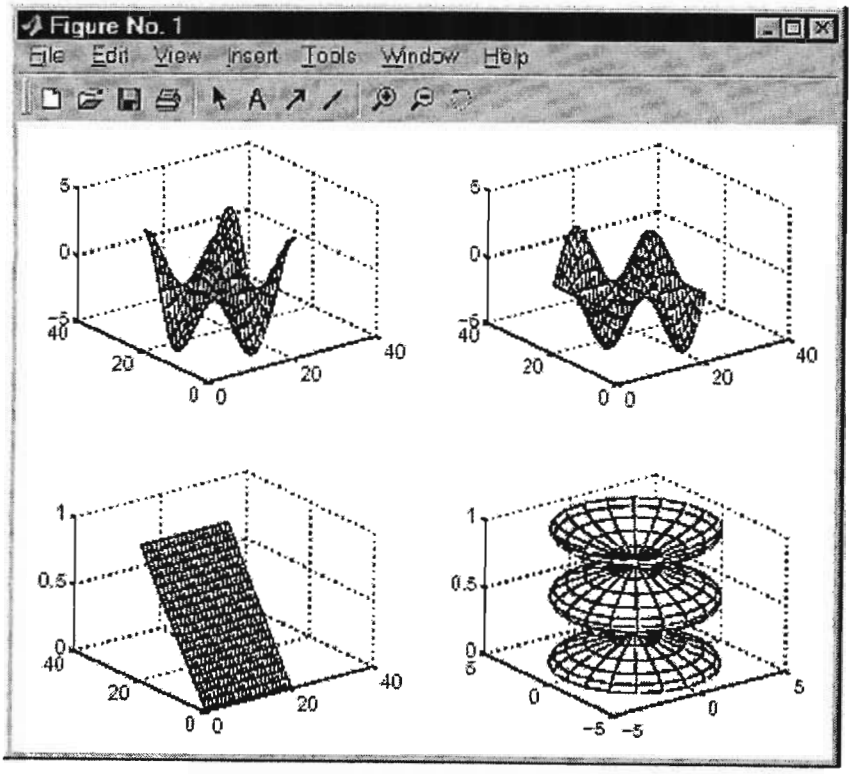

Figure B-3: Example of using the 'subplot' command in MATLAB

B4. Programming with MATLAB

MATLAB is a powerful programming language as well as an interactive computational environment. Files that contain code in the MATLAB language are called M-files. M-files are created using a text editor, then used as would any other MATLAB function or command. There are two kinds of M-files,

- Scripts, which do not accept input arguments or return output arguments. They operate on data in the workspace.
- Functions, which can accept input arguments and return output arguments. Internal variables are local to the function.

When a script is invoked, MATLAB simply executes the commands found in the file. Scripts can operate on existing data in the workspace, or they can create new data on which to operate. Although scripts do not return output arguments, any variables that they create remain in the workspace, to be used in subsequent computations. In addition, scripts can produce graphical output using functions like plot.

Functions are M-files that can accept input arguments and return output arguments. The name of the M-file and of the function should be the same. Functions operate on variables within their own workspace, separate from the workspace you access at the MATLAB command prompt.

If more than one function need to share a single copy of a variable, the variable is declared as global in all the functions. The same thing is done at the command line if the base workspace needs to access the variable. The global declaration must occur before the variable is actually used in a function.

Flow control constructs including if, switch and case, for, while, continue, and break are used for programming.

The 'if' statement evaluates a logical expression and executes a group of statements when the expression is true. The optional 'elseif' and 'else' keywords provide for the execution of alternate groups of statements. An 'end' keyword, which matches the 'if', terminates the last group of statements. The groups of statements are delineated by the four keywords - no braces or brackets are involved. The MATLAB algorithm for generating a magic square of order n involves three different cases: when n is odd, when n is even but not divisible by 4, or when n is divisible by 4. This is described by,

```
if rem(n,2) ~= 0
M = odd_magic(n)
elseif rem(n,4) ~= 0
M = single_even_magic(n)
else
M = double_even_magic(n)
end
```

In this example, the three cases are mutually exclusive, but if they weren't, the first true condition would be executed. It is important to understand how relational operators and 'if' statements work with matrices. When the equality between two variables needs to be checked, the following command can be used,

```
if A == B, ...
```

This is legal MATLAB code, and does what is expected when A and B are scalars. But when A and B are matrices, $A == B$ does not test if they are equal, but tests where they are equal; the result is another matrix of 0's and 1's showing element-by-element equality. In fact, if A and B are not the same size, then $A == B$ is an error. The proper way to check for equality between two variables is to use the 'isequal' function,

```
if isequal(A,B), ...
```

The 'switch' statement executes groups of statements based on the value of a variable or expression. The keywords 'case' and 'otherwise' delineate the groups. Only the first matching case is executed. There must always be an 'end' to match the 'switch'. The logic of the magic squares algorithm can also be described by,

```
switch (rem(n,4)==0) + (rem(n,2)==0)
case 0
M = odd_magic(n)
case 1
M = single_even_magic(n)
case 2
M = double_even_magic(n)
otherwise
```

```
error('This is impossible')
end
```

Note: Unlike the C language switch statement, MATLAB 'switch' does not fall through. If the first case statement is true, the other case statements do not execute. So, break statements are not required.

The 'for' loop repeats a group of statements a fixed, predetermined number of times. A matching 'end' delineates the statements.

```
for n = 3:32
r(n) = rank(magic(n));
end
r
```

The semicolon terminating the inner statement suppresses repeated printing, and the *r* after the loop displays the final result.

The 'while' loop repeats a group of statements an indefinite number of times under control of a logical condition. A matching 'end' delineates the statements. The cautions involving matrix comparisons that are discussed in the section on the 'if' statement also apply to the 'while' statement.

The 'continue' statement passes control to the next iteration of the 'for' or 'while' loop in which it appears, skipping any remaining statements in the body of the loop. In nested loops, 'continue' passes control to the next iteration of the 'for' or 'while' loop enclosing it. The example below shows a 'continue' loop that counts the lines of code in the file, magic.m, skipping all blank lines and comments. A 'continue' statement is used to advance to the next line in magic.m without incrementing the count whenever a blank line or comment line is encountered.

```
fid = fopen('magic.m','r');
count = 0;
while ~feof(fid)
line = fgetl(fid);
if isempty(line) | strncmp(line,'%',1)
continue
end
```

count = *count* + 1;
end
disp(sprintf('%d *lines*',*count*));

The 'break' statement allows early exit from a 'for' or 'while' loop. In nested loops, 'break' exits from the innermost loop only.

MATLAB is a sophisticated software package with tremendous capability and it is not the intention of the author to fully describe its functionality in just a few pages. Rather, this summary is provided to give the reader a glimpse into what MATLAB has offered in the development of the numerical model used in the current thesis.

B5. MATLAB Code for Numerical Analysis

```
clear
clc
format short

% Characteristics of physical system

gravity = 9.81;
mass = 2.6;
length = 0.055;
width = 0.01;
initial_depth = 0.008;
moment_of_inertia = (width*initial_depth^3)/12;
aspect_ratio = length/initial_depth;

% Damage modulus definition for various materials

al_strain = 0:0.0001:0.145;
dimen = size(al_strain);
n = dimen(2);

break1 = find(al_strain == 0.0025);
break2 = find(al_strain == 0.0037);
break3 = find(al_strain == 0.0059);
break4 = find(al_strain == 0.0114);
break5 = find(al_strain == 0.012);
```

```
break6 = find(al_strain == 0.0221);
break7 = find(al_strain == 0.0797);
break8 = find(al_strain == 0.121);

for i=1:break1
   al_modulus(i) = 73e9;
end

for i=break1+1:break2
   al_modulus(i) = 40e9+al_strain(break1)*(al_modulus(break1)-
40e9)/al_strain(i);
end

for i=break2+1:break3
   al_modulus(i) = 14e9+al_strain(break2)*(al_modulus(break2)-
14e9)/al_strain(i);
end

for i=break3+1:break4
   al_modulus(i) = 4e9+al_strain(break3)*(al_modulus(break3)-
4e9)/al_strain(i);
end

for i=break4+1:n
   al_modulus(i) = al_modulus(i-1);
end

for i=1:n
   al_stress(i) = al_strain(i)*al_modulus(i);
end

final_strain_fibre = 0.0064;
final_strain_sma = 0.145;

matrix_strength  =265e6;
fibre_strength = 2e9;
fibre_shear = 0.5*fibre_strength;
sma_strength = 1600e6;
sma_shear = 0.5*sma_strength;

fibre_length = 150e-6;
```

```
fibre_diam = 4e-6;
crit_length_fibre = fibre_strength*fibre_diam/(2*fibre_shear);
crit_length_sma = sma_strength*fibre_diam/(2*sma_shear);

for i = 1:65
   fibre_modulus(i) = 310e9;
end

for i = 66:n
   fibre_modulus(i) = 0;
end

for i = 1:n
   fibre_stress(i) = fibre_modulus(i)*al_strain(i);
end

for i = 1:break4
   sma_modulus(i) = 53e9;
end

for i = break4+1:break6
   sma_modulus(i) = 8.77e9+al_strain(break4)*(sma_modulus(break4)-
8.77e9)/al_strain(i);
end

for i = break6+1:break7
    sma_modulus(i) =
al_strain(break6)*(sma_modulus(break6))/al_strain(i);
end

for i = break7+1:break8
    sma_modulus(i) = 19e9+al_strain(break7)*(sma_modulus(break7)-
19e9)/al_strain(i);
end

for i = break8+1:n
    sma_modulus(i) = 3.88e9+al_strain(break8)*(sma_modulus(break8)-
3.88e9)/al_strain(i);
end

for i = 1:n
```

```
    sma_stress(i) = sma_modulus(i)*al_strain(i);
end

geometric_factor = 0.76;
fibre_fraction = 0.0001;
sma_fraction = 0.1499;
strength_factor = 0.65;

for i = 1:break4
   equiv_modulus(i) = geometric_factor*(fibre_modulus(i)*fibre_fraction +
sma_modulus(i)*sma_fraction+al_modulus(i)*(1-fibre_fraction-
sma_fraction));
end

for i = break4+1:n
   equiv_modulus(i) = geometric_factor*(fibre_modulus(i)*fibre_fraction +
sma_modulus(i)*sma_fraction+al_modulus(break4)*(1-fibre_fraction-
sma_fraction));
end

for i = 1:n
   comp_stress(i) = equiv_modulus(i)*al_strain(i);
end

comp_strength = strength_factor*(fibre_strength*(1-
(crit_length_fibre/(2*fibre_length)))*fibre_fraction+sma_strength*(1-
(crit_length_sma/(2*fibre_length)))*sma_fraction+matrix_strength*(1-
fibre_fraction-sma_fraction));

for i=1:n
   if comp_stress(i)>=comp_strength
      comp_stress(i)=0;
   end
end

% Strain energy Calculation

prestrain = 0.0;

impact_velocity = 1;
impact_height = (impact_velocity^2)/(2*gravity)
```

```
total_energy = 0.5*mass*impact_velocity^2;

strain_factor = 150;
depth_factor = 0.08;

time_interval = 4.5e-6;

velocity(1) = impact_velocity;
displacement(1) = velocity(1)*time_interval;
delta = velocity(1)*time_interval;
strainL = (((sin((pi/2)-
(3*displacement(1)/length))*(6*displacement(1)/length))/sin(6*displacemen
t(1)/length))-1)*strain_factor;
strain(1) = strainL+prestrain;

temp1 = find(al_strain<=strain(1));
temp2 = size(temp1);

stress(1) = equiv_modulus(temp2(2))*strain(1);
depth(1) = initial_depth;
stress_matrix(1) =al_modulus(temp2(2))*strain(1);
stress_fibre(1) = fibre_modulus(temp2(2))*strain(1);
stress_sma(1) = sma_modulus(temp2(2))*strain(1);
load_matrix(1) = (2*stress_matrix(1)*(1-fibre_fraction-
sma_fraction)*geometric_factor*width*depth(1)^2)/(3*length);
load_fibre(1) =
(2*stress_fibre(1)*fibre_fraction*geometric_factor*width*depth(1)^2)/(3*l
ength);
load_sma(1) =
(2*stress_sma(1)*sma_fraction*geometric_factor*width*depth(1)^2)/(3*lengt
h);
load_comp(1) = (load_fibre(1)+load_sma(1)+load_matrix(1));
strain_energy(1) =
(load_matrix(1)*delta)+(load_fibre(1)*delta)+(load_sma(1)*delta);

for i=2:break4
   velocity(i) = sqrt(2*(total_energy-strain_energy(i-1))/mass);
   delta = velocity(i)*time_interval;
   displacement(i) = displacement(i-1)+velocity(i)*time_interval;
```

```
   strainL = (((sin((pi/2)-
(3*displacement(i)/length))*(6*displacement(i)/length))/sin(6*displacemen
t(i)/length))-1)*strain_factor;
   strain(i) = strainL+prestrain;

   temp1 = find(al_strain<=strain(i));
   temp2 = size(temp1);
   stress(i) = equiv_modulus(temp2(2))*strain(i);

   depth(i) = initial_depth;

   stress_matrix(i) =al_modulus(temp2(2))*strain(i);
   stress_fibre(i) = fibre_modulus(temp2(2))*strain(i);
   stress_sma(i) = sma_modulus(temp2(2))*strain(i);
   load_matrix(i) = (2*stress_matrix(i)*(1-fibre_fraction-
sma_fraction)*geometric_factor*width*depth(i)^2)/(3*length);
   load_fibre(i) =
(2*stress_fibre(i)*fibre_fraction*geometric_factor*width*depth(i)^2)/(3*l
ength);
   load_sma(i) =
(2*stress_sma(i)*sma_fraction*geometric_factor*width*depth(i)^2)/(3*lengt
h);
   load_comp(i) = (load_fibre(i)+load_sma(i)+load_matrix(i));

   if strain(i)>=0.145
      strain_energy(i) = strain_energy(i-1);
   else
      strain_energy(i) = strain_energy(i-
1)+(load_matrix(i)*delta)+(load_sma(i)*delta)+(load_fibre(i)*delta);
   end;
end

for i=break4+1:n
   velocity(i) = sqrt(2*(total_energy-strain_energy(i-1))/mass);
   delta = velocity(i)*time_interval;
   displacement(i) = displacement(i-1)+velocity(i)*time_interval;
   strainL = (((sin((pi/2)-
(3*displacement(i)/length))*(6*displacement(i)/length))/sin(6*displacemen
t(i)/length))-1)*strain_factor;
   strain(i) = strainL+prestrain;
```

```
    temp1 = find(al_strain<=strain(i));
    temp2 = size(temp1);
    stress(i) = equiv_modulus(temp2(2))*strain(i);

    depth(i) = initial_depth;

    stress_matrix(i) =stress_matrix(break4);
    stress_fibre(i) = fibre_modulus(temp2(2))*strain(i);
    stress_sma(i) = sma_modulus(temp2(2))*strain(i);
    load_matrix(i) = (2*stress_matrix(i)*(1-fibre_fraction-
sma_fraction)*geometric_factor*width*depth(i)^2)/(3*length);
    load_fibre(i) =
(2*stress_fibre(i)*fibre_fraction*geometric_factor*width*depth(i)^2)/(3*l
ength);
    load_sma(i) =
(2*stress_sma(i)*sma_fraction*geometric_factor*width*depth(i)^2)/(3*lengt
h);
    load_comp(i) = (load_fibre(i)+load_sma(i)+load_matrix(i));

    if strain(i)>=0.145
       strain_energy(i) = strain_energy(i-1);
    else
       strain_energy(i) = strain_energy(i-
1)+(load_matrix(i)*delta)+(load_sma(i)*delta)+(load_fibre(i)*delta);
    end;
end

if max(stress)>=comp_strength
    failure1 = find(stress>comp_strength);
else
    failure1 = n;
end

if sma_fraction/fibre_fraction>2
    if max(strain)>=final_strain_sma;
       failure2 = find(strain>final_strain_sma);
    else
       failure2 = n;
    end
else
    if max(strain)>=final_strain_fibre
```

```
        failure2 = find(strain>final_strain_fibre);
    else
        failure2 = n;
    end
end

if min(velocity)<=0.03;
    failure3 = find(velocity<=0.05);
else
    failure3 = n;
end

if failure1(1)>failure2(1)
    if failure2(1)>failure3(1)
        failure=failure3(1);
    else
        failure=failure2(1);
    end
else
    if failure1(1)>failure3(1)
        failure=failure3(1);
    else
        failure=failure1(1);
    end
end

final_depth = (load_comp(failure)/comp_strength)/width;

    for i=failure+1:n
        velocity(i) = sqrt(2*(total_energy-strain_energy(i-1))/mass);
        delta = velocity(i)*time_interval;
        displacement(i) = displacement(i-1)+velocity(i)*time_interval;
        strainL = strain(i-1);
        strain(i) = strainL+prestrain;

        temp1 = find(al_strain<=strain(i));
        temp2 = size(temp1);

        stress(i) = stress(i-1);
        depth(i) = depth(i-1)-depth_factor*(initial_depth-final_depth);
```

```
      if depth(i)>=final_depth
         stress_matrix(i) = stress_matrix(i-1);
         stress_fibre(i) = stress_fibre(i-1);
         stress_sma(i) = stress_sma(i-1);
         load_matrix(i) = (2*stress_matrix(i)*(1-fibre_fraction-
sma_fraction)*geometric_factor*width*depth(i)^2)/(3*length);
         load_fibre(i) =
(2*stress_fibre(i)*fibre_fraction*geometric_factor*width*depth(i)^2)/(3*l
ength);
         load_sma(i) =
(2*stress_sma(i)*sma_fraction*geometric_factor*width*depth(i)^2)/(3*lengt
h);
         load_comp(i) = (load_fibre(i)+load_sma(i)+load_matrix(i));

         if strain(i)>=0.145
            strain_energy(i) = strain_energy(i-1);
         else
            strain_energy(i) = strain_energy(i-
1)+(load_matrix(i)*delta)+(load_sma(i)*delta)+(load_fibre(i)*delta);
         end;
      else
         load_matrix(i) = 0;
         load_fibre(i) = 0;
         load_sma(i) = 0;
         load_comp(i)= 0;
         strain_energy(i) = strain_energy(i-1);
      end
   end
end

stop_point = find(load_comp == 0);
stop = stop_point(1);

max_load = round(max(load_comp(1:stop)))
max_energy = max(strain_energy(1:stop))
velocity(stop)

figure(1)
plot(displacement(1:70),stress(1:70),'b.-')
figure(2)
```

```
plot(al_strain(1:70),equiv_modulus(1:70),'cx-')
figure(3)
plot(displacement(1:70),velocity(1:70))
figure(4)
plot(displacement(1:stop)*1e3,load_comp(1:stop))
title('LOAD CHARACTERISTICS OF SMA COMPOSITES')
xlabel('Displacement [mm]')
ylabel('Load [N]')
figure(5)
plot(displacement(1:stop)*1e3,strain_energy(1:stop))
title('ENERGY CHARACTERISTICS OF SMA COMPOSITES')
xlabel('Displacement [mm]')
ylabel('Strain Energy [J]')
figure(6)
plot(al_strain(1:115)*100,al_modulus(1:115)/1e9,'r')
title('AC8A MODULUS')
xlabel('STRAIN [%]')
ylabel('GOPAL''S MODULUS [GPa]')
figure(7)
plot(al_strain(1:65)*100,fibre_modulus(1:65)/1e9,'r')
title('ALUMINIUM OXIDE MODULUS')
xlabel('STRAIN [%]')
ylabel('GOPAL''S MODULUS [GPa]')
figure(8)
plot(al_strain*100,sma_modulus/1e9,'r')
title('NITINOL MODULUS')
xlabel('STRAIN [%]')
ylabel('GOPAL''S MODULUS [GPa]')
figure(9)
plot(al_strain(1:115)*100,al_stress(1:115)/1e6,'b')
title('AC8A STRESS-STRAIN CURVE')
xlabel('STRAIN [%]')
ylabel('STRESS [MPa]')
figure(10)
plot(al_strain(1:65)*100,fibre_stress(1:65)/1e6,'b')
title('ALUMINIUM OXIDE STRESS-STRAIN CURVE')
xlabel('STRAIN [%]')
```

```
ylabel('STRESS [MPa]')
figure(11)
plot(al_strain*100,sma_stress/1e6,'b')
title('NITINOL STRESS-STRAIN CURVE')
xlabel('STRAIN [%]')
ylabel('STRESS [MPa]')
```